

**STRUCTURE-PROPERTY RELATIONSHIP OF NANOPATELET-
REINFORCED POLYMER NANOCOMPOSITES**

A Dissertation

by

WOONG JAE BOO

Submitted to the Office of Graduate Studies of
Texas A&M University
in partial fulfillment of the requirements for the degree of

DOCTOR OF PHILOSOPHY

May 2007

Major Subject: Materials Science and Engineering

**STRUCTURE-PROPERTY RELATIONSHIP OF NANOPATELET-
REINFORCED POLYMER NANOCOMPOSITES**

A Dissertation

by

WOONG JAE BOO

Submitted to the Office of Graduate Studies of
Texas A&M University
in partial fulfillment of the requirements for the degree of

DOCTOR OF PHILOSOPHY

Approved by:

Chair of Committee,
Committee Members,

Hung-Jue Sue
Jaime Grunlan
Hong Liang
Tahir Cagin
Joseph H. Ross, Jr.

Chair of Interdisciplinary Faculty,

May 2007

Major Subject: Materials Science and Engineering

ABSTRACT

Structure-Property Relationship of Nanoplatelet-Reinforced
Polymer Nanocomposites. (May 2007)

Woong Jae Boo, B.S., Hankook Aviation University;
M.S., Texas A&M University

Chair of Advisory Committee: Dr. Hung-Jue Sue

As a part of a larger effort towards the fundamental understanding of structure-property relationship in nanoplatelet-reinforced polymer nanocomposites, a set of model epoxy systems containing α -Zirconium Phosphate (α -ZrP) have been prepared and studied in this dissertation. A new surface modification approach, *i.e.*, *the porous pathway approach*, for improving intercalation efficiency and exfoliation of layered nanoplatelets has been proposed and the effectiveness has been demonstrated. In order to clearly understand the roles of nanofillers and the effects of their geometric factors on the physical and mechanical properties of nanocomposites, variables such as nanoplatelet loading level, degree of exfoliation, and aspect ratio have been carefully controlled in the epoxy matrices. Morphological information of the prepared nanocomposites was unambiguously confirmed by carrying out X-ray diffraction and transmission electron microscopy (TEM). Tensile and thermo-mechanical properties of the model epoxy/ α -ZrP nanocomposites have been investigated. Furthermore, fracture behavior of the model nanocomposites is examined in this study. This work has enhanced the understanding of the effects of nanoplatelet, *i.e.*, *loading level, degree of*

exfoliation, aspect ratio, and the type of surface modifiers, on the mechanical properties and fracture behavior of polymer nanocomposites.

To
My parents
My sister and
My wife Jin

ACKNOWLEDGEMENTS

I would like to express my deep gratitude and great respect to my academic advisor, Dr. Hung-Jue Sue, for his guidance, advice and inspiration. I am grateful to my dissertation committee members, Dr. Hong Liang, Dr. Jaime Grunlan, and Dr. Tahir Cagin for their valuable discussions and support.

Special thanks are given to Dr. Abraham Clearfield for his help with the α -Zirconium phosphate-related experiments and discussions, Ms. Ann Ellis at the Microscopy & Imaging Center at Texas A&M University for her instructions with the TEM work, and Dr. Nattamai Bhuvanesh at the X-ray Diffraction Laboratory at Texas A&M University for his help with the small and wide-angle X-ray diffraction experiments.

I thank the State of Texas (000512-00311-2003), National Science Foundation (DMR-0332453), Defense Logistic Agency (SP0103-02-D-0024), and the Dow Chemical Company for the final supports.

Throughout my study, I have greatly benefited from working with my former and current colleagues: Mr. Chih-Wei Feng, Dr. Jong-Il Weon, Dr. Goyteck Lim, Dr. Ki Tak Gam, Dr. Luyi Sun, Mr. Ehsan Moghbelli, Mr. Ikeda Hidehito, Mr. Dazhi Sun, Mr. Jia Liu, Mr. Robert Browning, Mr. Sung-Min Lee, and Mr. Graham Warren. Their friendship and unconditional support will always be remembered.

TABLE OF CONTENTS

	Page
ABSTRACT	iii
DEDICATION	v
ACKNOWLEDGEMENTS	vi
TABLE OF CONTENTS	vii
LIST OF TABLES	x
LIST OF FIGURES.....	xi
 CHAPTER	
I INTRODUCTION.....	1
1.1 Background	1
1.2 α -Zirconium Phosphate-Reinforced Polymer Nanocomposites	2
1.3 Research Objectives and Significance	3
1.4 Dissertation Layout	4
II LITERATURE REVIEW	7
2.1 Polymer Nanocomposites.....	7
2.2 Toughening Mechanisms	8
2.2.1 Crack Deflection	10
2.2.2 Local Plastic Deformation	11
2.2.3 Microcracking	13
2.2.4 Crack Pinning.....	16
2.3 Fundamental Issues of Concern	18
2.4 Concluding Remarks	23
III EFFECTIVE INTERCALATION AND EXFOLIATION OF NANOPLATELETS IN EPOXY VIA CREATION OF POROUS PATHWAYS	25
3.1 Introduction	25
3.2 Experimental	27
3.2.1 Materials.....	27
3.2.2 Sample Preparation	28
3.2.3 Characterization	29

CHAPTER	Page
3.3 Results and Discussion.....	30
3.4 Summary	40
 IV MORPHOLOGY AND MECHANICAL BEHAVIOR OF EXFOLIATED EPOXY/ α -ZIRCONIUM PHOSPHATE NANOCOMPOSITES	41
4.1 Introduction	41
4.2 Experimental	43
4.2.1 Materials.....	43
4.2.2 Preparation of α -ZrP-Based Epoxy Nanocomposites	43
4.2.3 Morphology Characterization.....	45
4.2.4 Mechanical/Physical Property Characterization	45
4.2.5 Fracture Toughness and Toughening Mechanism Investigation.....	45
4.3 Results and Discussion.....	46
4.3.1 Morphology.....	46
4.3.2 A Simple Geometric Model	48
4.3.3 Mechanical Property.....	53
4.3.4 Fracture Behavior Study.....	56
4.4 Summary	59
 V EFFECTS OF NANOPLETELET DISPERSION ON MECHANICAL BEHAVIOR OF POLYMER NANOCOMPOSITES.....	61
5.1 Introduction	61
5.2 Experimental.....	65
5.2.1 Materials.....	65
5.2.2 Preparation of Epoxy/ α -ZrP Nanocomposites	66
5.2.3 Morphology Characterization.....	68
5.2.4 Mechanical Property Characterization	68
5.2.5 Fracture Behavior	69
5.3 Results and Discussion.....	69
5.3.1 Morphology	70
5.3.2 Mechanical Property.....	76
5.3.3 Fracture Behavior Study.....	81
5.4 Summary.....	86
 VI EFFECTS OF NANOPLETELET ASPECT RATIO ON MECHANICAL PROPERTIES OF EPOXY NANOCOMPOSITES	88
6.1 Introduction	88
6.2 Experimental.....	91
6.2.1 Materials.....	91
6.2.2 Preparation of Epoxy/ α -ZrP Nanocomposites	91
6.2.3 Morphology Characterization.....	93

CHAPTER	Page
6.2.4 Mechanical Property and Fracture Behavior Studies	94
6.3 Results and Discussion	95
6.3.1 Morphology	95
6.3.2 Mechanical Property	101
6.3.3 Fracture Behavior Study	106
6.4 Summary	111
VII CONCLUDING REMARKS AND RECOMMENDATIONS	112
7.1 Intercalation and Exfoliation of Nanoplatelets in Epoxy Nanocomposites	113
7.2 Morphology and Mechanical Behavior of Exfoliated Epoxy/ α -Zirconium Phosphate Nanocomposites	113
7.3 Effects of Nanoplatelet Dispersion on Mechanical Behavior of Polymer Nanocomposites	114
7.4 Effects of Nanoplatelet Aspect Ratio on Mechanical Properties of Epoxy Nanocomposites	115
7.5 Recommendations for Future Work	115
7.5.1 Intercalating Agent and Interface Study	116
7.5.2 Toughenability Study of Nanoplatelet-Dispersed Epoxy Nanocomposites	117
REFERENCES	119
APPENDIX A	129
VITA	157

LIST OF TABLES

TABLE	Page
2.1 Modulus and fracture toughness of epoxy and epoxy/ α -ZrP nanocomposites.....	21
2.2 Fracture toughness of nylon-6 and nylon-6/clay nanocomposites	22
3.1 Compositions of surface modifiers utilized for intercalation of α -ZrP.....	29
4.1 Compositions of model systems investigated (vol %)	44
4.2 The interlayer distances of nanoplatelets in polymer nanocomposites	53
5.1 Mechanical properties and T_g of epoxy/ α -ZrP nanocomposites.....	78
6.1 Material specification and source	92
6.2 Tensile properties and fracture toughness of epoxy/ α -ZrP nanocomposites	101

LIST OF FIGURES

FIGURE	Page
2.1 Fracture morphologies within the crack initiation region observed by SEM: (a) neat epoxy; (b) epoxy/clay (98/2), $\times 1000$. White arrows indicate the crack propagation direction (reproduced from [68])	9
2.2. Optical, (a) and (b), and SEM, (c) and (d), micrographs of DN-4PB crack tip in a 10 wt % clay sample, (b) and (d), as compared to an unfilled epoxy sample, (a) and (c) (reproduced from [69]).....	10
2.3 Micrographs illustrating compressive deformation in a 7 wt % clay sample: (a) macroscopic deformation illustrating a diffuse shear band, (b) SEM micrograph of a region outside the shear band, and (c) SEM micrograph of a region within the shear band with void detail (reproduced from [69]).....	12
2.4 TEM of the crack tip damage zone of epoxy/ α -ZrP nanocomposite. Delaminated cavities are observed at the crack tip region (reproduced from [15]).....	13
2.5 TEM micrographs of thin sections taken from the region in front of an arrested crack tip within epoxy/clay nanocomposites (reproduced from [45]).....	14
2.6 TEM micrographs of a propagated crack in epoxy-clay nanocomposites (reproduced from [45]).....	15
2.7 SEM micrographs of fracture surfaces of epoxy/organoclay nanocomposites (reproduced from [71]).....	16
2.8 Illustration of crack pinning in nanocomposites (reproduced from [71])	17
2.9 TEM micrographs of fully exfoliated epoxy/ α -ZrP nanocomposites (a) low and (b) high magnification. (reproduced from [27])	20
2.10 OM of crack tip damage zone of epoxy/ α -ZrP/CSR nanocomposite. Bright field and cross-polarized light. (reproduced from [15]).....	23
3.1 XRD of α -ZrP	31
3.2 SEM of α -ZrP	32

FIGURE	Page
3.3 XRD of intercalated α -ZrP and epoxy/ α -ZrP nanocomposites	34
3.4 Schematic illustrations of interlayer spacings of α -ZrP treated with different organic modifiers: (a) cyclohexylamine, (b) dodecylamine, and (c) an equal mixture of cyclohexylamine and dodecylamine	35
3.5 XRD of α -ZrP intercalated and exfoliated with a mixture of tetra-n-butyl ammonium hydroxide and Jeffamine M600	39
3.6 TEM of highly exfoliated α -ZrP nanoplatelets (2.0vol%) in epoxy	40
4.1 XRD patterns of (a) pristine α -ZrP powder (d-spacing: 7.6Å), (b) S-ZrP in solvent (d-spacing: 34Å), (c) S-ZrP mixed with epoxy monomer, and (d) Cured Epoxy/S-ZrP nanocomposite (2 vol%)	47
4.2 TEM images of Epoxy/S-ZrP nanocomposites showing a high degree of exfoliation of nanoplatelets in epoxy matrix. The nanocomposite with 2 vol% of ZrP is shown in (a) low magnification and (b) high magnification. The nanocomposite with 1 vol% of ZrP is shown in (c).....	49
4.3 Uniformly and orderly distributed nanoplatelets in polymer matrix	51
4.4 Tensile behavior of α -ZrP based DGEBA/DDS epoxy systems	54
4.5 DMA of neat epoxy, S-epoxy, and epoxy/S-ZrP nanocomposite systems	55
4.6 TEM images of DN-4PB damage zone of epoxy/S-ZrP nanocomposite (2 vol%) showing a straight crack, as shown in (a). In (b), the crack tip region is shown. The crack propagates from left to right.....	57
5.1 Schematic of categories of microcomposites and nanocomposites	63
5.2 Sample preparation procedures to control the degree of exfoliation of α -ZrP in epoxy.....	67
5.3 XRD patterns of (a) pristine α -ZrP powder (d-spacing 7.6Å), (b) Surface modified α -ZrP in solvent (d-spacing 38Å), (c) Exfoliated epoxy/ α -ZrP nanocomposite after curing	71
5.4 XRD patterns of epoxy/ α -ZrP nanocomposites with (a) poor exfoliation, (b) moderate exfoliation, and (c) good exfoliation	73
5.5 Images of neat epoxy and epoxy/ α -ZrP nanocomposites with different levels of exfoliation	73

FIGURE	Page
5.6 TEM of epoxy/ α -ZrP showing (a) poor exfoliation, (b) moderate exfoliation and (c) good exfoliation. All samples contain the same amount of α -ZrP (2.0 vol%) and intercalating agent in epoxy	75
5.7 Tensile behavior of α -ZrP based DGEBA/DDS epoxy systems	77
5.8 DMA of α -ZrP based DGEBA/DDS epoxy systems.....	80
5.9 TEM of DN-4PB damage zone of Epoxy/ α -ZrP nanocomposite with poor exfoliation (2.0 vol%), showing crack bifurcation and distortion: (a) low magnification and (b) high magnification. The crack propagates from left to right.....	82
5.10 TEM of DN-4PB damage zone of Epoxy/ α -ZrP nanocomposite with good exfoliation (2.0 vol%) showing straight crack propagation breaking through α -ZrP layers: (a) low magnification and (b) high magnification. The crack propagates from left to right.....	85
6.1 SEM of α -ZrP nanoplatelets having aspect ratios of (a) 100 and (b) 1,000	96
6.2 TEM of epoxy/ZrP-100 nanocomposite: (a) low magnification, (b) high magnification, and (c) the corresponding schematic.....	98
6.3 TEM of epoxy/ZrP-1000 nanocomposite: (a) low magnification, (b) high magnification, and (c) the corresponding schematic.....	100
6.4 Tensile behavior of neat epoxy and epoxy nanocomposites.....	102
6.5 DMA results of neat epoxy and epoxy nanocomposites.....	104
6.6 Molecular structure and size comparison of the intercalating agents between (a) tetra- <i>n</i> -butyl ammonium hydroxide and (b) monoamine-terminated polyether.....	105
6.7 TEM of DN-4PB damage zone of epoxy/ZrP-100: (a) the crack wake and (b) the crack tip region. The crack propagates from left to right	108
6.8 TEM of DN-4PB damage zone of epoxy/ZrP-1000 nanocomposite: (a) the crack wake region (low mag.) (b) the crack wake region (high mag.) and (c) the crack tip region. The crack propagates from left to right.....	109

CHAPTER I

INTRODUCTION

1. 1. Background

Polymer nanocomposites are a new class of materials that consist of a polymeric matrix containing well-dispersed particles or fillers with at least one of its dimensions to be at the nanometer scale. Since these materials can be ideal candidates for a vast majority of structural and functional material applications, polymer nanocomposites have drawn great deals of attention in recent years [1-13].

There are three types of nanoadditives that are categorized based on whether they possess (a) one, (b) two, or (c) three dimensions in the nanometer range. Among these, the nanoparticles of type (a), which possess a platelet-like structure that has only one dimension in the nanometer range, have been extensively studied as reinforcing nanofillers that yield exceptional properties due to its structural advantages such as high aspect ratio and large surface area [14-16]. These nanoplatelets usually exist in the form of sheets with 1-3 nm in thickness while having two or more orders of magnitude larger in the other two dimensions.

The dissertation follows the style of Polymer.

Among the wide variety of natural and synthetic inorganic fillers, montmorillonite (MMT) clay has been the most widely utilized filler to reinforce a variety of polymer matrices [17-21], mainly due to its relative high ion exchange capacity, high aspect ratio, low cost and ease of surface modification.

1. 2. α -Zirconium Phosphate-Reinforced Polymer Nanocomposites

Since the original work on montmorillonite (MMT) clay-modified nylon-6 [22] nanocomposites was reported about two decades ago, numerous efforts have followed to establish a better understanding of structure-property relationship in polymer nanocomposites reinforced with nanoplatelets [23,24]. Recently, in an effort to better understand the effects of nanoplatelets loading level, aspect ratio and dispersion of nanoplatelets on the physical and mechanical properties of polymer nanocomposites, significant efforts have been carried out to improve stiffness and strength [18,21], enhanced gas barrier properties [17,25], and flame retardancy [26].

Unfortunately, due to the typical high impurity content of MMT clays as well as their wide particle size distribution, it is unlikely that MMT clay based polymer nanocomposites can exhibit consistent properties for unambiguous fundamental structure-property relationship studies. Therefore, limited structure-property relationship can be gained from MMT-based polymer nanocomposite systems.

Stemming from the above concerns, synthetic α -zirconium phosphate (ZrP), $\text{Zr}(\text{HPO}_4)_2 \cdot \text{H}_2\text{O}$, has been chosen as a model nanofiller to probe the fundamental structure-property relationship of fully exfoliated polymer nanocomposites [15,27,28].

The ZrP has a higher ion exchange capacity than MMT clay; hence, it is relatively easy to achieve a higher degree of exfoliation for ZrP nanoplatelets [28]. In addition, the particle size and aspect ratio can be controlled by varying reactant concentrations, temperature, and reaction time [29]. As a result, α -ZrP can serve as an ideal nanofiller to study the fundamental structure-property relationship of polymer nanocomposites.

In this work, the structure-property relationship of epoxy/ZrP nanocomposites are studied, with an emphasis on how the nanoplatelets loading level, degree of exfoliation, aspect ratio and type of intercalating agents affect the properties of the nanocomposites.

1. 3. Research Objectives and Significance

The primary objectives of this research are to investigate the mechanical and fracture behavior of polymer nanocomposites and the improvement of their physical/mechanical properties by addition of α -zirconium phosphate nanoplatelets. The goal of the research is to gain fundamental understanding of the following:

- a) The effects of the nanofiller addition on the mechanical properties of the polymer matrix.
- b) The effects of the nanofiller structure, e.g., loading level, particle size, aspect ratio, and level of exfoliation, on the improvement of mechanical properties of the polymer nanocomposites.

- c) The effect of surface modifiers on the mechanical and physical properties of the polymer nanocomposites.
- d) The detailed fracture behavior and toughening mechanisms of exfoliated nanoplatelet-reinforced epoxy nanocomposites.

It is expected that the present work will contribute significantly to the fundamental understanding of the effect of not only the nanofiller addition to polymer matrices but also the influence of the nanofiller characteristics, such as loading level, particle size, aspect ratio, and state of exfoliation, on the structure-property relationship of nanoplatelet-reinforced polymer nanocomposites.

1. 4. Dissertation Layout

As mentioned earlier, a series of experimental approaches are employed in this study in order to understand the fundamental structure-property relationship of nanoplatelet-reinforced polymer nanocomposites. To further develop the background of polymer nanocomposites research, a compendious literature review of the fracture behavior of nanoplatelet-reinforced polymer nanocomposites has been performed and included in Chapter II.

Based on α -ZrP nanoplatelets, a new surface modification approach, *i.e. porous pathway*, to improve intercalation efficiency and exfoliation of layered nanoplatelets is

carefully laid out in Chapter III. The intercalation/exfoliation mechanisms accounting for the observed effectiveness are also discussed in this chapter.

In Chapter IV, the morphology of epoxy/ZrP nanocomposites with a high level of exfoliation is examined using TEM. A simple geometric model is utilized to describe an idealized relationship between interlayer d-spacing and filler loading level. The detailed fracture mechanisms and the influence of nanoplatelet loading level on physical and mechanical properties have also been addressed.

By altering the processing conditions *alone*, three distinctive levels of dispersion of α -ZrP nanoplatelets have been achieved. Thus, the effect of nanoplatelet dispersion on mechanical properties can be unambiguously addressed in Chapter V. The corresponding mechanical properties and fracture behaviors of the epoxy/ α -ZrP nanocomposites are investigated and the differences in the operative fracture mechanisms of the model nanocomposites are also described and discussed in this chapter.

As shown in Chapter VI, in order to study the effects of nanoplatelet aspect ratio on the mechanical properties of polymer nanocomposites, epoxy/ α -zirconium phosphate nanocomposites with two distinctive aspect ratios at 100 and 1,000 have been prepared and characterized. In this chapter, fundamental study on how the nanoplatelet aspect ratio influences the mechanical properties of polymer nanocomposites and the usefulness of high aspect ratio nanoplatelets in polymer nanocomposites for structural applications have also been discussed.

Finally, in Chapter VII, an overall conclusion of this study has been made and included, while recommendations and possible ideas and ambiguities for future work are given.

CHAPTER II

LITERATURE REVIEW

2. 1. Polymer Nanocomposites

Polymer nanocomposites have attracted a great deal of research attention in the past two decades because, if well-exfoliated and well-dispersed, they may exhibit substantially improved physical and mechanical properties compared with conventional composites that contain comparable amounts of reinforcement [4,7,9,30-41]. Polymer nanocomposites are a novel class of materials that are reinforced by one or more types of fillers of which at least one dimension of the dispersed particles in the polymer matrix is in the nanometer range. From the standpoints of reinforcement efficiency and cost consideration, the most commonly chosen nanoparticles exhibit nanoplatelet layer structure characteristics, such as montmorillonite (MMT) clay [5,11,37,39,42-51].

There are various types of layer-structured materials (i.e., MMT clay, $Zr(HPO_4)_2$, MoS_2 , graphite, etc.) [6,15,16,19,21,23,27,52-65]. Polymer nanocomposites containing these types of layer structures are usually produced *via* a multi-step process to achieve well-exfoliated nanocomposite systems. These multi-step processes include purification, surface modification, intercalation, and exfoliation of the nanolayers in the polymer matrix. If they are well exfoliated, significant improvements in physical and mechanical properties can be achieved by only a small amount (1-3 vol%) of filler addition due to their high elastic modulus, strength, and high aspect ratio [6,16,19,21,61-64].

In addition to the layer-structured nanofillers, there are also other nanometer-scale fillers, such as CaCO_3 and carbon nanotubes (CNTs), for reinforcing polymer matrices. Depending on their size, shape, surface characteristics, and the ductility of the host polymer, the corresponding fracture behaviors may vary significantly. These types of nanofillers do not need to be intercalated. Their mechanical properties and fracture behaviors also vary significantly from those of nanoplatelet-containing polymer nanocomposites [52,54,66,67]. They will not, however, be included in this review.

Herein, the fracture behavior of two types of nanoplatelet-containing polymer nanocomposites, which contain MMT clay and α -zirconium phosphate (α -ZrP), will be reviewed. The overall effect of nanofiller aspect ratio and level of exfoliation on the fracture behavior of polymer nanocomposites will also be discussed.

2.2. Toughening Mechanisms

Significant research has recently been pursued to examine the fracture process in MMT clay-based polymer nanocomposites. Yet, inconsistent claims have been made. Some researchers have observed an improvement in fracture toughness [45,68-71], while others have shown otherwise [15,53,72,73]. For instance, Liu *et al.* [68] found an improvement in critical stress intensity factor, K_{IC} , after clay addition to the epoxy matrix, and the K_{IC} value becomes higher as the clay concentration is increased. The fracture surfaces of neat epoxy and nanocomposites were compared (Fig. 2.1).

It can be seen that neat epoxy exhibits a relatively smooth fracture surface feature, which typifies a brittle fracture behavior. On the other hand, a much rougher fracture

surface is observed after adding clay into the epoxy matrix. The increased surface roughness implies that the path of the crack-tip is tortuous, making crack propagation more difficult. This finding also implies that the clay particles are not nanosize in nature. Micrometer and sub-micrometer aggregates on the fracture surface were observed. It is still uncertain whether or not the increased fracture toughness values obtained were mainly due to the presence of the micrometer-size particles.

Several key toughening mechanisms in MMT clay-modified epoxy have been observed in the literature; they are briefly summarized below.

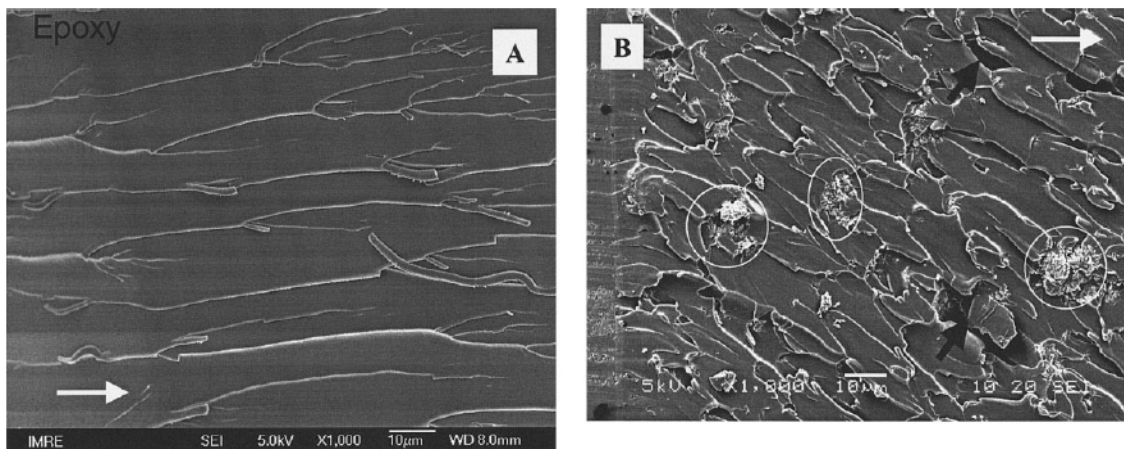


Fig. 2.1. Fracture morphologies within the crack initiation region observed by SEM: (a) neat epoxy; (b) epoxy/clay (98/2), $\times 1000$. White arrows indicate the crack propagation direction (reproduced from [68]).

2. 2. 1. Crack Deflection

Zerda and Lesser [69] utilized the double-notched four-point bend technique (DN-4PB) to study the fracture behavior of epoxy-clay nanocomposites. The DN-4PB method was first introduced by Sue and Yee [70] to probe the damage mechanisms around a loaded crack tip. Two cracks of equal length are introduced into a specimen and identically loaded. One crack propagates to failure and another propagates only subcritically. The survived crack can be utilized to unambiguously study the operative toughening mechanisms *via* optical microscopy (OM) and transmission electron microscopy (TEM). As illustrated in Fig. 2.2, the neat epoxy contains a straight crack with a smooth surface, whereas the intercalated nanocomposite shows a tortuous crack trajectory and exhibits evidence of crack branching along the crack path.

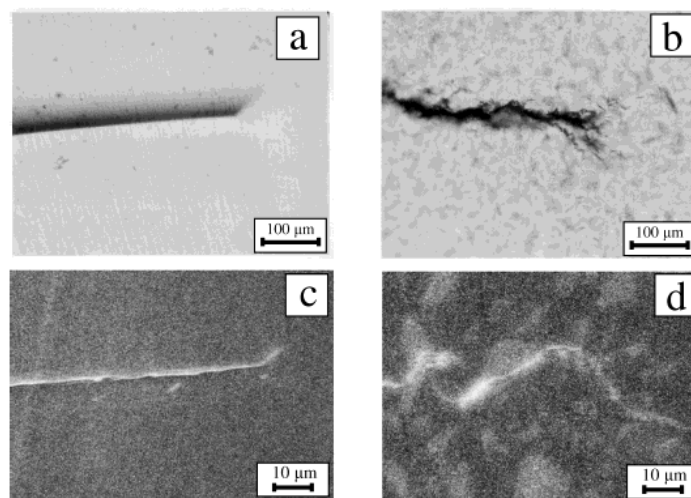


Fig. 2.2. Optical, (a) and (b), and SEM, (c) and (d), micrographs of DN-4PB crack tip in a 10 wt % clay sample, (b) and (d), as compared to an unfilled epoxy sample, (a) and (c) (reproduced from [69]).

Generally, the presence of clay causes perturbations along the crack front, altering the crack path. The crack propagates through either debonding along the particle/matrix interface or delamination between the agglomerated particles. As the clay concentration increases, the distance between clay particles decreases. This leads to a more tortuous crack path. Again, the abovementioned toughening mechanism appears to require the presence of aggregated particles to become effective.

2. 2. 2. Local Plastic Deformation

Zerda and Lesser [69] also reported that, upon compression, the clay-filled epoxy yields in shear with the evolution of a visible but diffuse shear-banding zone (Fig. 2.3). There is a creation of new surface area in this region, which is indicated by the scattering of visible light in the band. On further compression past the yield point, the shear-banding zone expands to consume the entire sample. This shear-banding zone was further examined using SEM. As shown in Fig. 2.3(c), voiding developed and was confined mostly within the large clay domains.

Upon fracture, the clay particles serve as stress concentration sites, thus resulting in either debonding at the clay-matrix interface or cleavage of clay tactoids that leads to the formation of micro- or nano-voids. These voids could initiate shear yielding of the epoxy matrix at the crack and microcrack tips throughout the entire volume, thereby absorbing a significant amount of energy before final fracture. The shear yielding of the matrix manifests itself as a kind of step structure that contributes to the increase in surface roughness.

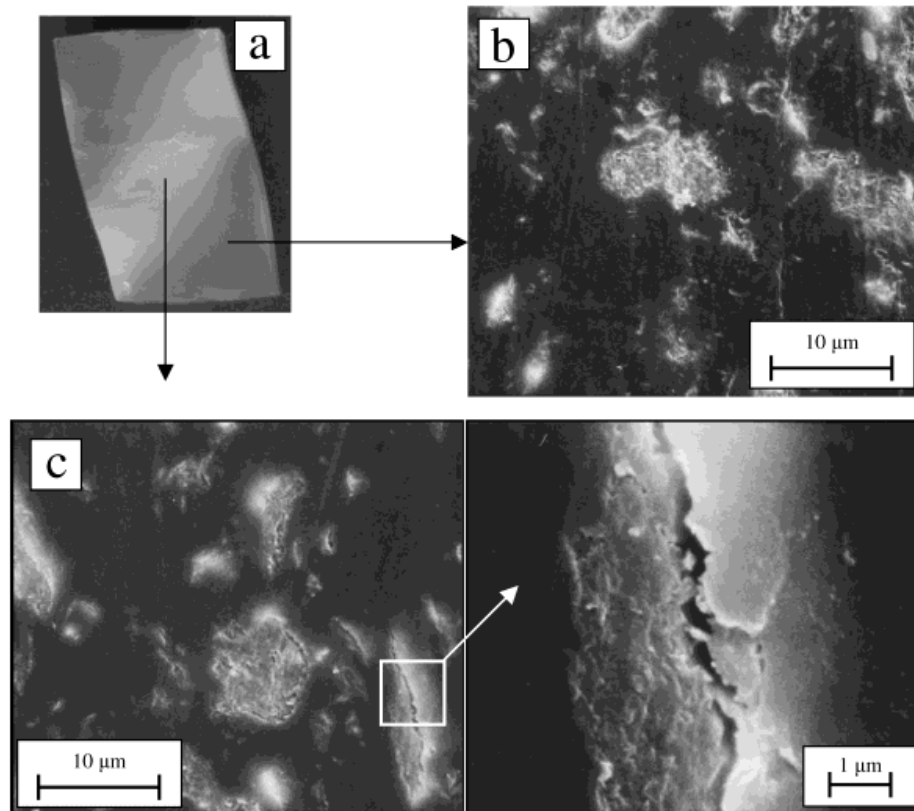


Fig. 2.3. Micrographs illustrating compressive deformation in a 7 wt % clay sample: (a) macroscopic deformation illustrating a diffuse shear band, (b) SEM micrograph of a region outside the shear band, and (c) SEM micrograph of a region within the shear band with void detail (reproduced from [69]).

2. 2. 3. Microcracking

Sue *et al.* [15,72] investigated the survived crack tip damage zone of DN-4PB specimens of a partially exfoliated epoxy/ α -ZrP nanocomposites. As shown in Fig. 2.4, microcracks are formed due to the voiding along the crack path in the crack tip region, and these voids come from the delamination of the intercalated α -ZrP platelets.

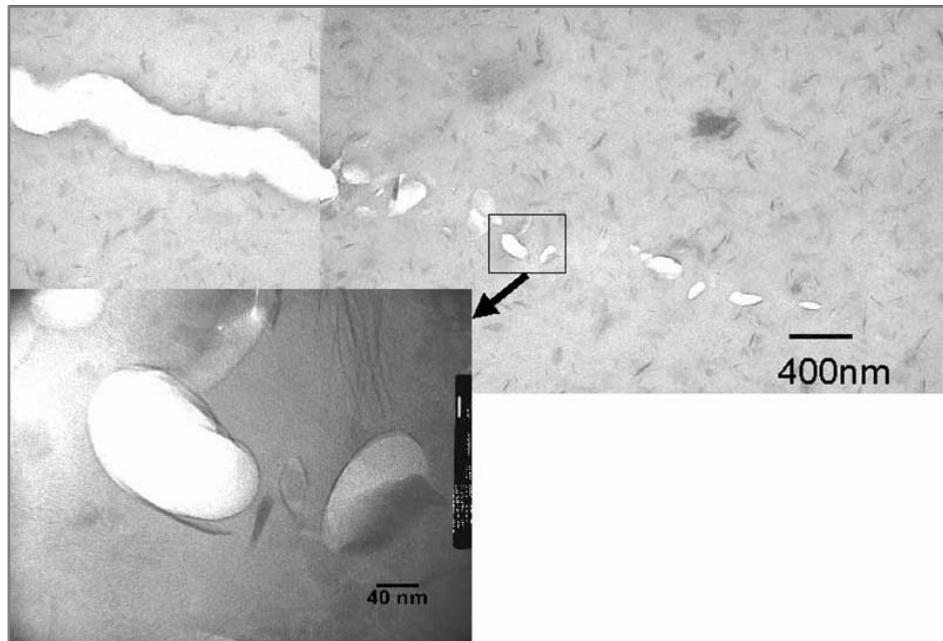


Fig. 2.4. TEM of the crack tip damage zone of epoxy/ α -ZrP nanocomposite. Delaminated cavities are observed at the crack tip region (reproduced from [15]).

Later on, Wang *et al.* [45] studied the vicinity of the arrested crack tip of an epoxy/clay nanocomposite from a DN-4PB specimen (Fig. 2.5). Some incipient cracks consist of several discontinuous cavities that are closely associated with clay platelets (Fig. 2.5(a)). Long, narrow microcavities or microcracks associated with clay were also found in the region ahead of the arrested crack tip (Fig. 2.5(b)). Most of the microcracks are formed either along the matrix-clay interface or on the delaminated clay platelets.

The crack propagation of a double-cantilever-beam specimen was also studied using TEM (Fig. 2.6 [45]). It is shown that microcracks finally develop into a main crack with a multitude of secondary cracks formed perpendicular to the main crack. These secondary cracks stop after a very short crack extension, and the tip is blunted (as shown in Fig. 2.6(c)).

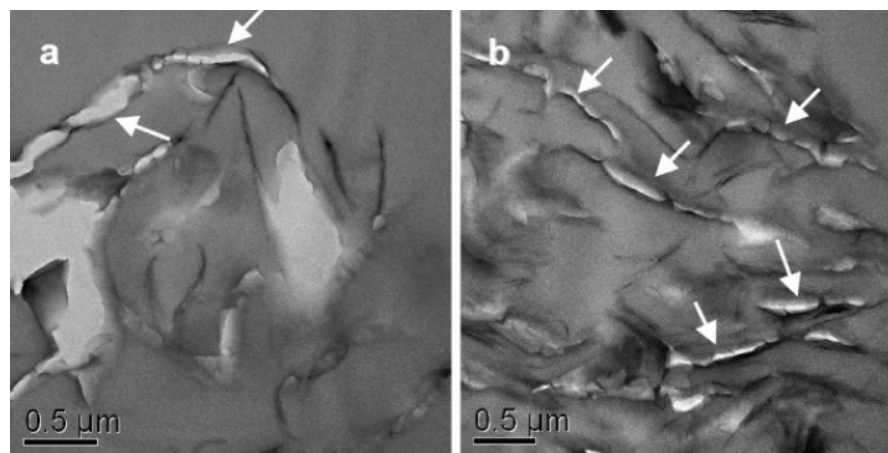


Fig. 2.5. TEM micrographs of thin sections taken from the region in front of an arrested crack tip within epoxy/clay nanocomposites (reproduced from [45]).

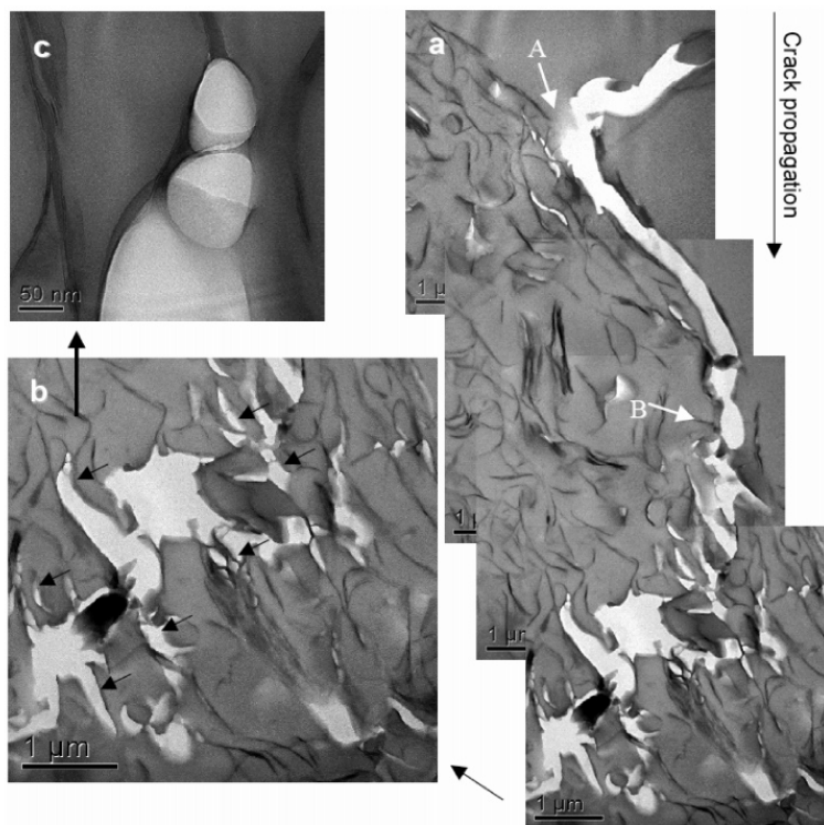


Fig. 2.6. TEM micrographs of a propagated crack in epoxy-clay nanocomposites (reproduced from [45]).

2. 2. 4. Crack Pinning

Liu *et al.* [71] compared the fracture surfaces of epoxy/organoclay and epoxy/pristine clay nanocomposites and found that, in their epoxy/organoclay system, only a small portion of the interfaces between the matrix and the clay are debonded and very few voids are seen (Fig. 2.7). This is due to the fact that the epoxy molecules were well intercalated into the clay platelets and had substantial interfacial adhesion between them, resulting in the formation of rigid and well-bonded agglomerates.

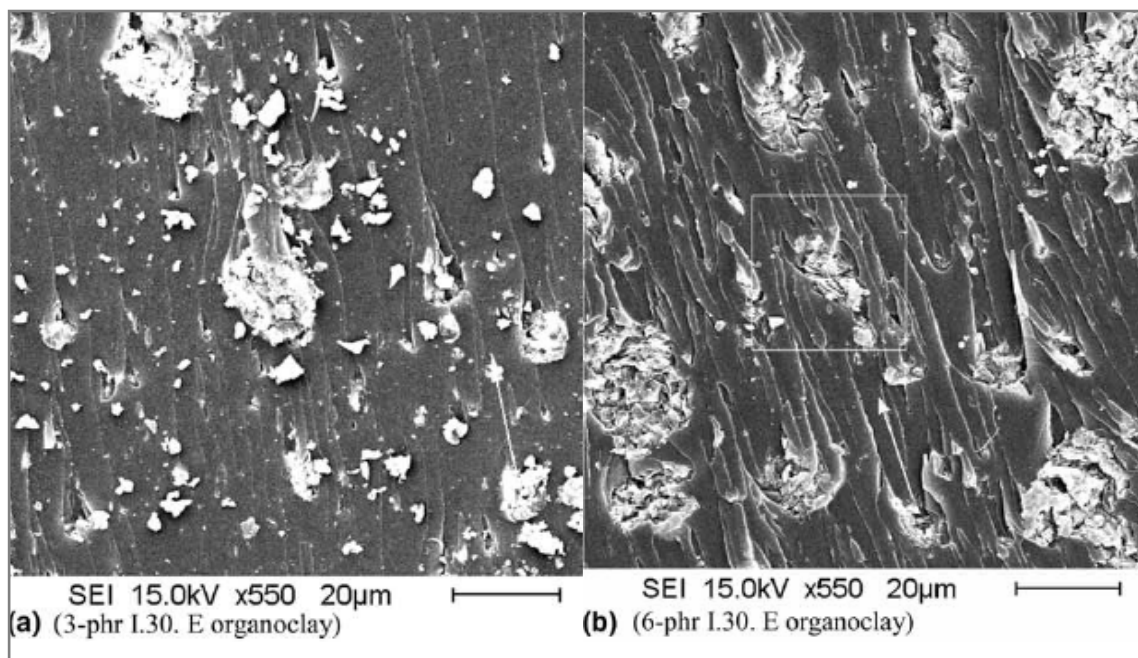


Fig. 2.7. SEM micrographs of fracture surfaces of epoxy/organoclay nanocomposites (reproduced from [71]).

When a propagating crack encounters the well-bonded rigid clay particles, it becomes temporarily pinned and tends to bow out between the rigid particles and form tails in front of the particles. Thus, it results in an increased absorption of energy. This includes not only the creation of new fracture surfaces but the formation of the new non-linear crack fronts that consume additional line energy. This pinning mechanism is demonstrated in the sketch shown in Fig. 2.8 [37].

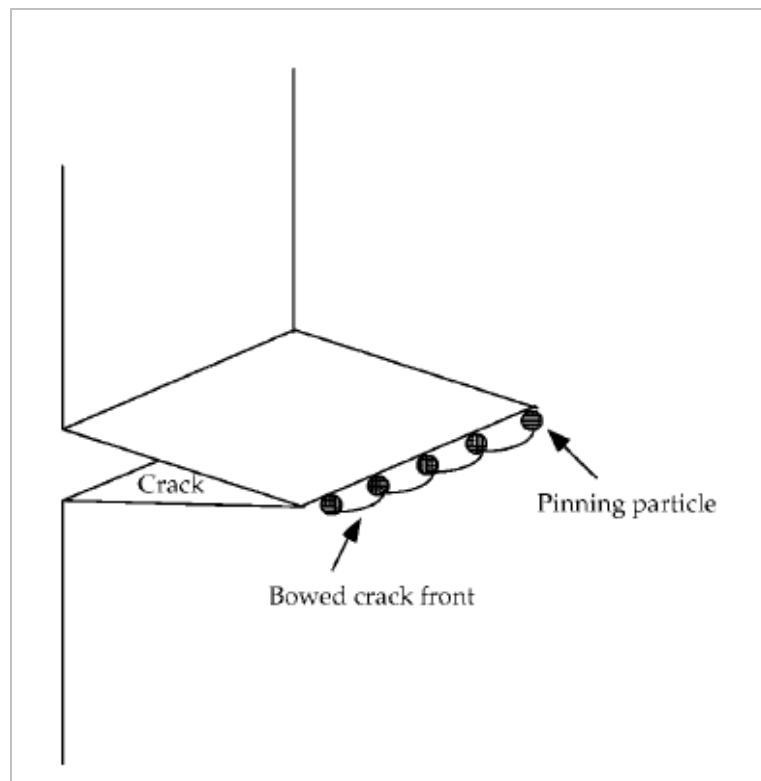


Fig. 2.8. Illustration of crack pinning in nanocomposites (reproduced from [71]).

2. 3. Fundamental Issues of Concern

There have been literally hundreds of papers attempting to fundamentally understand the mechanical and fracture behaviors of clay-based polymer nanocomposites [8,9,12,31,35,74-78]. Very little fundamental knowledge is gained, however. This is mainly due to the inability of researchers to prepare fully exfoliated clay-based polymer nanocomposites in a consistent manner. As a result, ambiguous findings are abundant.

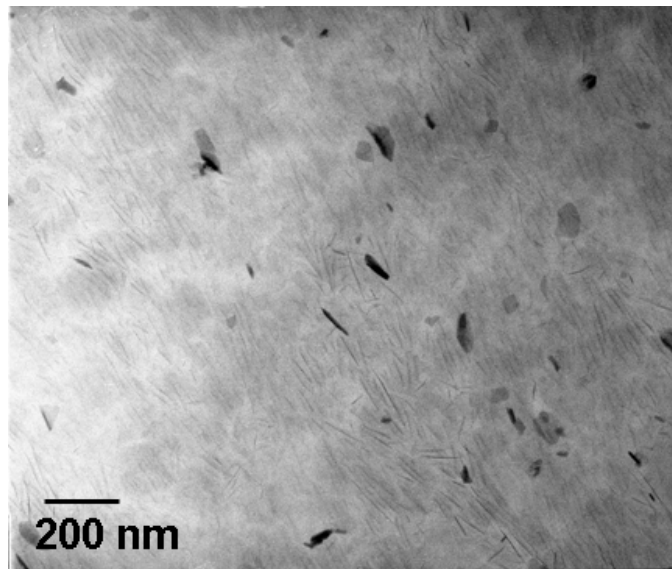
In general, for nanocomposite systems that exhibit an improved toughness, one or a combination of the previously mentioned toughening mechanisms can account for the improvement in fracture toughness for nanoplatelet-filled polymer nanocomposites. On the other hand, it should be noted that the effectiveness of toughening based on the above mechanisms is limited. Many of the improvements in toughness observed in the literature are not by design but rather a consequence of a lack of full exfoliation of the nanoplatelets in the polymer matrix. Most of the polymer matrices contain numerous intercalated tactoids or even micron-scale nanofiller agglomerates. Consequently, ineffective toughening mechanisms, such as crack deflection, delamination, and microcracking, prevail in the so-called “nanocomposites”. Two questions now arise: (1) what is the fracture behavior of fully exfoliated polymer nanocomposites and (2) is full exfoliation a necessity to achieve best mechanical properties?

Kinloch and Taylor [73] showed an interesting comparison between micro- and nano-composites. At almost every level of filler concentration, epoxy/mica microcomposites possess a higher fracture toughness than those of their epoxy/clay

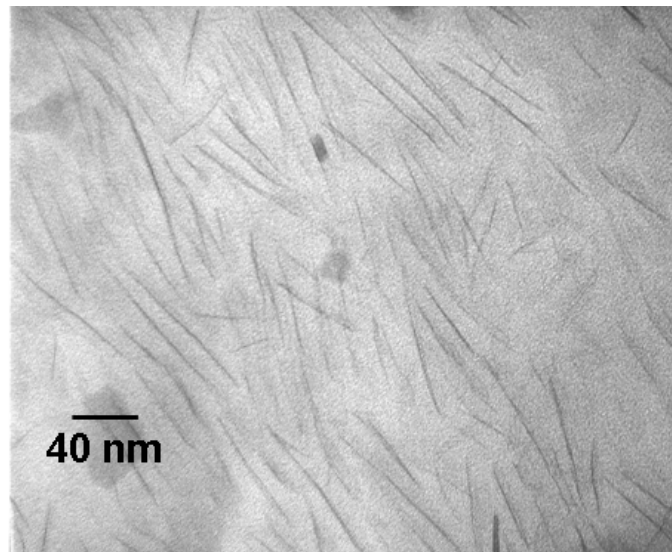
nanocomposites counterparts. Furthermore, the toughness value does not always increase with filler concentration. Instead, after a certain concentration level, addition of more fillers to the matrix will lower the fracture toughness.

Recently, Sue *et al.* [15,27] used α -ZrP as nanoplatelets to achieve a fully exfoliated epoxy nanocomposite, as shown in Fig. 2.9. The synthetic α -ZrP nanoplatelets have a much higher cation exchange capacity, are much purer than MMT clay, and the size distribution can be more tightly controlled. As a result, polymer nanocomposites containing fully exfoliated α -ZrP nanoplatelets can be easily prepared.

According to their findings, the fully exfoliated epoxy/ α -ZrP shows a slightly lower K_{IC} value than neat epoxy (Table 2.1). A similar result was also reported for fully exfoliated epoxy/clay and nylon/clay nanocomposites [79]. This suggests that a nearly perfect exfoliation and dispersion of nanofiller in the polymer matrix will not improve fracture toughness of the polymer matrix. It is believed that the intercalated or agglomerated domains can help trigger some limited degree of toughening that is unachievable in the fully exfoliated systems. It is possible that the exfoliated nanoplatelets effectively restrict large-scale molecular motions of the matrix, thus limiting the plastic deformation of the polymer matrix. Moreover, it is valuable to note that the nanoparticle dimensions are generally too small, compared with the natural crack tip radius of a typical polymer, to trigger effective toughening mechanisms such as crack bridging, crack deflection, and crack blunting.



(a)



(b)

Fig. 2.9. TEM micrographs of fully exfoliated epoxy/ α -ZrP nanocomposites (a) low and (b) high magnification. (reproduced from [27]).

Table 2.1. Modulus and fracture toughness of epoxy and epoxy/ α -ZrP nanocomposites (reproduced from [15])

	Neat epoxy	Epoxy/ α -ZrP	Epoxy/ α -ZrP/CSR
Modulus (GPa)	2.85±0.22	3.97±0.15	3.77±0.20
K_{IC} (MPa m ^{1/2})	0.76±0.05	0.70±0.04	1.64±0.04

More recently, Weon and Sue [40] studied how the aspect ratio and orientation of clay on the K_{IC} value of a commercially available fully exfoliated nylon 6/clay nanocomposite system (obtained from Ube Industries). Their study strongly supports the notion that, if the nanoplatelets are fully exfoliated in the polymer matrix, the K_{IC} value of the nanocomposites is nearly identical with the neat nylon matrix, irrespective of the variations in nanoplatelet orientation and aspect ratio (Table 2.2). In other words, if the nanoplatelets are about 100 nm in length and 1 nm in thickness, the composite system is unable to effectively promote microcracking, crack deflection, and crack blunting. The nanoplatelets do not appear to be able to serve as stress concentrators to promote the above toughening mechanisms. Actually, there is a consistent trend showing that a slight drop in fracture toughness is observed in fully exfoliated epoxy/clay [72], epoxy/ α -ZrP [15,27], and nylon/clay [80] nanocomposite systems.

Interestingly, when core-shell rubber (CSR) particles were used for toughening the epoxy/ α -ZrP nanocomposite, a two-fold increase in fracture toughness (K_{IC}) was observed (Table 2.1, [15]). This implies that the conventional route of using rubber

particles for toughening polymer nanocomposites can still be viable. As shown in Fig. 2.10, large-scale rubber particle cavitation and matrix shear banding are found to be responsible for such an impressive toughening effect.

Table 2.2. Fracture toughness of nylon-6 and nylon-6/clay nanocomposites (reproduced from [15])

	Neat Nylon-6	NC_Ref ^a	NC_A1 ^b	NC_C2 ^c
K_{IC} (MPa m ^{1/2})	3.0	2.7±0.07	3.1±0.13	3.0±0.11

^aNylon-6/clay nanocomposite, as received (aspect ratio = 132).

^bNylon-6/clay nanocomposite showing unidirectional orientation (aspect ratio = 87).

^cNylon-6/clay nanocomposite exhibiting random orientation (aspect ratio = 78).

In summary, well-exfoliated nanoplatelets in the polymer matrix will not give any improvements in fracture toughness without the incorporation of additional toughening phase (e.g., CSR or nanoplatelet aggregates). A slight reduction in fracture toughness and ductility of the matrix is normally observed [15,68,72,80]. Only in the presence of numerous micro- or nano-sized aggregates of nanoplatelets in the polymer matrix will the composite system show improvements in fracture toughness. Upon rubber toughening, the presence of nanoplatelets does not limit the ability of the rubber particles to cavitate and undergo large-scale plastic deformation around the crack tip (Fig. 2.10). As a result, both modulus and toughness can be gained upon simultaneous

additions of nanoplatelets and rubber toughener (Table 2.1). This finding suggests that nanoplatelets-containing polymer nanocomposites exhibit a great potential as materials for load-bearing structural applications.

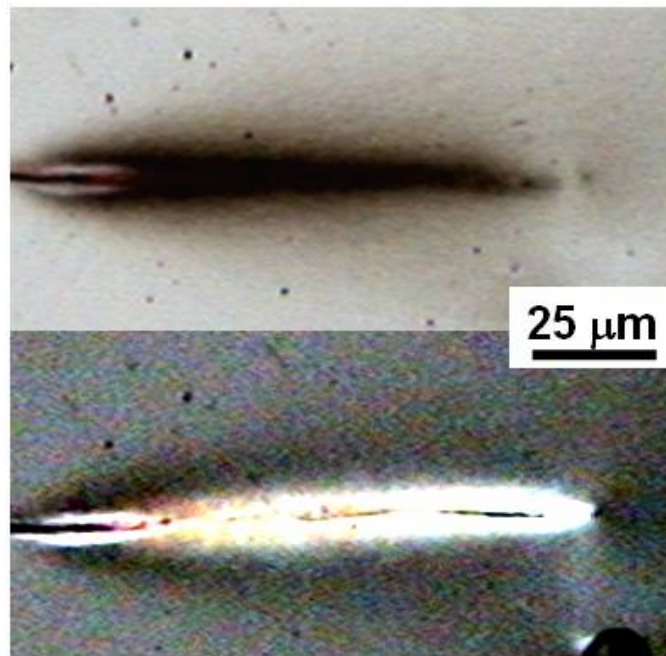


Fig. 2.10. OM of crack tip damage zone of epoxy/ α -ZrP/CSR nanocomposite. Bright field and cross-polarized light. (reproduced from [15]).

2.4. Concluding Remarks

This review has reviewed a number of key research advances in understanding toughening mechanisms observed in the literature for polymer nanocomposites reinforced by nanoplatelets. Several nanocomposite systems have been presented here, including MMT clay and α -ZrP reinforced polymer nanocomposites. The effectiveness

of nanoplatelet inorganic fillers on improving mechanical and physical properties of composites with polymer matrices strongly depends on the filler type, size, loading level, dispersion, and degree of exfoliation. Especially for the nanoplatelet reinforced polymer nanocomposites, the degree of exfoliation of the fillers is one of the most critical factors in determining the physical and mechanical properties of the composites as well as fracture behavior and toughening mechanisms. Yet, despite significant research efforts in the past two decades, the mechanisms by which the structural characteristics of nanofillers, especially when fillers are on the nanometer scale, influence the physical and mechanical properties of polymer matrices still remains inconclusive and demands further investigation.

CHAPTER III

EFFECTIVE INTERCALATION AND EXFOLIATION OF NANOPATELETS IN EPOXY VIA CREATION OF POROUS PATHWAYS

3. 1. Introduction

Since the original work on montmorillonite clay-modified nylon-6 nanocomposites was reported about two decades ago [23,24], research on inorganic layered compound-based polymer nanocomposites has attracted worldwide attention because they exhibit significantly improved physical and mechanical properties compared with conventional polymer composites [18,81]. In preparing polymer nanocomposites, no matter what layered compound is selected, intercalation and exfoliation have always been the two most critical steps for the preparation of polymer nanocomposites. Effective intercalation has been shown to be essential for the preparation of fully exfoliated polymer nanocomposites with greatly improved modulus and barrier properties [15,27,82,83].

Among a number of routes to prepare polymer nanocomposites developed in the past few years, the most traditional and probably also most popular approach is to intercalate the layered compounds in advance with an organophilic surface modifier, followed by intercalation of monomers or polymers into the layers to achieve final exfoliation [23,81,82,84,85].

To render hydrophilic nanoplatelet fillers to become miscible with polymer matrices, the hydrophilic nanoplatelet surfaces need to be converted to an organophilic ones so that they can be more compatible with monomers or polymer chains. Generally, this surface modification process can be achieved by ion-exchange reactions with cation-based intercalating agent, such as ammonium or phosphonium salts, to lower the surface energy of the inorganic nanoplatelets and improve the wetting with the polymer matrix. Also, by employing appropriate intercalating agent(s), functional groups on the nanoplatelet surfaces may be tailored to trigger *in-situ* polymerization of monomers for improved interfacial strength between the inorganic nanoplatelets and the polymer matrix [86,87].

When preparing intercalated layered compounds, most of the researchers emphasize the importance of interlayer distance to achieve exfoliation [77,83,88,89]. As a result, the larger the interlayer distance for the surface modified nanoplatelets, the easier the monomers or polymers can be introduced into the interlayer galleries to achieve full exfoliation. Typically, a larger interlayer distance leads to weaker inter-layer binding strength to allow for easier intercalation and exfoliation when external driving forces, such as mixing, shearing, ultrasonication, etc, are applied. Surprisingly, in some cases, the conformational freedom of the intercalating chains is more critical than a large interlayer distance to result in an improved intercalation and exfoliation [84,85,90]. The reason for such an unexpected outcome may lie in the fact that when the interlayer galleries are fully occupied by intercalating molecules, there is no room for monomers or

polymers to diffuse into the galleries. Thus, further intercalation and/or exfoliation cannot be easily realized.

To overcome the above undesirable outcome, the present study focuses on creating porous pathways in the interlayer galleries to facilitate effective intercalation of monomer or polymer chains. To demonstrate the importance of porous pathways for effective intercalation, a set of model intercalating agents containing long chain and short chain amines, and their combination, were selected to study the intercalation process in α -zirconium phosphate (α -ZrP) nanoplatelets. The utilization of α -ZrP for preparation of polymer nanocomposites has been shown to be ideal for fundamental study of structure-property relationship of polymer nanocomposites [28,91,92]. The usefulness of porous pathways for the intercalation process in epoxy was monitored using X-ray diffraction (XRD) and transmission electron microscopy (TEM). Approaches for achieving effective intercalation and exfoliation of polymer nanocomposites are also discussed.

3. 2. Experimental

3. 2. 1. Materials

The α -ZrP was synthesized by refluxing 10.0 grams of zirconium oxychloride octahydrate ($\text{ZrOCl}_2 \cdot 8\text{H}_2\text{O}$, 98%, Aldrich) in 100 mL 3.0 M phosphoric acid (Aldrich) at 100 °C for 24 hours. The detailed chemistry and procedures for the synthesis of α -ZrP can be found elsewhere [28,91,92]. Cyclohexylamine ($\text{C}_6\text{H}_{11}\text{NH}_2$, 99%, Aldrich), dodecylamine ($\text{CH}_3(\text{CH}_2)_{11}\text{NH}_2$, 99%, Aldrich), polyoxyalkyleneamine (Jeffamine[®]

M600, Huntsman Chemical), and tetra-*n*-butyl ammonium hydroxide (TBA, $(\text{CH}_3\text{CH}_2\text{CH}_2\text{CH}_2)_4\text{N}(\text{OH})$, Aldrich) were used as surface modifiers to intercalate α -ZrP layers. The epoxy monomer used in this study was diglycidyl ether of bisphenol-A (DGEBA) epoxy resin (DER332[®], The Dow Chemical Company). The curing agent utilized was 4,4'-diamino-diphenyl sulfone (DDS, Aldrich). All the chemicals were used as received.

3. 2. 2. Sample Preparation

All intercalation reactions were carried out at room temperature. Three sets of samples were prepared in round-bottom flasks. In each flask, 1.0 mmol of α -ZrP powder was mixed with 50 mL acetone and ultrasonicated (1510R, Branson, 70 W-42 kHz) for 30 minutes. Afterwards, the α -ZrP powder was well dispersed in acetone to facilitate intercalation reactions. Mixture of 1.0 mmol of cyclohexylamine and 1.0 mmol of dodecylamine were pre-dissolved in 50 mL acetone and added dropwise into α -ZrP dispersion (CD-ZrP) during which the reactants were vigorously stirred.

For comparison, the same amount of α -ZrP dispersion was intercalated separately by 2.0 mmol of cyclohexylamine and 2.0 mmol of dodecylamine, denoted as C-ZrP and D-ZrP, respectively, *via* the same procedure. After finishing the drop-by-drop mixing, each sample was ultrasonicated for 30 minutes. For clarity, the compositions of all the samples prepared for this study are given in Table 3.1.

To investigate the effect of interlayer distance of surface modified α -ZrP on diffusion, 20 mmol epoxy monomer was pre-dissolved in 50 mL of acetone and added

into amine-intercalated α -ZrP/acetone mixtures, followed by 30 minutes of stirring and 15 minutes of ultrasonication. XRD was performed on every step to monitor the changes on interlayer distance of α -ZrP during intercalation and subsequent diffusion of epoxy monomers.

Table 3.1. Compositions of surface modifiers utilized for intercalation of α -ZrP

	α -ZrP (mmol, dispersed in acetone)	cyclohexylamine (mmol, 0.02 M solution in acetone)	dodecylamine (mmol, 0.02 M solution in acetone)
C-ZrP	1	2	—
D-ZrP	1	—	2
CD-ZrP	1	1	1

3. 2. 3. Characterization

XRD analysis was performed on a Bruker D8 diffractometer with Bragg-Brentano θ — 2θ geometry (40 kV and 40 mA). For the α -ZrP powder sample, it was gently packed on a sample holder. The diffraction pattern was obtained for 2θ in the range from 1° to 60° with a step size of 0.04° and a count time of 1 s per step. For the intercalated α -ZrP samples, they were cast as a thin film on a clean silicon wafer and dried overnight at room temperature prior to XRD characterization. Their diffraction

patterns were obtained for 2θ in the range from 1° to 15° with a step size of 0.04° and a count time of 2 s per step.

Scanning electron microscopy (SEM) images were acquired using a Zeiss Leo 1530 VP Field Emission-SEM (FE-SEM). The samples were sputter-coated with a thin layer (ca. 3 nm) of Pt/Pd (80/20) prior to SEM imaging.

For TEM observation, the thin-section samples were prepared by microtoming (Ultracut E) to prepare thin sections (~ 80 nm thickness) and deposited on carbon coated Cu grids. Sample grids were examined on a JEOL 1200 EX electron microscope operated at an accelerating voltage of 100 kV.

3.3. Results and Discussion

Fig. 3.1 shows the XRD pattern of the α -ZrP sample synthesized, which has an interlayer distance of 7.6 \AA . The relatively broad peaks in the XRD pattern indicate that the crystallinity of α -ZrP is relatively low. But the corresponding SEM image (Fig. 3.2) clearly shows that sheet structures with lateral dimensions of 80-100 nm have been formed. It has been confirmed by previous studies [15,27,28] that α -ZrP with relatively low crystallinity is actually beneficial for the intercalation process. The low crystallinity α -ZrP can be easily intercalated by a series of polyoxyalkyleneamines (Jeffamines[®], Huntsman) to an interlayer distance to about 70 \AA , which is over 10 times of its original interlayer distance [28].

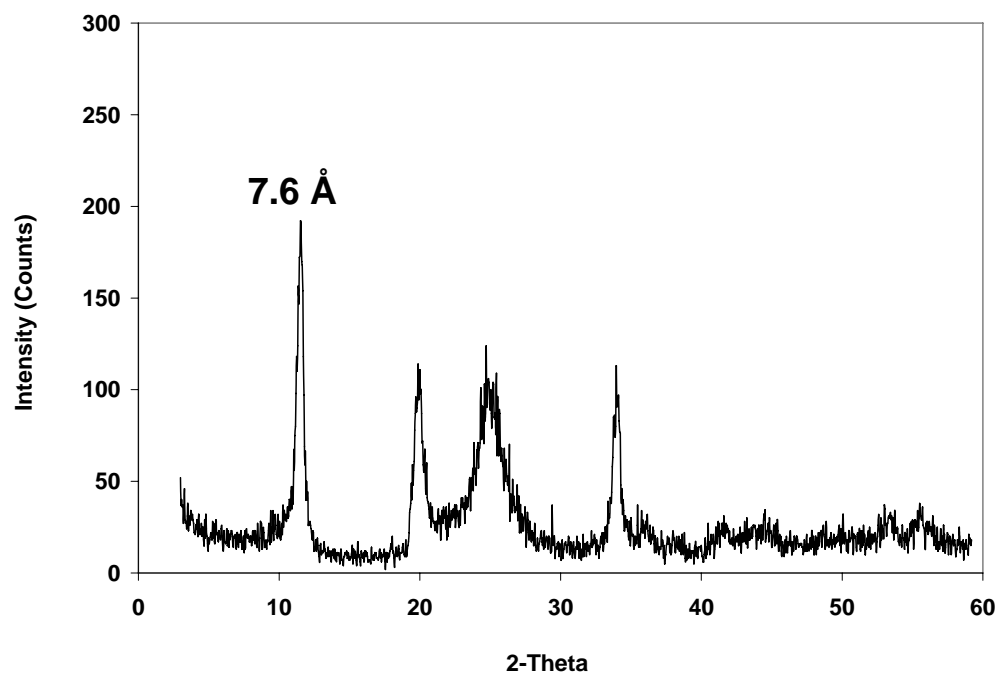


Fig. 3.1. XRD of α -ZrP.

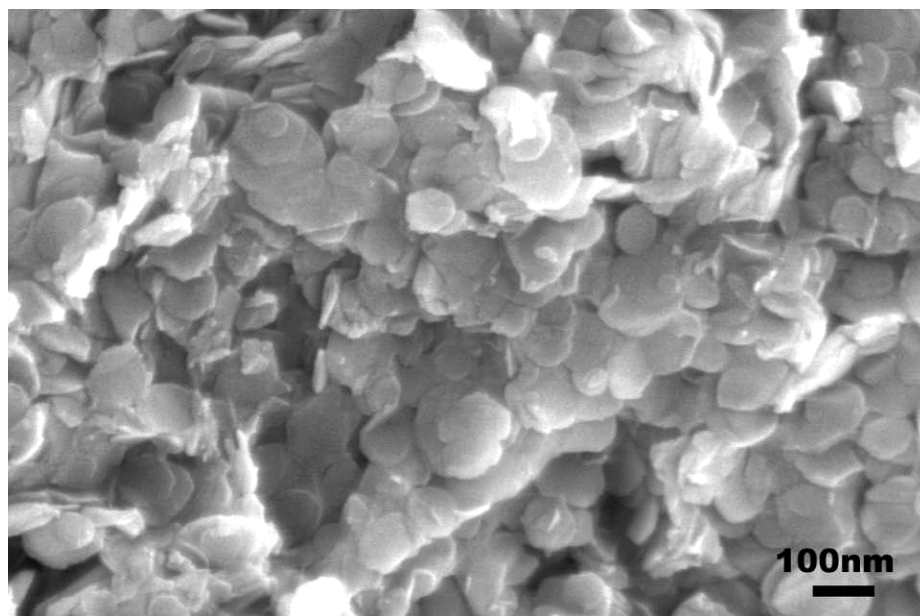


Fig.3.2. SEM of α -ZrP.

The XRD patterns of intercalated α -ZrP are shown in Fig. 3.3. XRD patterns (1) and (2) in Fig. 3.3 show the intercalated d -spacing of 18 Å and 36 Å for C-ZrP and D-ZrP, respectively. These interlayer distances correspond to the static state molecular sizes of cyclohexylamine and dodecylamine at room temperature [28,93]. XRD pattern (3) in Fig. 3.3 shows a d -spacing of 28 Å for CD-ZrP, which has been intercalated by a mixture with equal amount of cyclohexylamine and dodecylamine. It is noted that this d -spacing is in between 18Å and 36Å, which is expected. Generally, when certain aliphatic amine is used to intercalate layered compounds at a maximum stoichiometric ratio, the

linear molecule chains tend to pack tightly with each other and form a highly ordered structure [28,93].

However, by adding cyclohexylamine molecules as a co-intercalating agent with an aliphatic amine, it can prevent tight packing of intercalating molecules inside the galleries. As a result, a decreased d -spacing is observed. Compared with the XRD patterns of C-ZrP and D-ZrP, the peaks in CD-ZrP are broader. This indicates that the structure of CD-ZrP intercalated compound is less ordered and less uniform compared with those of C-ZrP and D-ZrP.

After addition of epoxy monomers into samples C-ZrP, D-ZrP, and CD-ZrP with stirring and followed by ultrasonication, XRD patterns were recorded and shown as (1-E), (2-E) and (3-E) in Fig. 3.3, respectively. Compared with XRD patterns (1) and (2), it is noted that no appreciable change in d -spacing occurred in (1-E) and (2-E) after the addition of epoxy monomers. However, (3-E) clearly shows an expanded d -spacing from 28 Å to 33 Å.

To assist the description of the observed intercalation process, schematic illustrations of the intercalation mechanisms and d -spacing are presented in Fig. 3.4. In both Case (a) and Case (b), the interlayer spacing is fully occupied by cyclohexylamine and dodecylamine, respectively. Although an increased interlayer distance is achieved, there is little room for possible further intercalation. Therefore, there is little change in d -spacing after the addition of epoxy monomer as shown in (1-E) and (2-E) in Fig. 3.3. In Case (c), even though the d -spacing is smaller than Cases (b), a mixture of a linear chain and a bulky chain will inevitably create porous pathways inside the galleries to facilitate

fast diffusion of epoxy monomer into the gallery. The difference in size and structure of the two types of amine molecules creates porous pathways to accommodate the epoxy monomer diffusion.

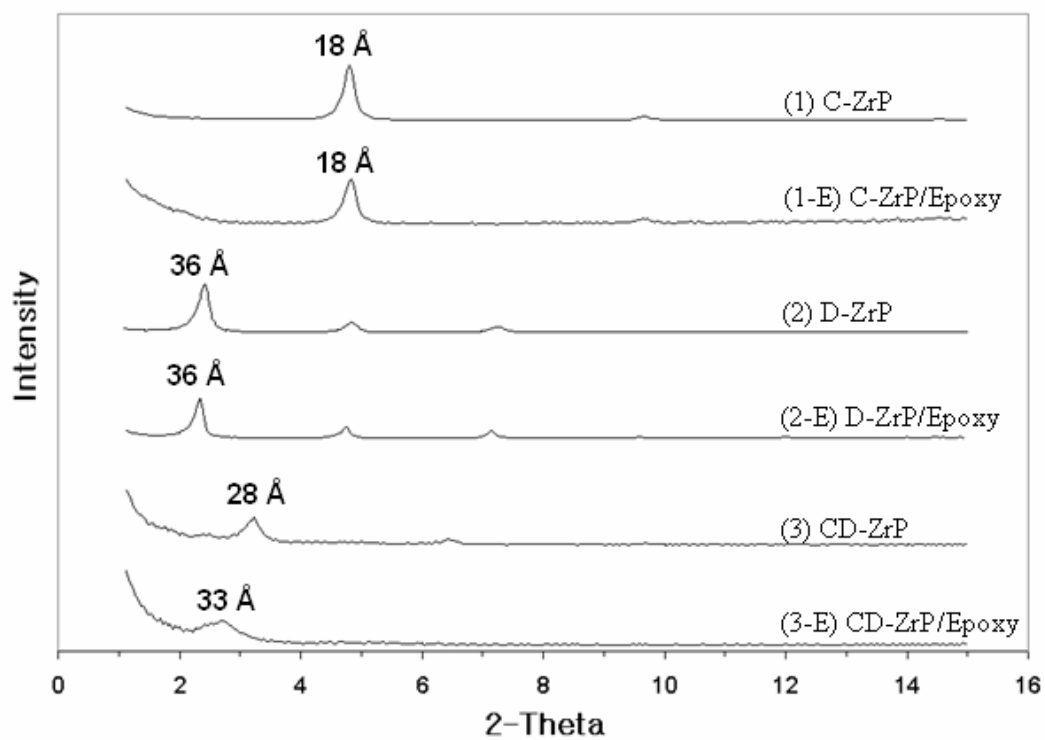
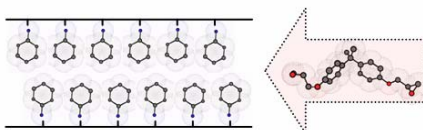


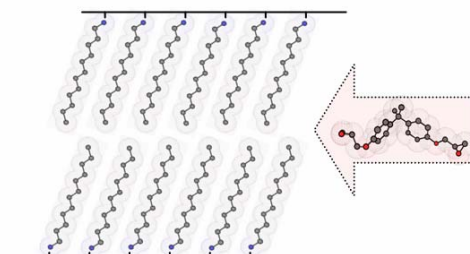
Fig. 3.3. XRD of intercalated α -ZrP and epoxy/ α -ZrP nanocomposites.

Consequently, the d -spacing between intercalated layers is expanded by the diffusion of epoxy monomer into α -ZrP interlayer galleries, as illustrated in Fig. 3.4(c) and supported by XRD pattern (3-E) in Fig. 3.3. To be noted, after further intercalation of epoxy monomer, the peak in XRD pattern (3-E) becomes much broader and less intense. The widening of the peak is because of the loosening of the layered structure. The lowered intensity is probably due to the delamination of a portion of α -ZrP nanoplatelets, which result in exfoliation. Even though the layered structure in case (3-E) of Fig. 3.3 is still not completely exfoliated, the strategy of creating porous pathways clearly shows an advantage over the conventional intercalation approach where only one intercalating agent is used.

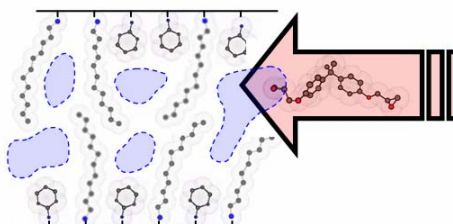


(a)

Fig. 3.4. Schematic illustrations of interlayer spacings of α -ZrP treated with different organic modifiers: (a) cyclohexylamine, (b) dodecylamine, and (c) an equal mixture of cyclohexylamine and dodecylamine.



(b)



(c)

Fig. 3.4. Continued.

The above favorable intercalation phenomenon has been well explained and supported by the work of Vaia *et al.* [84,85] and Pinnavaia *et al.* [38,90]. Vaia *et al.* employed the concept of internal energy and entropic factors associated with intermolecular interactions to show the importance of conformational freedom of intercalating molecular chains for effective intercalation and exfoliation. Pinnavaia *et al.* reported that low charge density nanoplatelets are desirable to achieve nanocomposites with a high degree of layer exfoliation due to the low areal density of onium ion and prepolymer in the intergallery region. The porous pathway concept follows the preferences for intercalation and exfoliation described above. The porous pathways can be created by many choices of combination of intercalating agents, depending on the polymer matrices involved and the size and interfacial characteristics desired.

Another significant side benefit of the porous pathway approach, in addition to the high level of exfoliation is its fast intercalation and exfoliation rate. In all the samples prepared, all reach their maximum intercalation and exfoliation state within 30 min. This finding is consistent with the work of Ginzburz *et al.*, [94,95] who uses a “kink model” to explain the fast intercalation rate due to the increased intergallery spacing created by the kinking of nanoplatelets. The fast intercalation and exfoliation rate phenomenon can also be supported by the free energy concept described by Vaia *et al.* [84].

Because of the aforementioned porous pathway concept, a mixture of TBA and polyoxyalkyleneamines (Jeffamines[®] M600) were utilized as intercalating agents to maximize the sizes of the porous pathways for intercalation and exfoliation of α -ZrP

nanoplatelets (TM-ZrP) in epoxy before curing. The molecular size differences between TBA and M600 are much more than those of cyclohexylamine and dodecylamine [96,97], leading to extremely effective intercalation and exfoliation in epoxy.

Fig. 3.5 presents the XRD patterns of (a) pristine α -ZrP, (b) intercalated TM-ZrP, and (c) exfoliated TM-ZrP after the addition of epoxy monomers. The XRD pattern of TM-ZrP shows an increase in basal spacing from 7.6Å (pristine α -ZrP) to 33Å, which is between the d-spacing values of α -ZrP intercalated with only TBA or M600 [28,98], meaning that the disruption of molecular packing took place and porous pathways, which is favorable for the diffusion of epoxy monomers, have been created. The XRD of epoxy/TM-ZrP indicates that exfoliation of α -ZrP have been achieved through the diffusion of epoxy monomer into the intercalated TM-ZrP galleries. It should be noted that the broad hump at 18° in 2 θ corresponds to the amorphous halo of epoxy resin.

To confirm the high degree of exfoliation of α -ZrP nanoplatelets in epoxy matrix, TEM investigations were performed after curing of epoxy/TM-ZrP with DDS curing agent. Fig. 3.6 displays TEM images showing exfoliated and well-dispersed TM-ZrP nanoplatelets (2.0 vol%) in epoxy with no sign of aggregation or intercalated nanoplatelets.

To obtain the benefit of polymer nanocomposites, it is required that high degrees of exfoliation of nanoplatelets be achieved. In this study, a new approach to facilitate effective diffusion of monomers, and possibly polymer chains, into the intergalleries of nanoplatelets is presented. In addition to the previously proposed intercalating approaches proposed by others [38,84,90,93], the porous pathway approach reported in

this study can be an effective alternative to achieve the preparation of exfoliated polymer nanocomposites.

This present study also gives insights toward the intercalation/exfoliation mechanisms of nanoplatelets in polymer nanocomposites. It is evident that, in addition to the functionalities of the intercalating agents which affect the thermodynamic state, a kinetic pathway has to be created to facilitate a realistic preparation of exfoliated nanoplatelets in a polymer matrix.

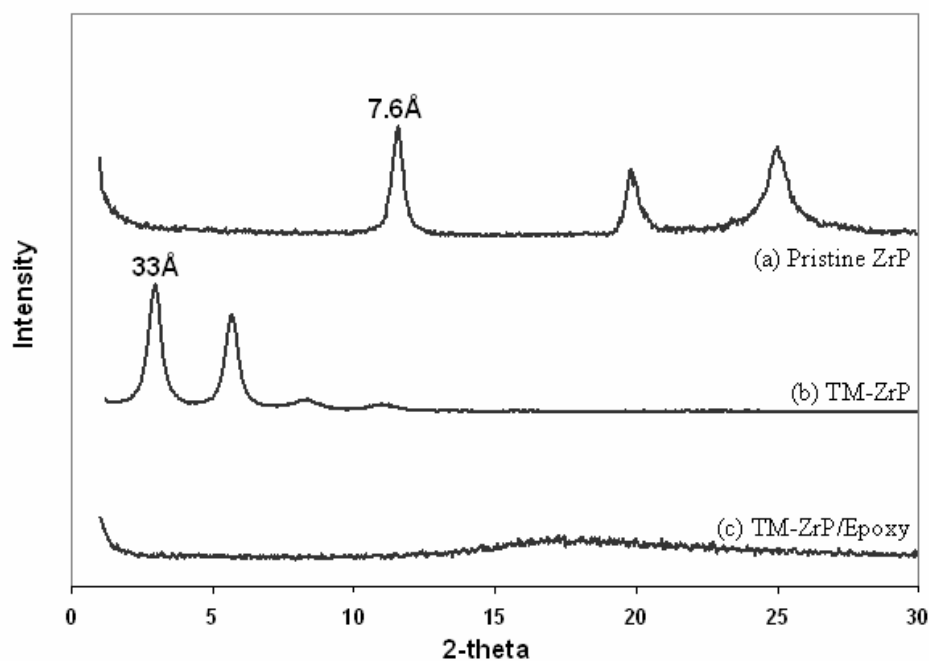


Fig. 3.5. XRD of α -ZrP intercalated and exfoliated with a mixture of tetra-n-butyl ammonium hydroxide and Jeffamine M600.

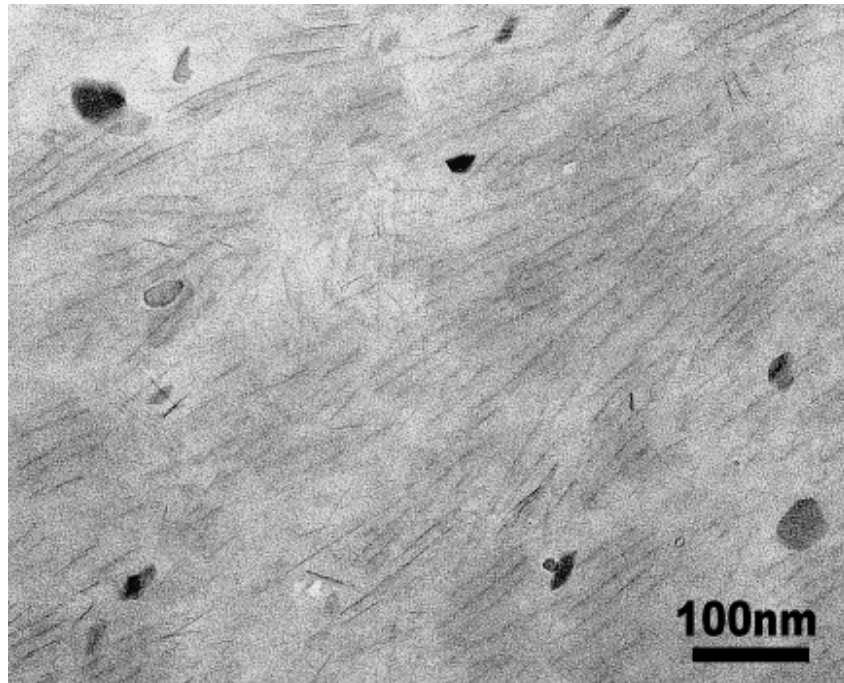


Fig. 3.6. TEM of highly exfoliated α -ZrP nanoplatelets (2.0vol%) in epoxy.

3.4. Summary

A simple and effective approach to achieve intercalation/exfoliation of nanoplatelets in polymer matrices by using a mixture of intercalating agents with different sizes is introduced. The results show that the intercalation *via* creation of porous pathways using two different sizes of intercalating agents is an effective way to achieve effective intercalation and subsequent exfoliation. The approach allows for effective intercalation and exfoliation of nanoplatelets for practical manufacturing of polymer nanocomposites.

CHAPTER IV

MORPHOLOGY AND MECHANICAL BEHAVIOR OF EXFOLIATED EPOXY/ α -ZIRCONIUM PHOSPHATE NANOCOMPOSITES*

4. 1. Introduction

Polymer nanocomposites containing layered silicates have been studied extensively as a new generation of advanced composites that exhibit greatly improved stiffness and strength [18,21], enhanced gas barrier properties [17,25], and flame retardancy [26]. Among the layered nanofillers, montmorillonite (MMT) clay is one of the most widely used nanofiller for preparing polymer nanocomposites due to its advantages in high ion exchange capacity, high aspect ratio, and low cost [6,16,17,19,21,61,63,99]. However, the main drawbacks of MMT clay are its wide particle size distribution and difficulty in achieving full exfoliation in polymer matrices. As a result, only limited success is achieved in establishing fundamental structure-property relationship of MMT clay-based polymer nanocomposite systems.

The effectiveness of nanoplatelet fillers on improving physical and mechanical properties of polymer nanocomposites strongly depends on the filler type, size, loading level, dispersion, and degree of exfoliation, etc. In particular, for nanoplatelet-reinforced

* Reprinted with permission from “Morphology and mechanical behavior of exfoliated epoxy/ α -zirconium phosphate nanocomposites” by W.-J. Boo *et al.*, 2007. *Composites Science and Technology*, 67, 262-269. ©2006 by Elsevier Ltd.

polymer nanocomposites, the degree of exfoliation of the nanofiller in the polymer matrix is critical for physical and mechanical property enhancements.

In recent years, extensive research efforts have been focused on fracture behavior of polymer nanocomposites. Some researchers have reported that nanoplatelets can help improve fracture toughness of the polymer matrix *via* crack deflection, delamination, and crack tip blunting [68,69]. However, aggregation of nanoplatelets in their polymer matrices is evident. The observed toughening mechanisms appear to be strongly related to the presence of the aggregated nanoplatelets. In the case of an exfoliated polymer nanocomposite system, it is still uncertain whether or not crack deflection or crack tip blunting can take place to lead to a higher fracture toughness value. It is also uncertain if debonding of the individual nanoplatelet from the polymer matrix can take place. It is critical that the above questions be answered for optimal mechanical performance of polymer nanocomposites.

Stemming from the above concerns, synthetic α -zirconium phosphate (ZrP), $\text{Zr}(\text{HPO}_4)_2 \cdot \text{H}_2\text{O}$, has been chosen as a model nanofiller to study the fundamental structure-property relationship of exfoliated polymer nanocomposites [15,27,28]. The ZrP has a higher ion exchange capacity than MMT clay; hence, it is relatively easy to achieve a higher degree of exfoliation for ZrP nanoplatelets [28]. Moreover, the particle size and aspect ratio can be controlled by varying reactant concentration, temperature, and reaction time [29]. As a result, ZrP is ideal for studying the fundamental structure-property relationship of polymer nanocomposites.

In this study, the morphology of epoxy/ZrP nanocomposites with a high level of exfoliation is studied using TEM. A simple geometric model describing an idealized relationship between interlayer d-spacing and filler loading level is presented to correlate with our experimental findings. The detailed fracture mechanisms of an exfoliated nanoplatelet-reinforced epoxy nanocomposite are reported and discussed. The influence of nanoplatelet loading level on physical and mechanical properties is also addressed.

4. 2. Experimental

4. 2. 1. Materials

The epoxy monomer used in this study, which has a narrow monomer molecular weight distribution (172-176 g/mol), is diglycidyl ether of bisphenol-A (DGEBA) epoxy resin (D.E.R.TM 332 epoxy resin (The Dow Chemical Company)). The curing agent is 4,4'-diamino-diphenyl sulfone (DDS, Aldrich).

The ZrP nanoplatelets were synthesized by refluxing zirconium oxychloride octahydrate ($\text{ZrOCl}_2 \cdot 8\text{H}_2\text{O}$, 98% Aldrich) in phosphoric acid (Aldrich). The detailed chemistry and procedures for the synthesis of ZrP can be found elsewhere [29,91,100]. Monoamine surface modifier, Jeffamine M600 (Huntsman Chemical), was used as the intercalating agent for ZrP. All chemicals were used as received.

4. 2. 2. Preparation of α -ZrP-Based Epoxy Nanocomposites

The interlayer spacing of ZrP crystal prior to surface treatment is 7.6Å. The addition of amine-based surface modifier at 0.75:1 molar ratio through dropwise mixing

at room temperature expands the interlayer spacing of ZrP to 34 Å (i.e., S-ZrP). The intercalated ZrP was mixed with epoxy monomer (epoxy/S-ZrP) to achieve a finally inorganic ZrP loading of 1 and 2 vol% in epoxy, respectively. After removal of solvent with a Rotarvapor® in a water bath at about 70°C, DDS was added at stoichiometric ratio. The resin mixture was cast in a preheated glass mold and cured in an oven at 180°C for 2 hrs, followed by 2 hrs of post-cure at 220°C.

For comparison purposes, a neat epoxy plaque (Neat Epoxy), an epoxy plaque with only surface modifier addition (S-epoxy), and an epoxy panel with 1 and 2 vol% of ZrP without surface treatment (epoxy/ZrP) were also prepared (Table 4.1).

Table 4.1. Compositions of model systems investigated (vol %)

Materials	α -zirconium phosphate	Surfactants
Neat epoxy (DGEBA/DDS)	none	none
S-epoxy	none	3.5
Epoxy/ZrP	1.0	none
Epoxy/S-ZrP (1vol%)	1.0	3.5
Epoxy/S-ZrP (2vol%)	2.0	7.0

4. 2. 3. Morphology Characterization

X-ray diffraction (XRD) analysis was performed on a Bruker D8 diffractometer with Bragg-Brentano θ - 2θ geometry (40kV and 40mA). Diffraction patterns were obtained for 2θ in the range from 2° to 30° with a step size of 0.04° and a count time of 2s per step. Transmission electron microscopy (TEM) was performed using a JEOL 1200EX, operated at 100keV. The detailed sample preparation procedures for XRD and TEM can be found elsewhere [27].

4. 2. 4. Mechanical/Physical Property Characterization

A series of tensile tests were performed, based on ASTM D638-98, using a Sintech-2 screw-driven mechanical testing machine at a crosshead speed of 5.08 mm/min (0.2 in/min) at ambient temperature. To report modulus, yield stress, and elongation at break, average values were taken from at least five specimens per sample type. Dynamic mechanical analysis (DMA) was conducted using RSA-III (TA Instrument) at a fixed frequency of 1 Hz and with increasing temperature 5°C per step, ranging from -150 to 250°C . A sinusoidal strain-amplitude of 0.05% was chosen for the analysis. The maximum point on the $\tan \delta$ curve was chosen as the glass transition temperature (T_g) of the sample.

4. 2. 5. Fracture Toughness and Toughening Mechanism Investigation

Fracture toughness measurements were performed based on the linear elastic fracture mechanics (LEFM) approach. The single-edge-notch 3-point-bending (SEN-

3PB) test, based on ASTM D5045-96, was used to obtain the mode-I critical stress intensity factor (K_{IC}) of the neat epoxy and epoxy/ZrP nanocomposite systems. Care was taken to ensure that the initial crack, generated by one tapping with a fresh razor blade, exhibited a thumbnail shape crack front prior to testing. At least five specimens were used to determine K_{IC} of the samples.

The double-notch four-point-bend (DN-4PB) test [101] was employed to investigate the detailed fracture behavior of the epoxy nanocomposites. Detailed methods of sample preparation and testing can be found elsewhere [15,72]. The DN-4PB tests were carried out at room temperature. The arrested crack tip damage zone was isolated, trimmed, and thin-sectioned for TEM observation.

4. 3. Results and Discussion

4. 3. 1. Morphology

Fig. 4.1 presents the XRD patterns of pristine ZrP, S-ZrP, exfoliated S-ZrP in epoxy monomer, and cured epoxy/S-ZrP nanocomposite with 2 vol% of ZrP. In the case of the pristine α -ZrP, the powder pattern shows a peak at 7.6\AA for the interlayer distance of the (002) plane (Fig. 4.1a). The XRD pattern of S-ZrP shows an increase in basal spacing to 34\AA and no pristine α -ZrP peaks are observed (Fig. 4.1b). The XRD of S-ZrP in epoxy monomer indicates that, even before the curing, signs of exfoliation have been achieved on the S-ZrP layered structure through the diffusion of epoxy monomer into the ZrP galleries (Fig. 4.1c). In the case of cured epoxy/S-ZrP nanocomposite, the XRD pattern only exhibits a broad hump at 18° in 2θ , which corresponds to the structure of

the amorphous epoxy matrix (Fig. 4.1d). In the case of the 1vol% epoxy/S-ZrP system, the XRD is exactly the same as the 2vol% system. As a result, they are omitted.

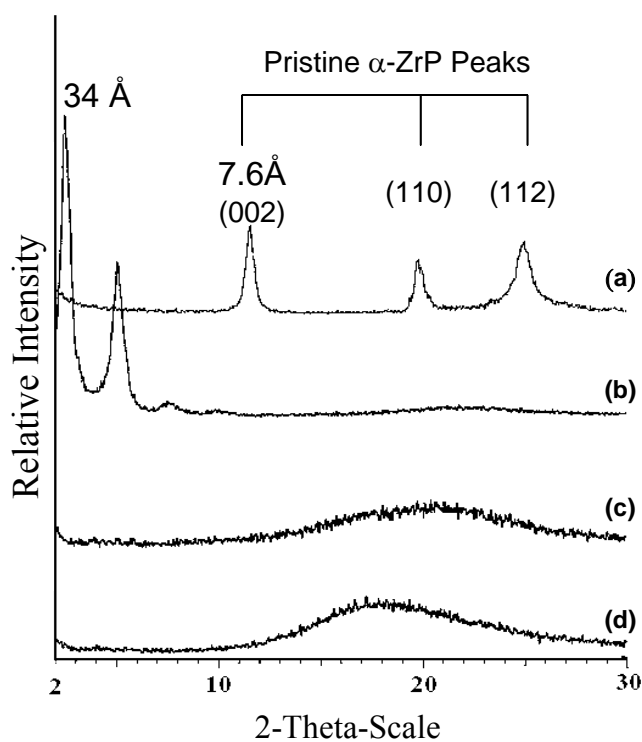


Fig. 4.1. XRD patterns of (a) pristine α -ZrP powder (d-spacing: 7.6Å), (b) S-ZrP in solvent (d-spacing: 34Å), (c) S-ZrP mixed with epoxy monomer, and (d) Cured Epoxy/S-ZrP nanocomposite (2 vol%).

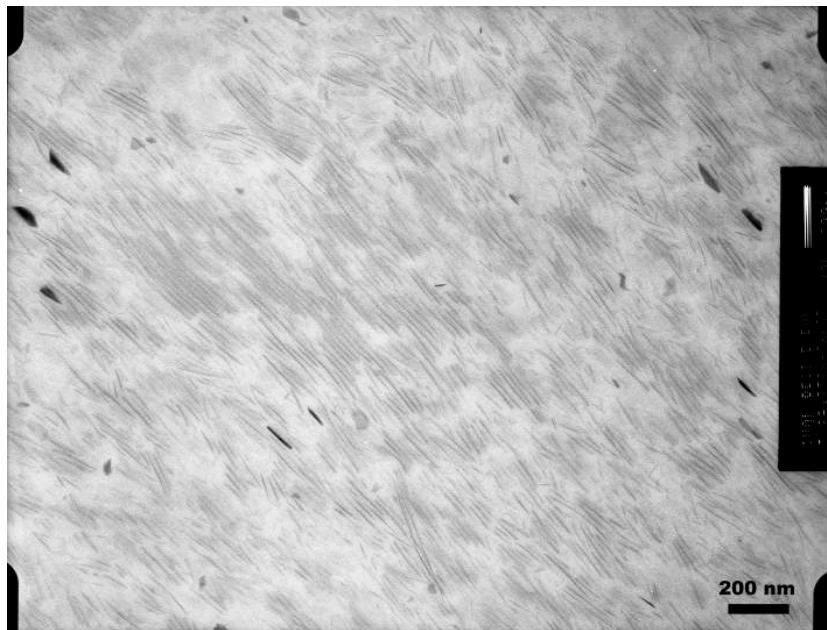
To confirm the high degree of exfoliation and an overall dispersion of S-ZrP layers in the epoxy matrix, additional optical microscopy (OM), scanning electron microscopy (SEM), and TEM investigations were performed. In this report, only TEM images are presented since no signs of S-ZrP aggregation were detected in the epoxy matrix at OM and SEM length scales. Fig. 4.2 displays TEM images showing highly exfoliated and well-dispersed S-ZrP nanoplatelets (2 vol%) in epoxy.

It is interesting to note that the ZrP nanoplatelets in epoxy show signs of strong orientation. As explained by Sue *et al.* [27], the orientation of ZrP nanoplatelets is mainly due to the “excluded volume” effect of the neighboring nanoplatelets. Based on this argument, a lower volume fraction of ZrP in epoxy should lead to random orientation of ZrP nanoplatelets in epoxy. Indeed, as shown in Fig. 4.2(c), the morphology of 1 vol% of Epoxy/S-ZrP nanocomposite shows random orientation of ZrP nanoplatelets. It is also interesting to note that, as shown in Fig. 4.2c, the population of ZrP oriented parallel to the thin-section direction, i.e., the surface of the micrograph, appears to be higher than that of the 2 vol% scenario. The nanoplatelets that are oriented parallel to the thin section direction are encircled by the dotted-lines as shown in Fig. 4.2c.

4. 3. 2. A Simple Geometric Model

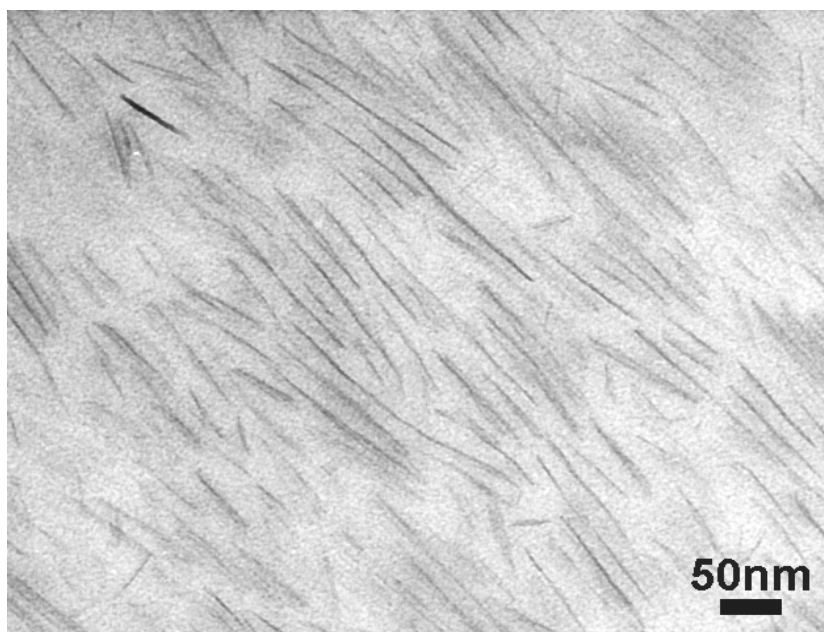
A simple geometric model is utilized here to gain an insight into the expected spacing between nanoplatelets in an exfoliated polymer nanocomposite. To make the analysis simple, the following assumptions are made: (1) the layered compound is

completely exfoliated into individual nanoplatelets, (2) all of the exfoliated sheets are rectangular and have identical size and shape, (3) all the sheets are uniformly distributed in the polymer matrix and oriented in the same direction, and (4) the distances between the sheets are equal. For clarity, the simple model is depicted in Fig. 4.3.

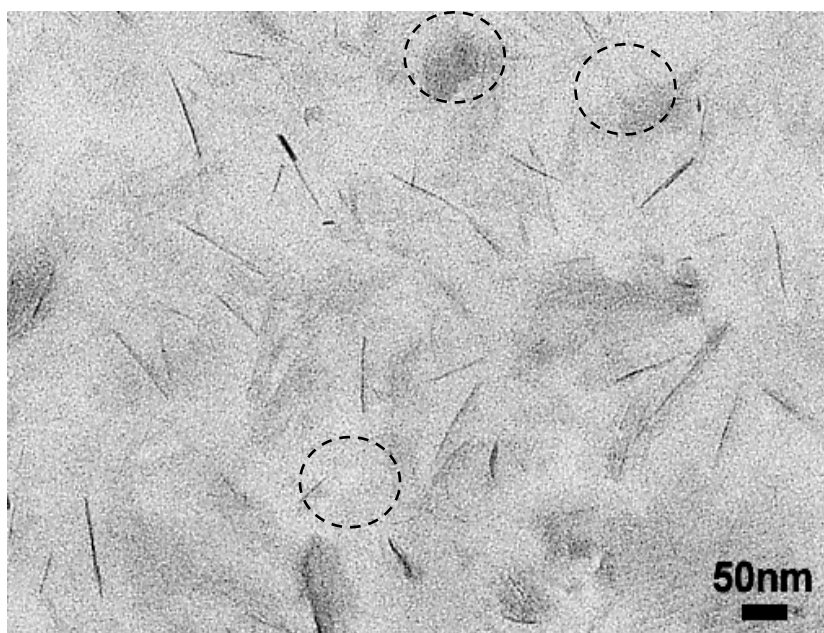


(a)

Fig. 4.2. TEM images of Epoxy/S-ZrP nanocomposites showing a high degree of exfoliation of nanoplatelets in epoxy matrix. The nanocomposite with 2 vol% of ZrP is shown in (a) low magnification and (b) high magnification. The nanocomposite with 1 vol% of ZrP is shown in (c).



(b)



(c)

Fig. 4.2. Continued.

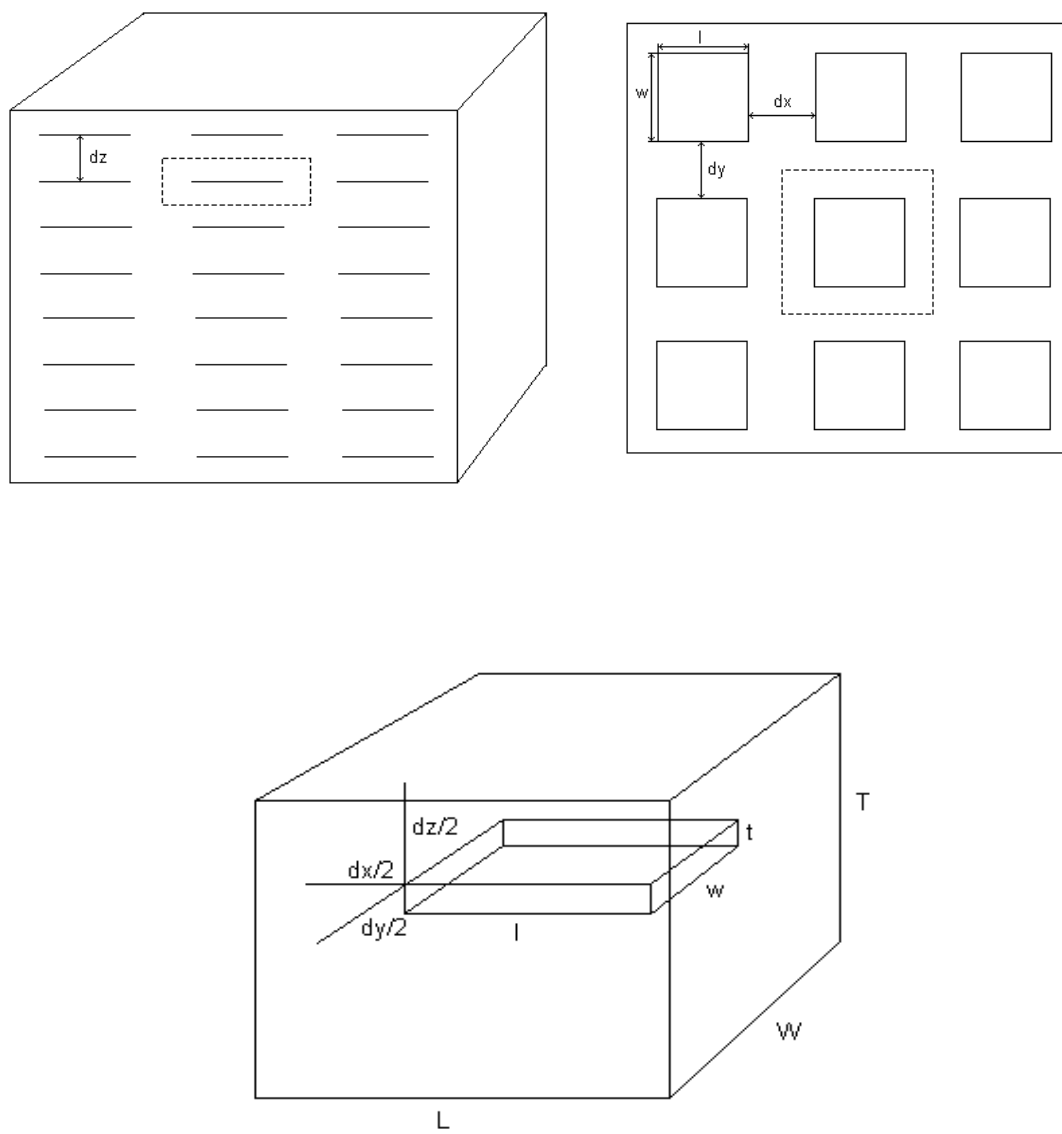


Fig. 4.3. Uniformly and orderly distributed nanoplatelets in polymer matrix.

According to Fig. 4.3, the volume fraction of nanoplatelets is

$$(lwt / LWT) \times 100 = vol\% \quad (4.1)$$

Thus,
$$\frac{lwt}{(l + d_x)(w + d_y)(t + d_z)} \times 100 = vol\% \quad (4.2)$$

$$\left(1 + \frac{d_x}{l}\right)\left(1 + \frac{d_y}{w}\right)\left(1 + \frac{d_z}{t}\right) = \frac{100}{vol\%} \quad (4.3)$$

By further assuming that $d_x/l = d_y/w$, the interlayer d-spacing can be calculated as shown in Table 4.2. In this study, the thickness of a single α -ZrP nanoplatelet is estimated to be 0.68 nm [98]. In cases where doublets of nanoplatelets are formed throughout the polymer nanocomposite, and there is not any intercalation in between the doublet layer, the thickness of the doublet becomes approximately 1.44 nm. The distance between the uniformly dispersed doublet layers can also be calculated and are shown in Table 4.2. Also, it is worth noting that the estimated values from the above simple geometric model are in good agreement with the experimental results and modeling reported by Chin *et al.* [102].

In Fig. 4.2b, the TEM image shows d_x/l and d_y/w are about 0.2 and the interlayer d-spacing is approximately 30 nm, which is consistent with the single-layer case calculated from the above simple model (Table 4.2). The above results, in turn, indicate that the ZrP nanoplatelets have been exfoliated in epoxy matrix.

Table 4.2. The Interlayer Distances of Nanoplatelets in Polymer Nanocomposites

vol%	Distance between layers (nm)					
	$dx/l=dy/w=0.1$		$dx/l=dy/w=0.2$		$dx/l=dy/w=0.3$	
	single-layer	double-layer	single-layer	double-layer	single-layer	double-layer
1	55.5	117.6	46.5	98.6	39.6	83.8
2	27.4	58.1	22.9	48.6	19.4	41.2
3	18.1	38.2	15.1	31.9	12.7	27.0

4.3.3. Mechanical Property

The tensile stress-strain curves of neat epoxy and epoxy nanocomposite systems are shown in Fig. 4.4. The incorporation of 1 and 2 vol% of S-ZrP nanoplatelets into epoxy matrix improves the tensile modulus by 20 and 52%, respectively. With an addition of monoamine surface modifier to neat epoxy, the tensile modulus, yield stress, and elongation at break are decreased by about 10%, 60%, and 70%, respectively. This reduction in tensile properties is likely due to the participation of curing reaction of monoamine surface modifier with the DGEBA epoxy. The addition of 1 vol% unmodified ZrP, which exhibits aggregated platelet structure, to neat epoxy only leads to a mere 3% improvement in modulus.

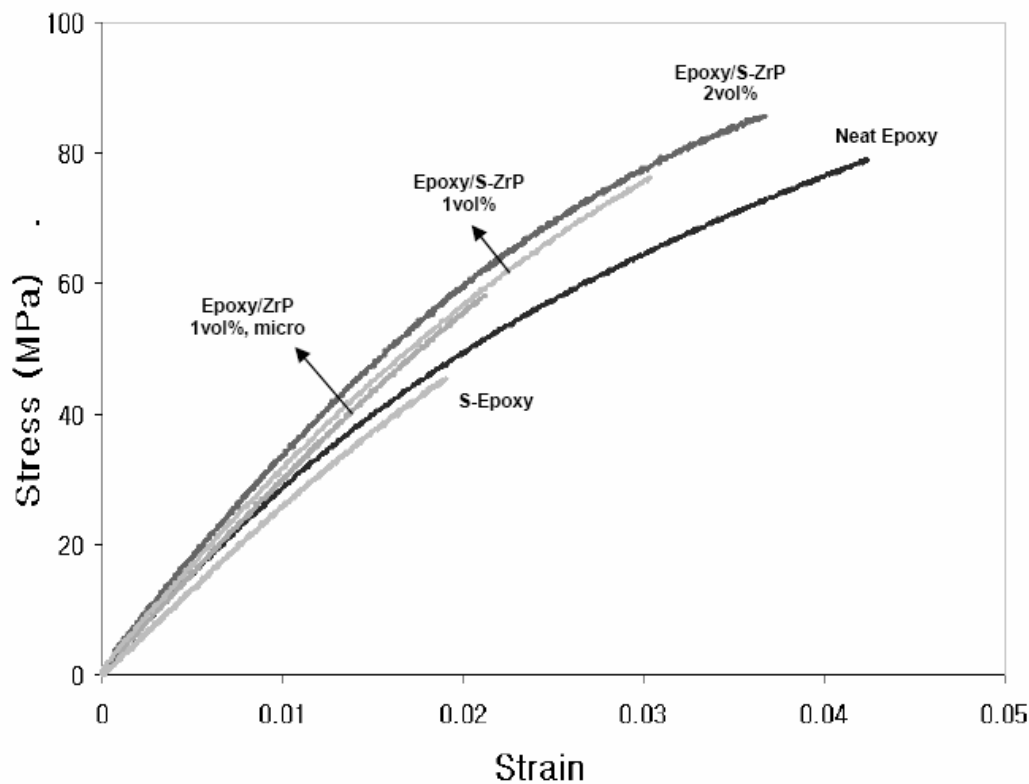


Fig. 4.4. Tensile behavior of α -ZrP based DGEBA/DDS epoxy systems.

Fig. 4.5 shows DMA spectra of Neat Epoxy, S-Epoxy, and Epoxy/S-ZrP (2 vol%). The T_g of Epoxy/S-ZrP (2 vol%) is found to be 155°C, which is 50°C lower than the T_g of Neat Epoxy (214°C). This T_g drop is attributed to the unintended reaction of monoamine surface modifier with the epoxy monomers [27,38]. For comparison purposes, S-Epoxy was also determined and the T_g is found to be 135°C.

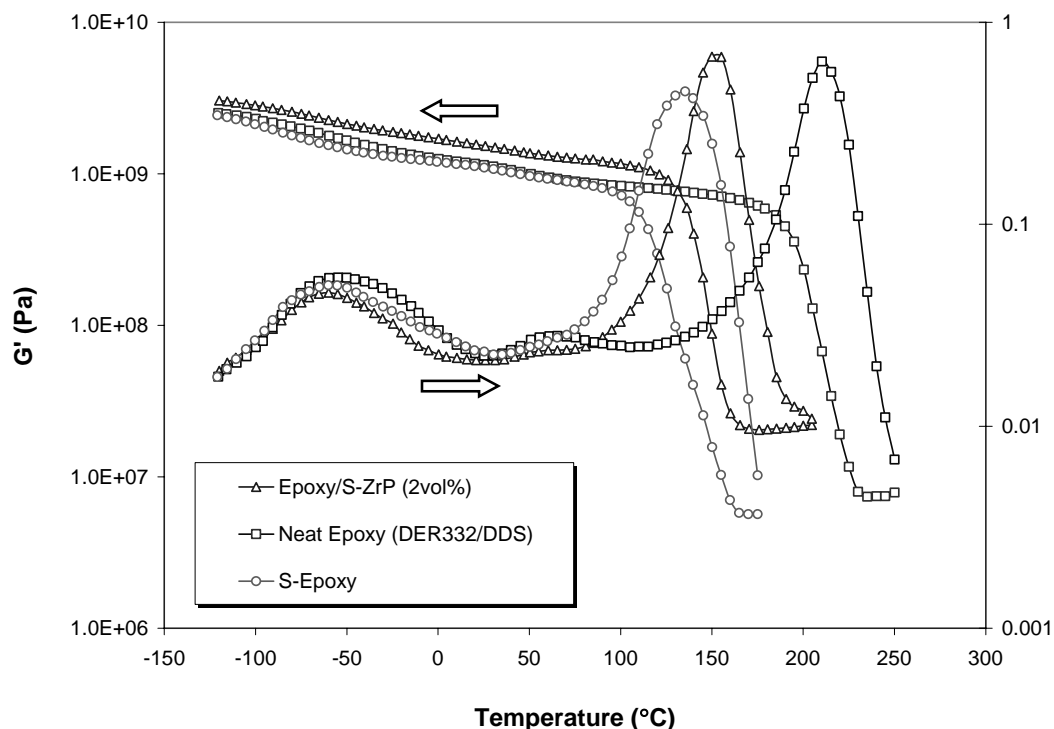


Fig. 4.5. DMA of neat epoxy, S-epoxy, and epoxy/S-ZrP nanocomposite systems.

The addition of 2 vol% of surface-modified ZrP to the epoxy matrix (Epoxy/S-ZrP), compared to the case of S-epoxy, have led to the changes of the following properties: (1) the T_g is increased from 135°C to 155°C; (2) the storage modulus is increased much more at temperatures above T_g , but the increase is reduced significantly as the temperature drops below T_g ; and (3) the magnitude of mechanical damping is suppressed. According to Sue *et al.* [15], the above changes are probably due to the combined effects of (1) the reduced amount of free monoamine to react with epoxy monomers during curing, (2) a decreased amount of relative molecular chain mobility,

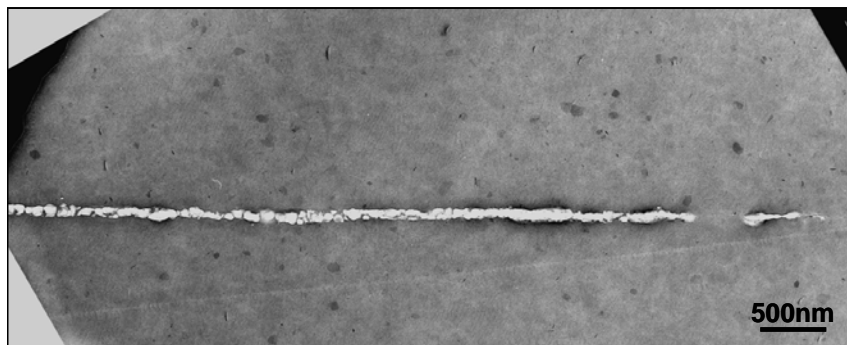
especially at temperatures above T_g , and (3) hindered molecular mobility leading to increased modulus.

4. 3. 4. Fracture Behavior Study

The Mode-I fracture toughness (K_{IC}) values of neat epoxy and epoxy nanocomposite systems (1 and 2 vol%) have been measured. However, there is no noticeable difference in K_{IC} between the neat epoxy and epoxy/ZrP nanocomposites having 1 and 2 vol% of nanofiller loadings. This result is consistent with our earlier study on both clay-filled and ZrP-reinforced epoxy nanocomposites systems [72,103]. Furthermore, it is noted that the ductility of the exfoliated epoxy nanocomposite is at least as good as that of the S-Epoxy or the neat epoxy, which suggests that the presence of the exfoliated nanoplatelets is unlikely to act as defects or stress concentrators during tensile loading and fracture.

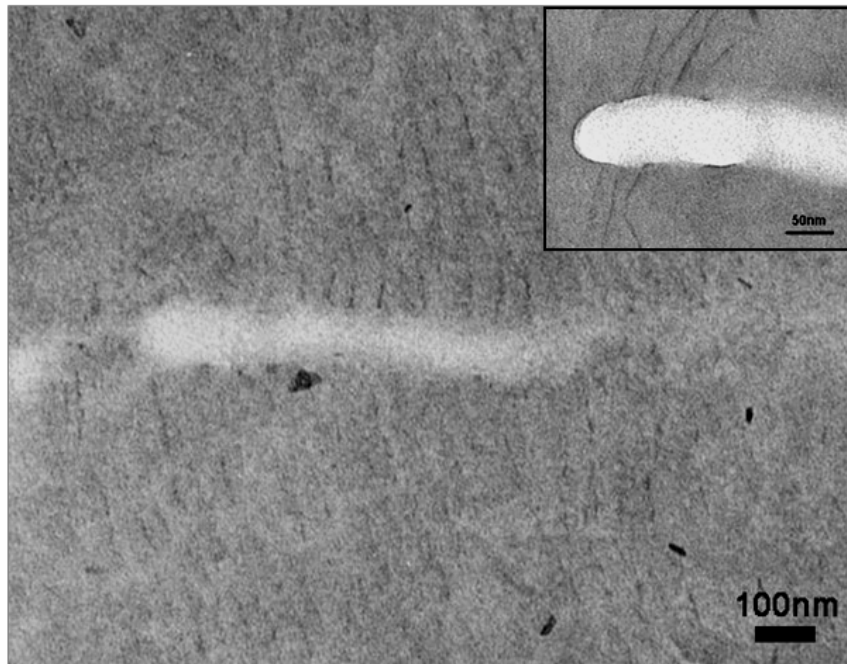
To investigate the fracture mechanisms in epoxy nanocomposites, it is critical that a subcritical crack growth damage zone be preserved upon fracture. By employing the DN-4PB technique, a survived subcritical crack tip damage zone can be successfully attained. In this study, an attempt is made to determine how the individually exfoliated nanoplatelets affect the fracture process. As shown in Fig. 4.6a, when the nanoplatelets are individually exfoliated, the subcritically propagated crack would grow in a straight manner. No signs of delamination or crack deflection can be found. Since the ZrP nanoplatelets are exfoliated in this case, each individual layer exhibits excellent bonding to the matrix and is well dispersed at the nanometer scale.

As a result, as compared to the size scale of the crack tip radius which is at the sub-micrometer scale, the crack is not able to “sense” any inhomogeneity in epoxy matrix. In other words, an exfoliated epoxy nanocomposite would exhibit a property like a one-phase homogeneous polymer, not a two-phase polymer. As a result, the crack propagates in a straight fashion.



(a)

Fig. 4.6. TEM images of DN-4PB damage zone of epoxy/S-ZrP nanocomposite (2 vol%) showing a straight crack, as shown in (a). In (b), the crack tip region is shown. The crack propagates from left to right.



(b)

Fig. 4.6. Continued.

If the ZrP nanoplatelets were either agglomerated or intercalated, the crack tip blunting and crack deflection mechanisms might take place due to the relatively weak van der Waals forces between aggregated ZrP layers [68,69,72,103]. Moreover, it is worth noting that the nanoplatelet dimensions are too small to trigger effective toughening mechanisms, such as crack bridging, crack deflection, and crack blunting. This claim is also in good agreement with that of Kinloch *et al.* [73]. As a result, the crack would propagate in a straight fashion. The above argument is supported by the fact

that ZrP nanoplatelets were fractured in the mid-plane upon crack propagation, as shown in Fig. 4.6b. Furthermore, the K_{IC} value of the nanocomposite remains the same as that of the neat epoxy. No improvement in fracture toughness of exfoliated nanocomposites is expected.

Based on the above findings, one would ask if the aspect ratio of the nanoplatelets becomes high and one of the dimensions is larger than the crack tip radius or when the interfacial adhesion between the matrix and the nanoplatelets is weakened, would it be possible for crack deflection and crack blunting mechanisms to occur. In other words, can the fracture toughness of an exfoliated nanocomposite be increased, in addition to a greatly improved modulus? To answer the above question, our future work will focus on preparing epoxy/ZrP nanocomposites with ZrP aspect ratio to be greater than 1,000. It is hoped that more fundamental knowledge regarding structure-property relationship in polymer nanocomposites can be gained.

4.4. Summary

A high degree of exfoliation of ZrP nanolayers in an epoxy matrix was achieved and the morphology of epoxy/ZrP nanocomposites investigated. The exfoliated epoxy/S-ZrP nanocomposite with 2 vol% of ZrP exhibits an ordered orientation due to geometric confinement of the surrounding ZrP nanoplatelets. This phenomenon is not observed in the nanocomposite with only 1 vol% of ZrP loading. The interlayer d-spacing of 2 vol% of ZrP layers in epoxy matrix observed in TEM is in good agreement with that

calculated from a simple geometric model. An addition of a small amount of rigid nanoplatelets into epoxy matrices can significantly improve tensile modulus of epoxy.

Upon fracture, the crack propagates in a straight manner in the exfoliated epoxy nanocomposite because the exfoliated nanoplatelets do not lead to significant crack tip blunting and/or crack deflection. Consequently, the fracture toughness of the exfoliated epoxy nanocomposite remains the same as that of the neat epoxy system.

CHAPTER V

EFFECTS OF NANOPATELET DISPERSION ON MECHANICAL BEHAVIOR OF POLYMER NANOCOMPOSITES

5. 1. Introduction

Polymer nanocomposites containing well-dispersed inorganic nanoplatelets, which have at least one dimension in the nanometer range, have been extensively studied [37,39,41,44-46,50,68,77,104-108]. Among the various nanoplatelets considered for polymer reinforcement, such as montmorillonite (MMT), hectorite, saponite, graphite, etc., MMT clay is the most popular choice for preparing polymer nanocomposites because of its relatively high ion exchange capacity, high aspect ratio, and economic advantages [17-21]. Unfortunately, MMT clay usually contains impurities and has a wide particle size distribution. As a result, it is unlikely that MMT clay based polymer nanocomposites can exhibit consistent properties for unambiguous fundamental structure-property relationship studies.

Compared with MMT clay, synthetic α -zirconium phosphate (α -ZrP), $\text{Zr}(\text{HPO}_4)_2 \cdot \text{H}_2\text{O}$, that exhibits similar structural characteristics as natural MMT clay is ideal for fundamental structure-property relationship study of polymer nanocomposites. The advantages of α -ZrP as a model system over MMT clay include a much higher purity and ion exchange capacity, ease of particle size, aspect ratio, and surface functionality control, and ease of intercalation and exfoliation [29,91,100]. Owing to the above

advantages of α -ZrP nanoplatelets, we have successfully achieved the preparation of epoxy nanocomposites reinforced with fully exfoliated α -ZrP nanoplatelets [15,27] and launched a series of fundamental studies to reveal the physics behind the reinforcement effects of fully exfoliated nanoplatelets on the physical and mechanical properties of nanoplatelet-reinforced polymer nanocomposites [109].

As has been well agreed [110], polymer nanocomposites can be categorized into two distinctive dispersion states: intercalated and exfoliated states (Fig. 5.1). The state of dispersion of nanoplatelets in polymer nanocomposites is expected to be crucial in affecting the mechanical properties of polymer nanocomposites. A systematic study to determine how important the state of nanoplatelets dispersion and its influences on mechanical properties of polymer nanocomposites is needed.

Furthermore, it has been well-recognized that technical difficulties and the cost involved for achieving full exfoliation of clay in some polymer matrices may be insurmountable. Thus, it would be of great interest to learn (1) whether or not it is ideal to obtain full exfoliation of nanoplatelets in a polymer matrix for best performance, (2) to what extent a certain degree of intercalation or nano-aggregation in the polymer nanocomposite will compromise its mechanical properties, and (3) how the fracture toughness is affected by the nanoplatelet dispersion of the nanocomposites. To answer the above questions, systematic investigation of a set of model epoxy nanocomposite systems having variations in levels of nanoplatelets dispersion needs to be carried out.

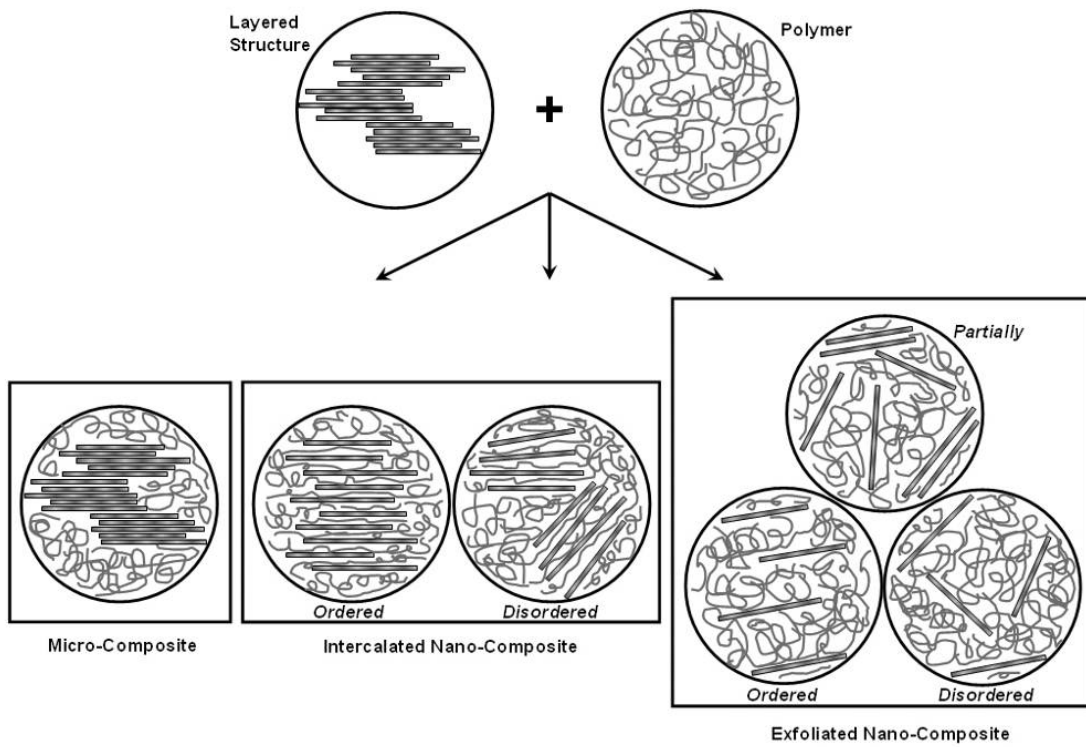


Fig. 5.1. Schematic of categories of microcomposites and nanocomposites.

To find out how the nanoplatelet dispersion influences the properties of polymer nanocomposites, significant research efforts have been carried out in recent years [62,111-115]. For instance, Wang *et al.* [62], developed elastomeric polymer-layered magadiite nanocomposites by *in-situ* polymerization. To obtain intercalated or exfoliated tactoids of Na⁺ magadiite layers, they used primary, secondary, tertiary, and quaternary onium ions as intercalating agents. Depending on the nature of the onium ions, several levels of intercalation/exfoliation of magadiite layers was achieved. Another example is to study moisture barrier and thermomechanical properties of organoclay-epoxy nanocomposites. Kim *et al.* [111] selected three different types of clays, including a quaternary alkylamine-modified montmorillonite, a quaternary ammonium-modified montmorillonite, and an octadecylamine-modified montmorillonite as nanofillers. In all cases, exfoliated silicate nanolayers were found to be more effective than intercalated or aggregated assemblies of nanolayers in optimizing mechanical properties.

Unfortunately, the above approaches employed the use of different intercalating agents to achieve different levels of nanoplatelet dispersion. Consequently, uncertainties regarding how the intercalating agents affect the polymer matrix properties as well as interfacial characteristics are introduced. Alternative approaches have to be considered to unambiguously investigate how the nanoplatelets dispersion influences the mechanical properties of polymer nanocomposites.

In this study, three distinctive levels of dispersion of α -ZrP nanoplatelets have been achieved by altering processing conditions *alone*. In this fashion, the chemical composition of the nanocomposites with the three levels of exfoliation is kept the same.

Thus, the effect of nanoplatelet dispersion on mechanical properties can be unambiguously addressed. The three distinctive levels of dispersion of α -ZrP nanoplatelets in epoxy matrix are qualitatively confirmed by transmission electron microscopy (TEM) and wide angle X-ray diffraction (WAXD). The corresponding tensile and fracture behaviors of the epoxy/ α -ZrP nanocomposites are investigated. The differences in the operative fracture mechanisms of the model nanocomposites are also described and discussed.

5. 2. Experimental

5. 2. 1. Materials

The α -ZrP was synthesized by refluxing zirconyl chloride octahydrate ($\text{ZrOCl}_2 \cdot 8\text{H}_2\text{O}$, 98%, Aldrich) in 3 M phosphoric acid for 24 hrs. Detailed chemistry and procedures for the synthesis of α -ZrP can be found elsewhere [29,91,100]. A commercial monoamine, polyoxyalkyleneamine (Jeffamine[®] M600, Huntsman Chemical), was used as an intercalating agent for α -ZrP. The epoxy matrix is composed of diglycidyl ether of bisphenol-A (DGEBA) epoxy resin (D.E.R.[™] 332 epoxy resin, The Dow Chemical Company), with an epoxy equivalent weight of 171-175 g/mol, and the curing agent, 4,4'-diamino-diphenyl sulfone (DDS, Aldrich). All the chemicals, except the epoxy resin which was dried in a vacuum oven for 24 hrs prior to curing, were used as received.

5. 2. 2. Preparation of Epoxy/ α -ZrP Nanocomposites

Without any surface treatment, the interlayer spacing of pristine α -ZrP crystal is 7.6Å. After the addition of monoamine (0.75 to 1 ratio to α -ZrP) intercalating agent at room temperature, the interlayer spacing of α -ZrP expands to 38 Å.

To control the degree of exfoliation of α -ZrP in epoxy, the rate of intercalating agent addition and ultrasonication time were altered systematically during the intercalation process to achieve various levels of α -ZrP dispersion in the epoxy. The detailed procedures for achieving the intercalation and exfoliation of α -ZrP in epoxy are summarized in Fig. 5.2. Three distinctive levels of α -ZrP exfoliation were achieved. In Fig. 5.2, samples (a), (b), (c) and (a'), (b'), (c') were separately prepared to show reproducibility. After the complete removal of solvent by using Rotarvapor[®] in a water bath at about 90°C, the curing agent (DDS) was added at a stoichiometric ratio and followed by further degassing and mixing at 140°C in an oil bath. The degassed resin mixture was cast in a preheated glass mold and cured in an oven at 180°C for 2 hrs, followed by 2 hrs of post-cure at 220°C. In all cases, two net volume percentage loading of inorganic α -ZrP with an addition of the same amount of intercalating agent was prepared for all epoxy nanocomposite systems.

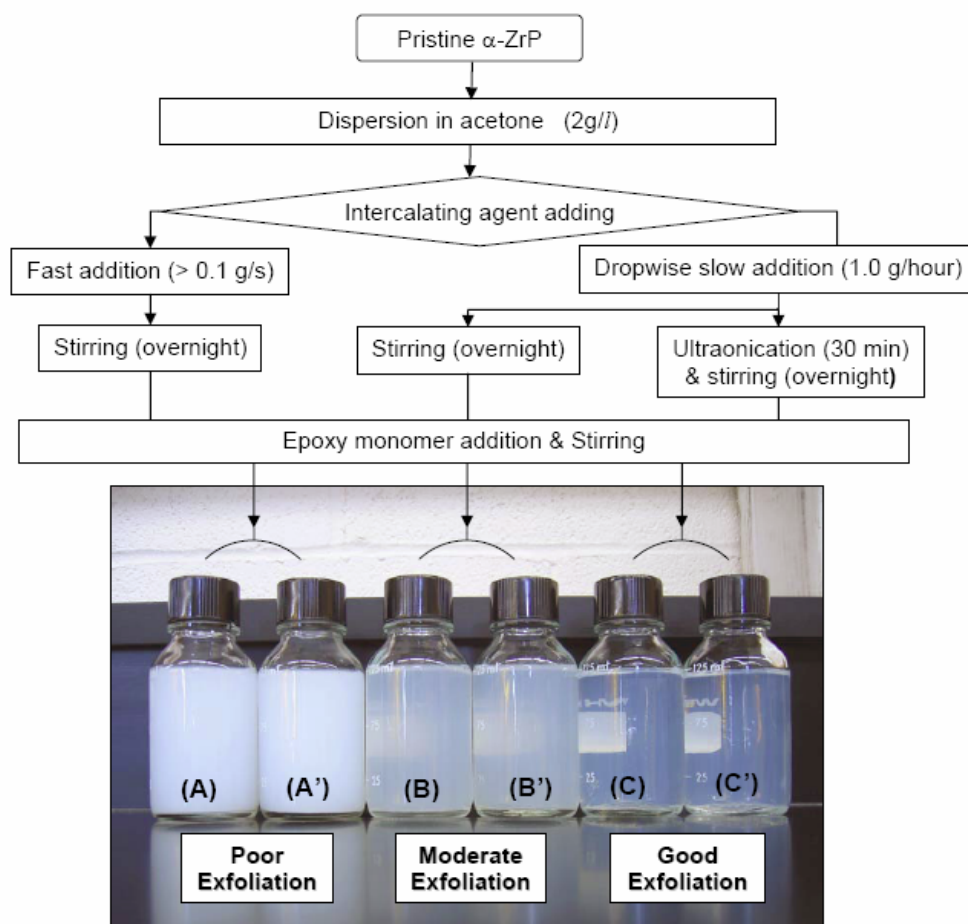


Fig. 5.2. Sample preparation procedures to control the degree of exfoliation of α -ZrP in epoxy.

5. 2. 3. Morphology Characterization

WAXD analysis was performed on a Bruker D8 diffractometer with Bragg-Brentano θ – 2θ geometry at a set operating voltage and current of 40 kV and 40 mA, respectively. Diffraction patterns were obtained for 2θ in the range from 2° to 30° with a step size of 0.04° and a count time of 2 seconds per step. For TEM observation, the thin-section samples were prepared by microtoming (Ultracut E) and the thin sections ($\sim 100\text{nm}$ thickness) deposited on carbon coated Cu grids. Sample grids were examined on a JEOL 1200 EX electron microscope operated at an accelerating voltage of 100 keV. TEM micrographs were taken using a calibrated Kodak[®] electron microscope film.

5. 2. 4. Mechanical Property Characterization

Tensile properties of epoxy/ α -ZrP nanocomposites were obtained following the ASTM D638-98 method. The tensile tests were performed using an MTS[®] servo-hydraulic test machine at a crosshead speed of 5.08 mm/min at ambient temperature. Young's modulus, tensile strength, and elongation at break of each sample were obtained based on at least five specimens per sample and the average values and standard deviations were reported.

Dynamic mechanical analysis (DMA) was performed on an RSA III (TA Instruments), ranging from -150 to 250°C at a fixed frequency of 1 Hz and a temperature increase at 5°C per step with a 3-point bending mode. A sinusoidal strain-amplitude of 0.05% was chosen for the analysis. The maximum point on the $\tan \delta$ curve was chosen as the glass transition temperature (T_g) of the samples.

5. 2. 5. *Fracture Behavior*

Fracture toughness tests were conducted based on the linear elastic fracture mechanics (LEFM) approach. The single-edge-notch 3-point-bending (SEN-3PB) test, based on ASTM D5045-96, was performed to obtain the mode-I critical stress intensity factor (K_{IC}) of the neat epoxy and epoxy/ α -ZrP nanocomposites. Care was taken to ensure that the initial sharp crack, generated by tapping with a fresh razor blade, exhibited a thumbnail shape crack front prior to testing. At least five specimens per sample were tested to determine K_{IC} values of the samples.

The double-notch four-point-bend (DN-4PB) test [101,116] was carried out to probe the detailed fracture mechanisms in the epoxy nanocomposites with variation in levels of nanoplatelet dispersion. Detailed methods of sample preparation and testing can be found elsewhere [101,116]. The DN-4PB tests were performed at room temperature. The arrested sub-critical crack tip damage zone was isolated, trimmed, and thin-sectioned for TEM observation.

5. 3. **Results and Discussion**

With rare exceptions [15,24,27,117], most of the literature results do not show consistent, full exfoliation of nanoplatelets in a polymer matrix. In cases where the effects of exfoliation state on mechanical properties are being studied, the intercalating agents have been altered to achieve different levels of nanoplatelets dispersion.²¹⁻²⁶ As a result, uncertainties still persist regarding fundamental structure-property relationship of polymer nanocomposites. It remains unclear if a full exfoliation of nanoplatelets in a

polymer matrix is essential to realize the benefits of polymer nanocomposites. It is also unclear if nanoplatelets can be utilized both as a toughening agent and a reinforcement filler to improve modulus, strength, and toughness of polymer matrices.

The significance of this study lies in that three distinctive levels of exfoliation of α -ZrP nanoplatelets in epoxy matrix has been successfully achieved by simply altering the process conditions. No structural or compositional changes were made. As a result, the present study can unambiguously reveal how the nanoplatelet dispersion can affect tensile and fracture behaviors of polymer nanocomposites.

5. 3. 1. Morphology

Fig. 5.3 presents the WAXD patterns of (a) pristine α -ZrP powder, (b) monoamine-modified α -ZrP (d-spacing 38Å), and (c) fully exfoliated epoxy/ α -ZrP nanocomposite after curing (from sample C in Fig. 5.2). In the case of the pristine α -ZrP powder (Fig. 5.3(a)), the WAXD pattern shows a peak for (002) plane of α -ZrP at about 11.7° of 2θ , corresponding to 7.6 Å for the distance between the pristine α -ZrP layers. The WAXD pattern of the intercalated α -ZrP (Fig. 5.3(b)) shows an increase in the interlayer spacing to 38Å after intercalation. The disappearance of the peaks of pristine α -ZrP suggests that a homogeneous and complete intercalation has been achieved. Finally, the WAXD pattern of the exfoliated α -ZrP/epoxy nanocomposite presents the evidence of a high degree of exfoliation of the surface-modified α -ZrP nanoplatelets in epoxy matrix

(Fig. 5.3(c)). The WAXD pattern in Fig. 5.3(c) only exhibits a broad hump at around 18° in 2θ , which corresponds to the amorphous epoxy structure [15,27].

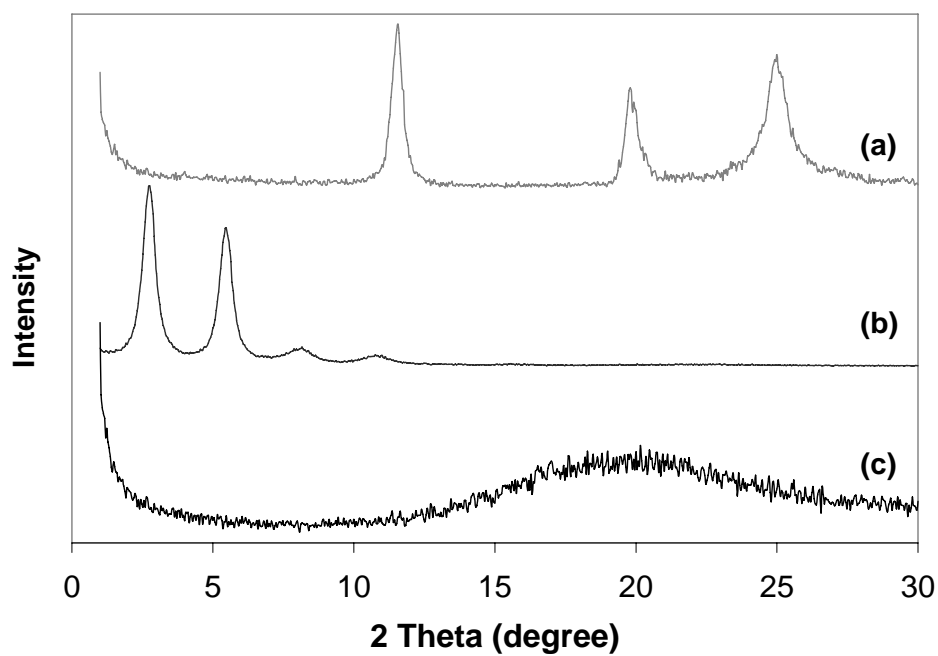


Fig. 5.3. XRD patterns of (a) pristine α -ZrP powder (d-spacing 7.6\AA), (b) Surface modified α -ZrP in solvent (d-spacing 38\AA), (c) Exfoliated epoxy/ α -ZrP nanocomposite after curing.

Fig. 5.4 shows the WAXD patterns of epoxy/ α -ZrP nanocomposites with three different levels of exfoliation. All three WAXD patterns show an amorphous epoxy hump at around 18° of 2θ . In the poorly exfoliated system (Fig. 5.4(a)), even though all the peaks from pristine α -ZrP have disappeared, new peaks due to the intercalated α -ZrP layers can be observed. This indicates that intercalated α -ZrP layers are still present in epoxy matrix. WAXD patterns obtained from the moderate and well exfoliated nanocomposites, as shown in (b) and (c), do not show any intercalation peaks, indicating that both of these nanocomposites do not have detectable intercalated nanoplatelets in the epoxy matrix. However, a minor distinction between WAXD patterns in Fig. 5.4(b) and Fig. 5.4(c) can still be distinguished. The XRD pattern (b) shows a noticeable hump at a 2θ position of $2-5^\circ$. This hump indicates the presence of a small amount of loosely formed intercalated nanoplatelets. In order to definitively discern the differences in the morphology variations among the three nanocomposite systems, direct TEM observation is further performed.

Fig. 5.5 shows a photograph of neat epoxy and epoxy/ α -ZrP with three different levels of exfoliation. It clearly shows that epoxy/ α -ZrP nanocomposite panels of good exfoliation and moderate exfoliation can maintain the transparency which is very close to that of neat epoxy. In comparison, the epoxy/ α -ZrP nanocomposite of poor exfoliation is opaque. The variations on the transparency are resulted from the presence of aggregated nanoplatelets which scatter visible light.

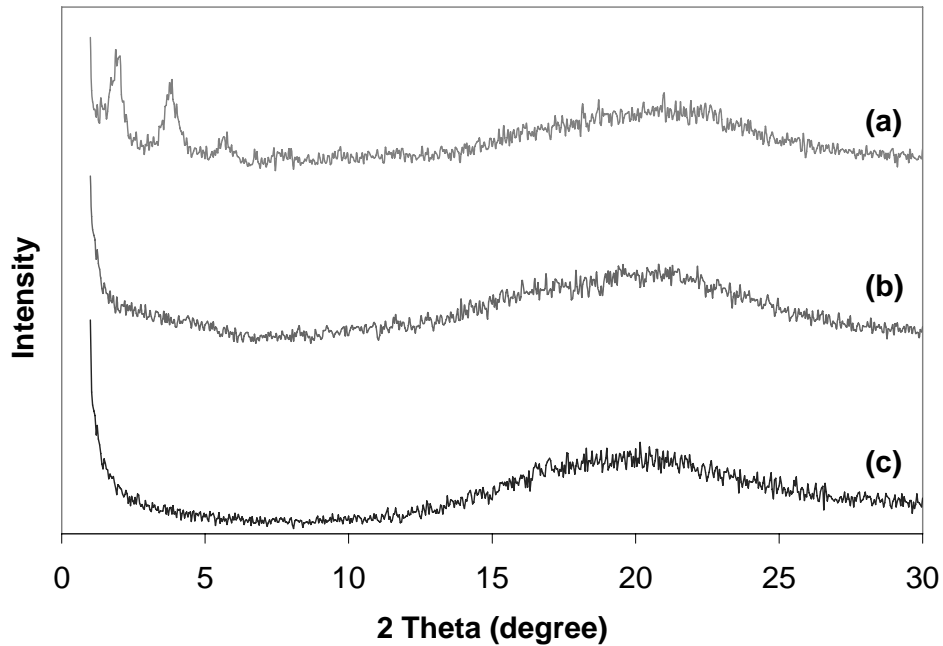
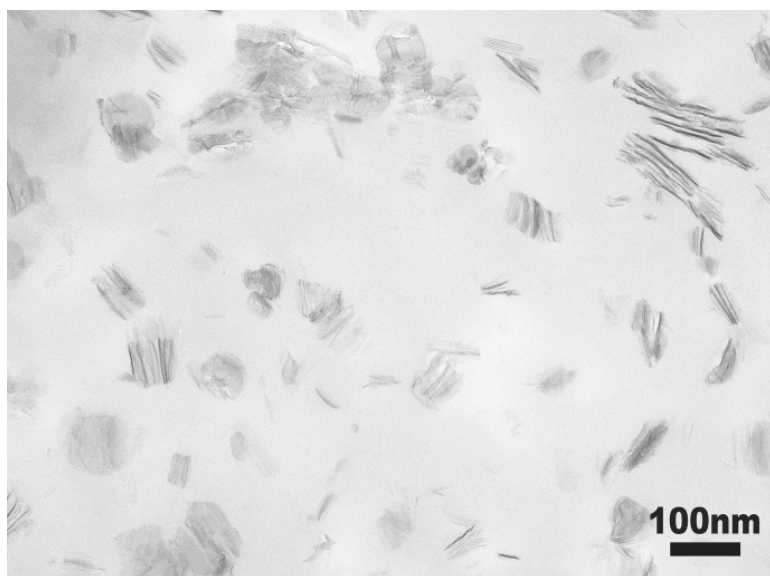


Fig. 5.4. XRD patterns of epoxy/ α -ZrP nanocomposites with (a) poor exfoliation, (b) moderate exfoliation, and (c) good exfoliation.

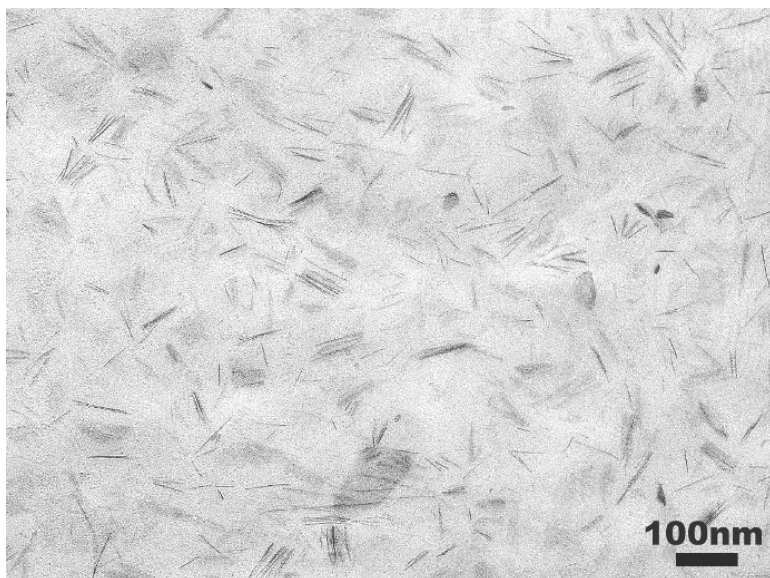


Fig. 5.5. Images of neat epoxy and epoxy/ α -ZrP nanocomposites with different levels of exfoliation.

Fig. 5.6 shows the three distinctly different levels of dispersion of α -ZrP nanoplatelets in the epoxy matrix: (a) poorly exfoliated, (b) moderately exfoliated, and (c) fully exfoliated. All the samples contain 2.0 vol% loading level of α -ZrP nanoplatelets. As expected from the XRD patterns, the TEM image of epoxy with poorly exfoliated α -ZrP shows a large number of intercalated α -ZrP domains (Fig. 5.6(a)). In the case of the moderate and good exfoliation cases, TEM can clearly differentiate their morphological differences (Figs. 5.6(b) and 5.6(c)). In Fig. 5.6(b), α -ZrP layers are well dispersed throughout the epoxy matrix. However, both exfoliated and loosely formed intercalated α -ZrP layers are present. In the case of the fully exfoliated system, Fig. 5.6(c), all of the α -ZrP layers have been exfoliated in the epoxy matrix. As pointed out earlier [27], the presence of 2.0 vol% of exfoliated nanoplatelets shows a local orientation of nanolayers in the matrix due to geometric constraint by the adjacent nanoplatelets. This geometric constraint-induced orientation is loosely formed with a domain size of about 1 μm or so. Globally, there is no preferred orientation in the fully exfoliated nanocomposites. It should be noted that when the nanoplatelet loading is at 1 vol% or lower, no sign of nanoplatelet local orientation is found [96].

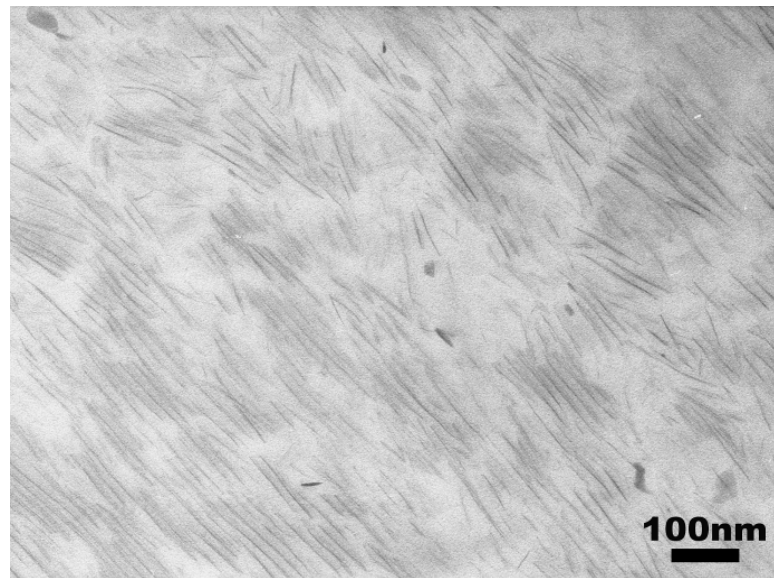


(a)



(b)

Fig. 5.6. TEM of epoxy/ α -ZrP showing (a) poor exfoliation, (b) moderate exfoliation and (c) good exfoliation. All samples contain the same amount of α -ZrP (2.0 vol%) and intercalating agent in epoxy.



(c)

Fig. 5.6. Continued.

5. 3. 2. Mechanical Property

The tensile stress-strain curves of neat epoxy and epoxy nanocomposite systems with three different levels of exfoliation are shown in Fig. 5.7 and the key tensile properties are presented in Table 5.1. The addition of 2.0 vol% of poorly exfoliated, i.e., mostly intercalated, α -ZrP nanoplatelets into epoxy matrix improves only the tensile modulus by 8%, but reduces strength and elongation-at-break by 30% and 50%, respectively. These big drops in strength and elongation-at-break are possibly caused by the intercalated tactoids [110] which may act as defects to weaken the epoxy matrix.

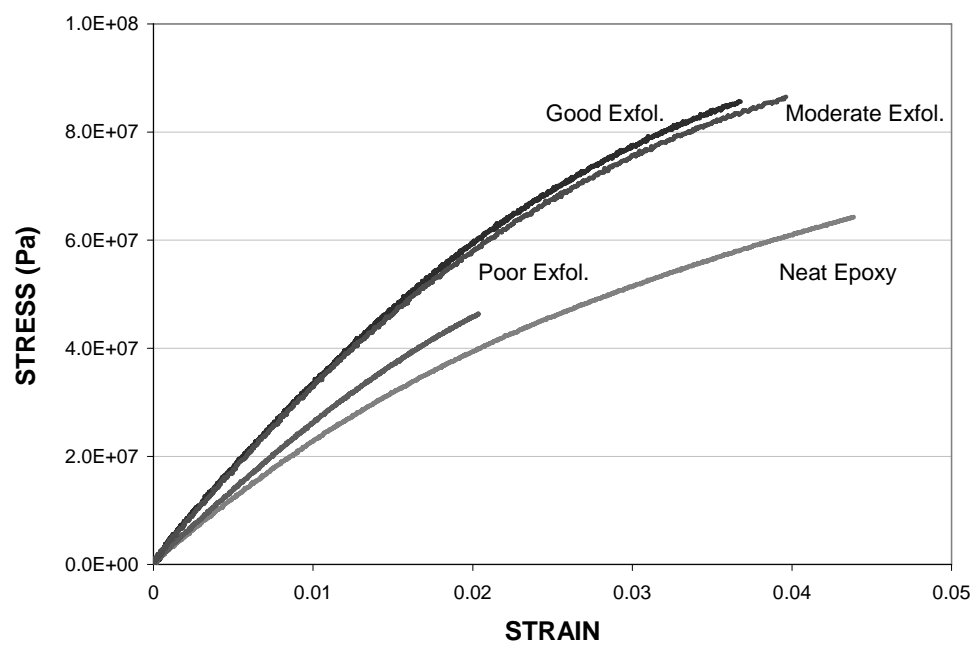


Fig. 5.7. Tensile behavior of α -ZrP based DGEBA/DDS epoxy systems.

Table 5.1. Mechanical Properties and T_g of Epoxy/ α -ZrP Nanocomposites

		Neat	Poor	Moderate	Good
Young's Modulus	GPa	2.90 \pm 0.05	3.13 \pm 0.20	3.72 \pm 0.21	4.39 \pm 0.25
Tensile Strength	MPa	75.3 \pm 6.4	53.2 \pm 8.4	86.5 \pm 7.8	86.0 \pm 6.7
Elongation at Break	%	4.1 \pm 0.4	2.0 \pm 0.3	3.9 \pm 0.3	3.8 \pm 0.3
K_{IC}	MPa·m ^{1/2}	0.72 \pm 0.02	0.64 \pm 0.05	0.79 \pm 0.04	0.76 \pm 0.05
T_g	°C	215	145	150	150

On the other hand, the incorporation of the same amount of α -ZrP nanoplatelets with good exfoliation can significantly improve the tensile modulus by about 50%. Yet, the elongation-at-break is practically unaffected. The great improvement in tensile modulus is surely due to the presence of the well-exfoliated, high aspect ratio α -ZrP nanoplatelets. In the case of the moderately exfoliated system, its tensile properties fall in between the poorly dispersed and fully exfoliated systems.

Fig. 5.8 shows DMA spectra of neat epoxy and epoxy nanocomposite systems with both poorly and well exfoliated α -ZrP nanoplatelets. Since the DMA of the moderately exfoliated system shows virtually the same spectrum as that of the well exfoliated system, it is omitted in Fig. 5.8. The T_g of the well exfoliated system is found

to be 150°C. As discussed previously [27], the drop in T_g is due to the reaction of monoamine intercalating agents with epoxy monomers.

With the case of the T_g drop, one may be skeptical of our claim saying that all of the samples in this study are of chemical identity due to the added surfactants into the systems. In this regard, there is a chemical difference between the neat epoxy and the three nanocomposites, each with different levels of nanofiller dispersion. The negative effects by the added surfactant have been well documented in our previous reports [15,27]. However, since all three nanocomposite samples used in this study contain the same amount of surfactant in their systems, there is no difference among the three samples in terms of network structure or chemical composition.

The DMA of the poorly exfoliated system shows a similar T_g range as that of the well exfoliated system, but showing a slightly higher low-temperature damping characteristic (γ -relaxation peak) and a broader α peak. The above behavior can be explained by the level of nanoplatelets dispersion/exfoliation. When the nanoplatelets are intercalated or agglomerated, the system behaves as if it is a conventional micro-composite. Thus, for the poorly exfoliated system, even though it has the same amount of nanoplatelets in the matrix, it exhibits a higher damping characteristic than the well exfoliated system. In terms of α peak (T_g) shape in the $\tan \delta$ curve, the well exfoliated system has a sharper α peak than that of the poorly exfoliated system. This suggests that the well exfoliated system contains more homogeneous network characteristics due to a higher degree of exfoliation and dispersion of nanoplatelets in epoxy.

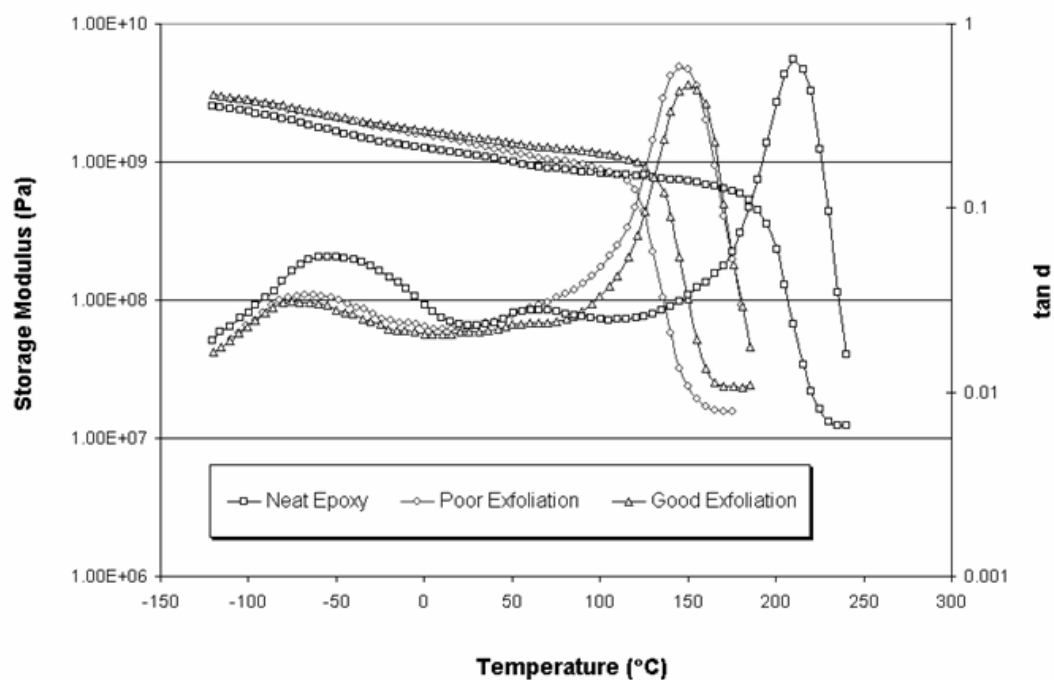


Fig. 5.8. DMA of α -ZrP based DGEBA/DDS epoxy systems.

Interestingly, it should be noted that, with a careful observation, at low temperatures the DMA curves of the poorly exfoliated system overlap with the well exfoliated system in terms of storage modulus and $\tan \delta$ curves. As the temperature increases, however, both storage modulus and $\tan \delta$ curves of the poorly exfoliated system begin to deviate from those of the well exfoliated system, and approach those of the neat epoxy. As the temperature reaches above T_g , the well exfoliated system exhibits

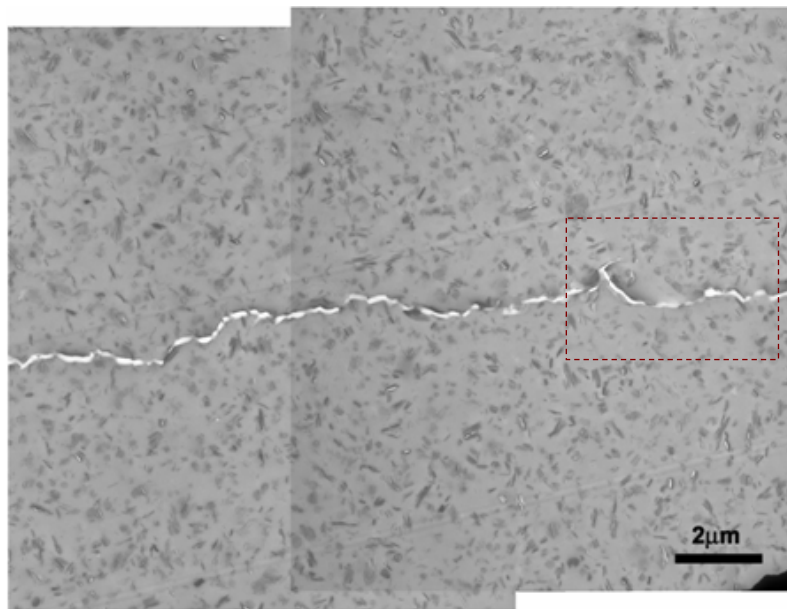
a much higher rubbery plateau modulus than the poorly dispersed system. The above phenomenon is consistent with what was reported recently by Sue *et al.*¹⁹

5. 3. 3. Fracture Behavior Study

The Mode-I fracture toughness (K_{IC}) values of neat epoxy and epoxy nanocomposites with three levels of exfoliation are presented in Table 5.1. There is no noticeable difference in K_{IC} between the neat epoxy and epoxy/ α -ZrP nanocomposites with moderate and good exfoliation systems. This finding is again consistent with our earlier study on both clay-filled and α -ZrP-reinforced epoxy nanocomposites systems [15,27,72]. However, the poorly dispersed system shows a slightly lower K_{IC} value. Furthermore, it is noted that the ductility of the poorly dispersed system is also dramatically reduced when it is compared to that of neat epoxy and well exfoliated system. This suggests that the presence of poorly dispersed nanoplatelets certainly act as defects during tensile loading and mode I fracture.

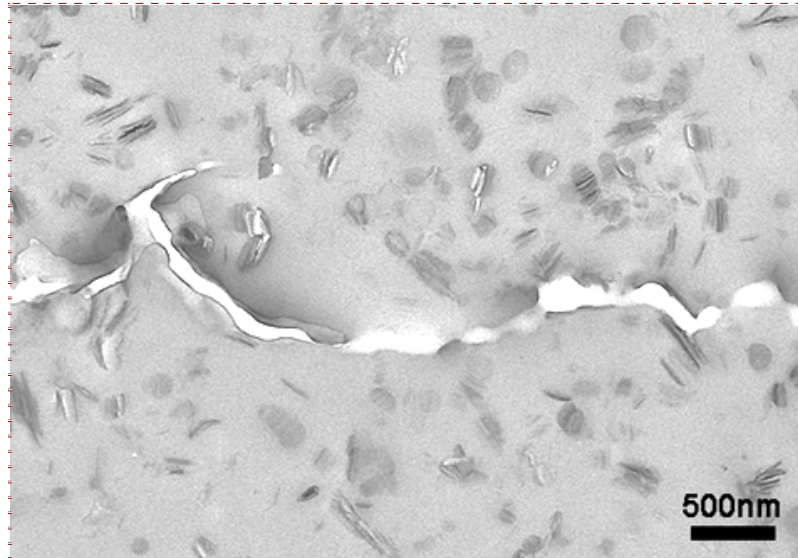
To further investigate into the effects of degree of exfoliation of nanoplatelets on the fracture behavior, the DN-4PB technique is employed on epoxy nanocomposites. As shown in Fig. 5.9, when the matrix contains poorly dispersed nanoplatelets, the arrested crack tip shows that crack deflection and bifurcation have taken place. With a careful observation, it is noticeable that the crack has a tendency to propagate along the weaker intercalated layers, which also act as stress concentration sites. Following this logic, the poorly dispersed nanocomposite would have shown an improved fracture toughness. As mentioned earlier, however, it actually has a lower K_{IC} value than neat epoxy. Again, the

reason of this drop is that intercalated or agglomerated platelets act as defects, which weakens the epoxy, in the nanocomposite. It should be noted that crack deflection and bifurcation are far less effective compared to crazing or shear banding in toughening.



(a)

Fig. 5.9. TEM of DN-4PB damage zone of Epoxy/ α -ZrP nanocomposite with poor exfoliation (2.0 vol%), showing crack bifurcation and distortion: (a) low magnification and (b) high magnification. The crack propagates from left to right.



(b)

Fig. 5.9. Continued.

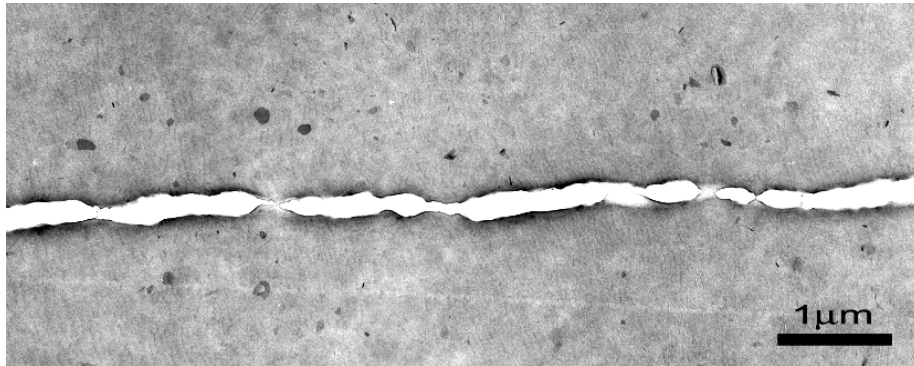
In contrast, as shown in Fig. 5.10, when the nanoplatelets are highly exfoliated throughout the matrix, no sign of delamination or crack deflection can be observed. Since all the α -ZrP nanoplatelets are highly exfoliated into an individual layer, there are no weak intercalated layers for the crack to propagate into. As a result, the crack can only grow in a straight fashion. Another explanation for the straight crack propagation is the “size” effect. Since the nanoplatelets are exfoliated and the nanoplatelet property is homogenized with the surrounding epoxy matrix, the crack can only “see” a one-phase matrix, not a two-phase matrix. Hence, the crack propagates in a straight fashion. Fig.

5.9 (b) supports the above claim that (1) the crack propagates in a straight manner through the mid-plane of the α -ZrP nanoplatelets and (2) the K_{IC} value of the well exfoliated system remains the same as that of the neat epoxy. The above findings are consistent with our earlier findings on epoxy nanocomposites with exfoliated α -ZrP [27].

Based on the above tensile, fracture, and DMA testing results, we are now able to understand how the different levels of exfoliation of nanoplatelets affect mechanical properties of epoxy/ α -ZrP nanocomposites. The results clearly show that the nanocomposite with good exfoliation is by far superior to the nanocomposites with moderate or poor exfoliation. This finding is also consistent with all of the previous literature results. It is worth noting that, except for the Young's modulus, the properties of the nanocomposite with good exfoliation are similar to those of the nanocomposites with moderate exfoliation. Considering the difficulty, time, and cost involved in preparing a fully exfoliated nanocomposite, one may raise a question: is it worthwhile and necessary to achieve good exfoliation to realize the full benefits of polymer nanocomposites? The present study can at least help answer one aspect of the question by allowing material engineers to tailor and optimize the performance of polymer nanocomposites at acceptable cost.

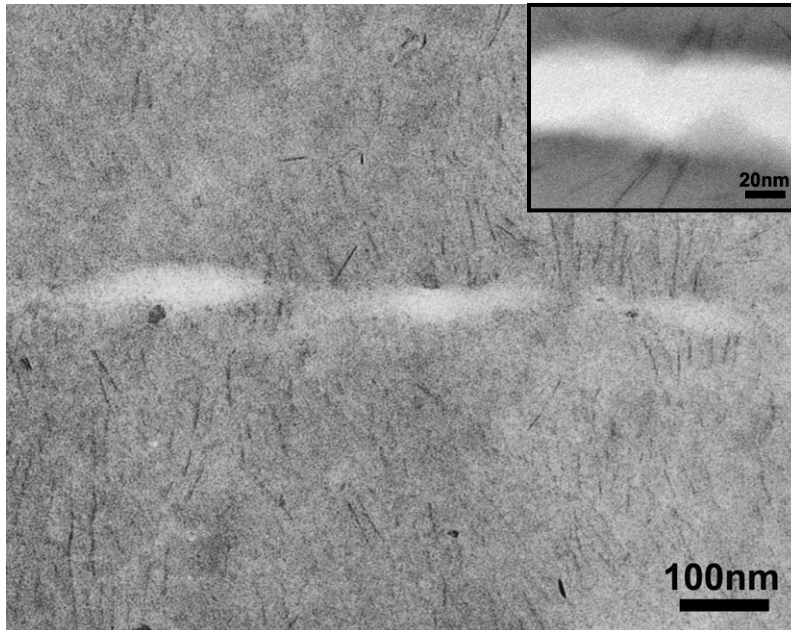
Another important finding of the present study is the unambiguous determination of the fracture behavior and toughening of polymer nanocomposites. It is evident that nanoplatelets with aspect ratio of about 100, if exfoliated, cannot introduce crack deflection and crack bifurcation mechanisms to toughen the polymer matrix. Even when nano-tactoids are present, they cannot effectively improve fracture toughness of an

epoxy matrix. The present finding implies that, for epoxy nanocomposite systems that show greatly improved fracture toughness in the literature, it may be due to other factors, such as the presence of large amount of intercalating agents in their systems. The effect of type of intercalating agents and their amount on mechanical properties and fracture behavior of polymer nanocomposites will be investigated and reported in the near future.



(a)

Fig. 5.10. TEM of DN-4PB damage zone of Epoxy/ α -ZrP nanocomposite with good exfoliation (2.0 vol%) showing straight crack propagation breaking through α -ZrP layers: (a) low magnification and (b) high magnification. The crack propagates from left to right.



(b)

Fig. 5.10. Continued.

5. 4. Summary

To understand how the levels of dispersion of nanoplatelets affect the mechanical properties of polymer nanocomposites, epoxy/ α -ZrP nanocomposites with various degrees of exfoliation were prepared by tuning the processing conditions. Morphological differences among the three distinctive sets of samples with various levels of exfoliation of α -ZrP nanoplatelets in epoxy matrices are clearly observed using TEM and WAXD. The mechanical and fracture testing results show that the level of nanoplatelet exfoliation

can strongly influence mechanical properties of the polymer nanocomposites. It also affects the fracture mechanisms of the nanocomposites. Unlike the poorly dispersed system, the well exfoliated system shows only straight crack propagation phenomena.

CHAPTER VI

EFFECTS OF NANOPATELET ASPECT RATIO ON MECHANICAL PROPERTIES OF EPOXY NANOCOMPOSITES[†]

6.1. Introduction

Since the successful development of nylon/clay nanocomposites that showed great improvements in physical and mechanical properties with only a small amount of clay introduced into the polymer matrix [22,23,25] in the late 1980s, the pursuits for high performance polymer nanocomposites have swamped both the scientific community and the industry in the past two decades. Numerous research efforts in this field have been focused on the incorporation of nanoplatelet fillers to greatly enhance their physical, mechanical, and chemical properties in various polymer matrices, including epoxy [34-36,40,42,47,68,78,107,108,118-121], polypropylene [114,122,123], polyethylene [113], polyimide [20,124], polystyrene [125-127], poly(methyl methacrylate) [26], etc. Most results have revealed great improvements of polymer properties by a small addition of nanoplatelets (< 5 wt%). Important factors that can affect the physical and mechanical properties of nanoplatelet-reinforced polymer nanocomposites include nanoplatelets [52-54,56,128] type, intercalating agents [62,111,115], filler loading levels [18,19,57], and processing [80,129]. In particular, significant efforts have emphasized on achieving maximum level of exfoliation of nanoplatelets in polymer matrices.

[†] Reprinted with permission from “Effect of nanoplatelet aspect ratio on mechanical properties of epoxy nanocomposites” by W.-J. Boo *et al.*, 2007. *Polymer*, 48, 1075-1082. ©2007 by Elsevier Ltd.

Recently, more emphases have been placed on investigating how the nanoplatelet aspect ratio, defined as the ratio of the long axis to platelet thickness, affects the physical and mechanical properties of polymer nanocomposites. For example, Maiti *et al.* [130] synthesized polylactide/layered silicate nanocomposites using organic phosphonium intercalating agents with different chain lengths to reveal the influence of nanoplatelet size and aspect ratio on the properties of polymer nanocomposites. To obtain exfoliated nanoplatelets with variations in aspect ratio in polymer matrices, they employed smectite, montmorillonite, and mica as nanofillers. Depending on the size of each type of layered silicates incorporated, the effects of dispersion, intercalation, and aspect ratio of nanoplatelets on mechanical and gas barrier properties of nanocomposites were investigated. More recently, Osman *et al.* [131] used *n*-benzyltrimethyl hexadecyl ammonium to intercalate and exfoliate montmorillonite clay in epoxy and polyurethane matrices, respectively, to investigate their gas barrier properties. The aspect ratios of the organoclay were varied by controlling the level of intercalation and exfoliation of the clay in the polymer matrix.

It should be pointed out that the above studies were performed based on the use of different types of natural silicates [130,132] or the use of different intercalating agents to obtain different filler aspect ratios in the nanocomposites. Consequently, in addition to the aspect ratio effect, uncertainties on the effect of different types of silicates and intercalating agents were introduced. Thus, it is unlikely that unambiguous results on how the aspect ratio of nanoplatelets affect physical and mechanical properties can be obtained.

Recently, alternative approaches have been undertaken to definitively investigate how the nanoplatelet size and aspect ratio influence the physical and mechanical properties of polymer nanocomposites. To avoid any possible ambiguities accompanied by the utilization of different fillers and surface functionalities to achieve the control of aspect ratios, synthetic α -zirconium phosphate (α -ZrP), $\text{Zr}(\text{HPO}_4)_2 \cdot \text{H}_2\text{O}$, that possesses well-controlled sizes and aspect ratios was prepared. The advantages of α -ZrP over that of clay has been highlighted elsewhere [28,29,91,100]. They will not be elaborated here. Because of the unique attributes of α -ZrP, a series of fundamental studies, including (1) the synthesis, intercalation, and exfoliation of α -ZrP [28] in epoxy, (2) the preparation of exfoliated epoxy/ α -ZrP nanocomposites [27], and (3) the study of fracture behaviors of epoxy/ α -ZrP [15,82] with various degrees of exfoliation have been carried out recently. Insightful information has been obtained.

In this work, fundamental study on how the nanoplatelet aspect ratio influences the mechanical properties of polymer nanocomposites was conducted. Considering the structure of nanoplatelet particles, it is expected that the higher aspect ratio of nanoplatelets will be more effective for the enhancement of mechanical properties due to the higher surface area of the nanoplatelets.

Instead of using high molecular weights monoamines, a small amount of less reactive intercalating agent, tetra-*n*-butyl ammonium hydroxide (TBA), is utilized [98] to minimize unintended reaction of intercalating agent with epoxy monomer. As a result, the glass transition temperature (T_g) of nanoplatelet-reinforced polymer nanocomposites can be maintained. Furthermore, the effect of intercalating agent type on nanocomposite

mechanical properties can be addressed by comparing the present findings against our earlier results where long-chain monoamine was utilized [82]. The usefulness of high aspect ratio nanoplatelets in polymer nanocomposites for structural applications is also discussed.

6. 2. Experimental

6. 2. 1. Materials

The materials used in this study are listed in Table 6.1. Two α -ZrP having two different aspect ratios, i.e., ca. 100 and 1000, were synthesized [82]. The detailed chemistry and procedures for the synthesis and control of aspect ratio of α -ZrP can be found elsewhere [28,29,91,100]. TBA (tetra-*n*-butyl ammonium hydroxide [CH₃CH₂CH₂CH₂)₄N(OH), Aldrich] was used as surface modifiers to intercalate α -ZrP layers. The diglycidyl ether of bisphenol-A (DGEBA) epoxy resin [D.E.R.TM 332 epoxy resin, The Dow Chemical Company], which has a narrow monomer molecular weight distribution (172-176 g/mol), was used in this study. The curing agent utilized is 4,4'-diaminodiphenylsulfone (DDS, Aldrich). All the chemicals were used as received except for epoxy resin, which was dried in a vacuum oven for 24 hrs prior to sample preparation.

6. 2. 2. Preparation of Epoxy/ α -ZrP Nanocomposites

The interlayer *d*-spacing of pristine α -ZrP is known to be 7.6Å [27]. The addition of TBA at a 0.75:1 molar ratio in deionized water at 0 °C can lead to full exfoliation of

α -ZrP layers into individual nanoplatelets. Detailed sample preparation procedures for achieving fully exfoliated α -ZrP in water and in epoxy can be found elsewhere.

Table 6.1. Material Specification and Source

Material	Comments / Specifications	Supplier
α -ZrP-100	3M phosphoric acid, refluxing at 100°C, aspect ratio 100	Synthesized in PTC*
α -ZrP-1000	Hydrofluoric acid, hydrothermal condition, aspect ratio 1,000	Synthesized in PTC
Intercalating agent	Tetra- <i>n</i> -Butyl Ammonium Hydroxide (TBA)	Aldrich
Epoxy resin	D.E.R. TM 332, diglycidyl ether of bisphenol-A (DGEBA)	DOW Chemical
Curing agent	DDS, 4,4'-diamino-diphenyl sulfone	Aldrich

* Polymer Technology Center, Texas A&M University

After exfoliation in deionized water, α -ZrP nanoplatelets with aspect ratios of ca. 100 and 1,000 were washed and transferred into acetone with an aid of centrifuge. DGEBA epoxy monomer which was pre-dissolved in acetone was added to achieve a final inorganic α -ZrP loading of 0.7 vol% in epoxy. After removal of solvent with Rotarvapor® in a water bath at about 90°C, DDS was added at stoichiometric ratio. After the DDS melted at 130°C, the resin mixture was cast in a preheated glass mold and

cured in an oven at 180 °C for 2 hrs, followed by 2 hrs of post-cure at 220 °C. The epoxy/ α -ZrP systems with aspect ratios of 100 and 1,000 are designated as epoxy/ZrP-100 and epoxy/ZrP-1000, respectively. For comparison, a neat epoxy plaque (neat epoxy) and an epoxy plaque with only intercalating agent, i.e., TBA, addition (epoxy/TBA) were also prepared.

It should be noted that attempts were made to increase the α -ZrP loading in epoxy. However, when α -ZrP loading is greater than 0.7 vol% for the epoxy/ α -ZrP-1000 system, the viscosity build-up will become so high that good quality epoxy nanocomposite plaques cannot be prepared. As a result, only epoxy nanocomposite panels with 0.7 vol% of α -ZrP were investigated.

6. 2. 3. Morphology Characterization

Scanning electron microscopy (SEM) images of α -ZrP nanoplatelets were acquired using a Zeiss Leo 1530 VP Field Emission-SEM (FE-SEM). The samples were sputter-coated with a thin layer (ca. 3 nm) of Pt/Pd (80/20) prior to SEM observation.

For transmission electron microscopy (TEM) observation, the thin-section samples extracted from the core region of the specimens were prepared by microtoming (Ultracut E) and the thin sections (~100nm thickness) were deposited on carbon coated Cu grids. Sample grids were examined on a JEOL 1200 EX electron microscope operated at an accelerating voltage of 100 kV. TEM micrographs were printed on a calibrated Kodak[®] electron microscope film. Complete details of the microtomy and microscopy techniques employed here are given in prior publications [15,27].

6. 2. 4. Mechanical Properties and Fracture Behavior Studies

Tensile properties of epoxy nanocomposites reinforced with α -ZrP having two different aspect ratios were obtained based on the ASTM D638-98 method. The tensile tests were performed using an MTS[®] servo-hydraulic test machine at a crosshead speed of 5.08 mm/min at ambient temperature. Young's modulus, tensile strength, and elongation at break of each sample were obtained based on at least five specimens per sample and the average values and standard deviations were reported.

Dynamic mechanical analysis (DMA) was conducted on a RSA III (TA Instruments) with a 3-point-bending mode, at a fixed frequency of 1 Hz and with a temperature increase of 5°C per step, ranging from -150 to 250 °C. A sinusoidal strain-amplitude of 0.05% was chosen for the measurement. The maximum point on the Tan δ curve was recorded as the T_g of the samples. Multiple scans were conducted to ensure reproducibility.

Fracture toughness tests were conducted based on the linear elastic fracture mechanics (LEFM) approach. The single-edge-notch 3-point-bending (SEN-3PB) test, based on ASTM D5045-96, was performed to obtain the mode-I critical stress intensity factor (K_{IC}) of the neat epoxy and epoxy nanocomposites with two different aspect ratios. Care was taken to ensure that the initial sharp crack, generated by tapping with a fresh razor blade, exhibited a thumbnail shape crack front prior to testing. At least five specimens per sample were tested to determine K_{IC} values of the samples. The critical stress intensity factors were calculated using the following equation:

$$K_{IC} = \frac{P_C S}{BW^{3/2}} f(a/W) \quad (6.1)$$

where P_C is the load at crack initiation, S is the span width, B is the thickness of the specimen, W is the width of the specimen, and a is the initial crack length.

The double-notch four-point-bend (DN-4PB) test was conducted to probe the detailed mechanisms on crack propagation phenomena in the epoxy nanocomposites with variation in filler aspect ratios. Detailed methods of sample preparation and testing can be found elsewhere [101,116]. The DN-4PB tests were performed at ambient temperature. The arrested sub-critical crack tip damage zone from the core region of the specimen was isolated, trimmed, and thin-sectioned for TEM observation.

6.3. Results and Discussion

6.3.1. Morphology

After synthesis, washing, and drying the powder of crystalline α -ZrP, SEM was employed to verify the size of the nanoplatelets synthesized. Fig. 6.1 displays the SEM micrographs of the α -ZrP nanoplatelets with their aspect ratios of (a) 100 and (b) 1,000, respectively.

Since all the detailed XRD patterns of intercalated and exfoliated α -ZrP with various aspect ratios and those of corresponding nanocomposites can be found elsewhere [82], only TEM micrographs of epoxy/ α -ZrP nanocomposites are reported here.

According to the XRD characterization in the previous reports [82], fully exfoliated α -ZrP layer in epoxy is obtained. To directly confirm the state of exfoliation and an overall dispersion of exfoliated α -ZrP nanoplatelets in epoxy matrix, the samples were imaged by TEM.

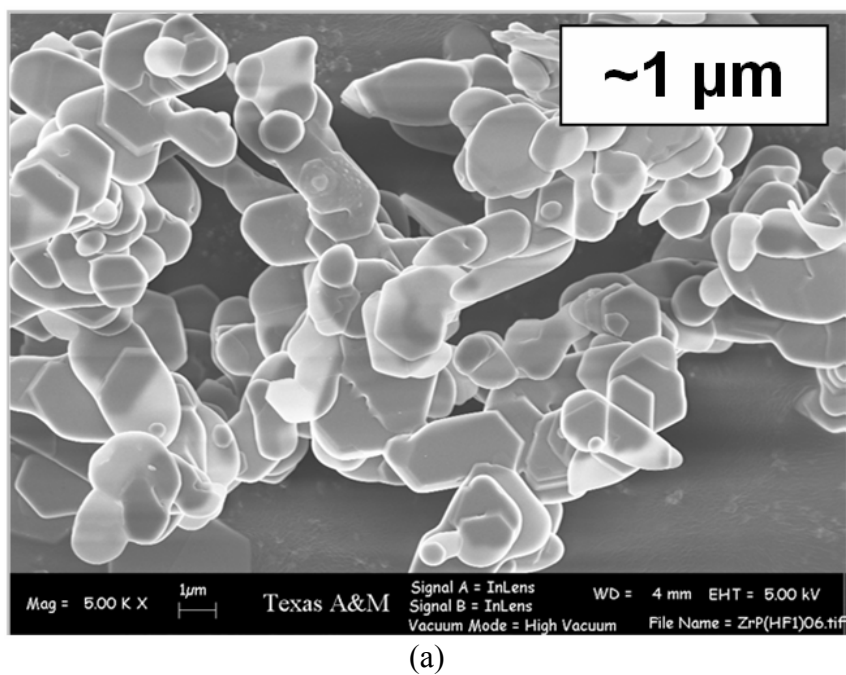


Fig. 6.1. SEM of α -ZrP nanoplatelets having aspect ratios of (a) 100 and (b) 1,000.

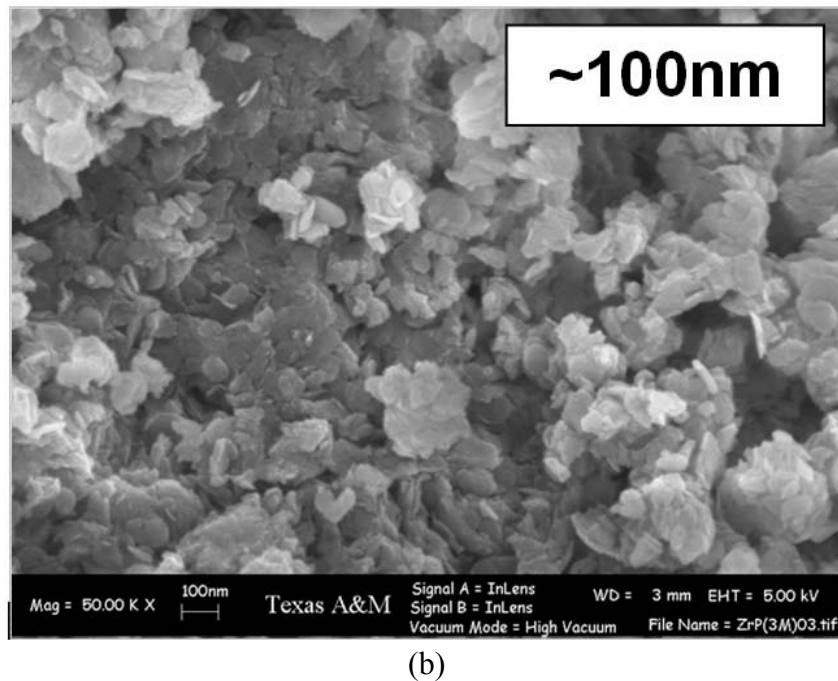
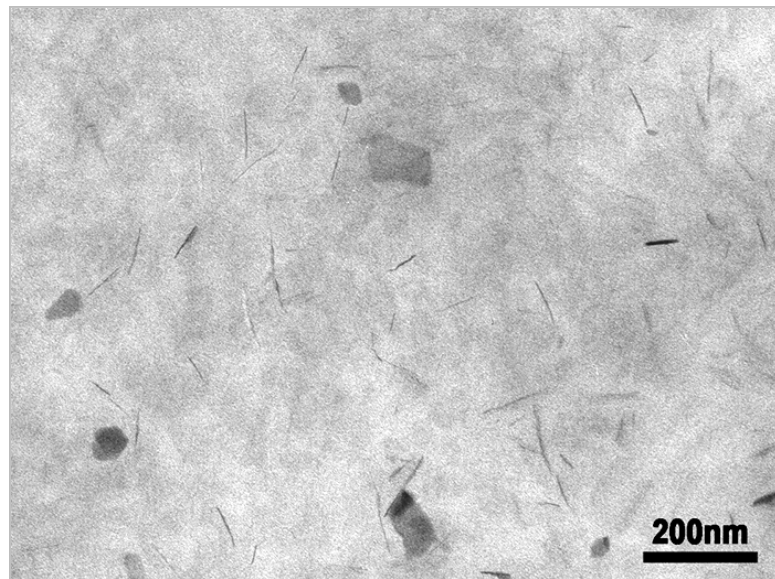
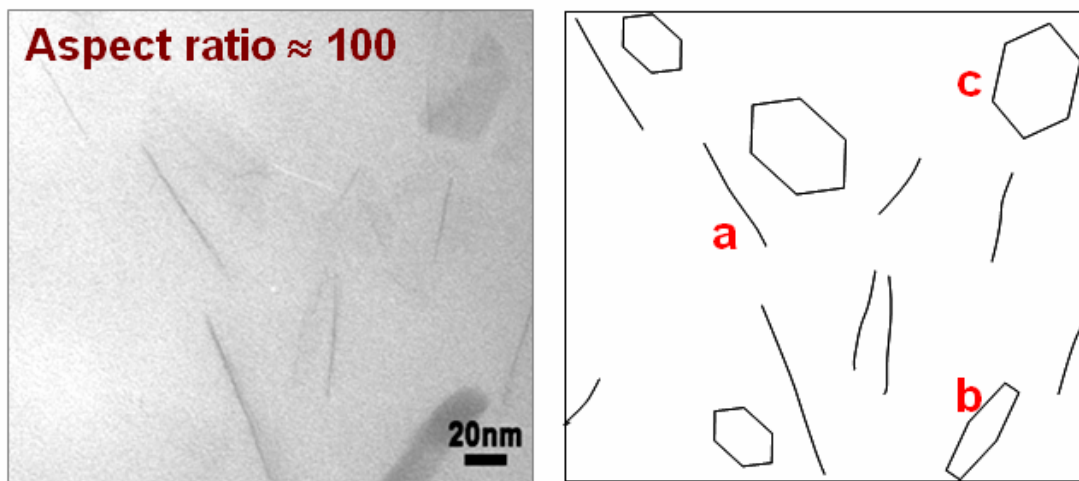


Fig. 6.1. Continued.

Fig. 6.2(a) displays highly exfoliated and well-dispersed α -ZrP-100 nanoplatelets (0.7 vol%) in epoxy. The TEM image clearly shows random orientation of α -ZrP nanoplatelets which are completely exfoliated. This random orientation is probably due to the low filler loading (0.7 vol%). In contrast, locally oriented nanoplatelet morphology has been observed at higher α -ZrP loadings [27,82].



(a)



(b)

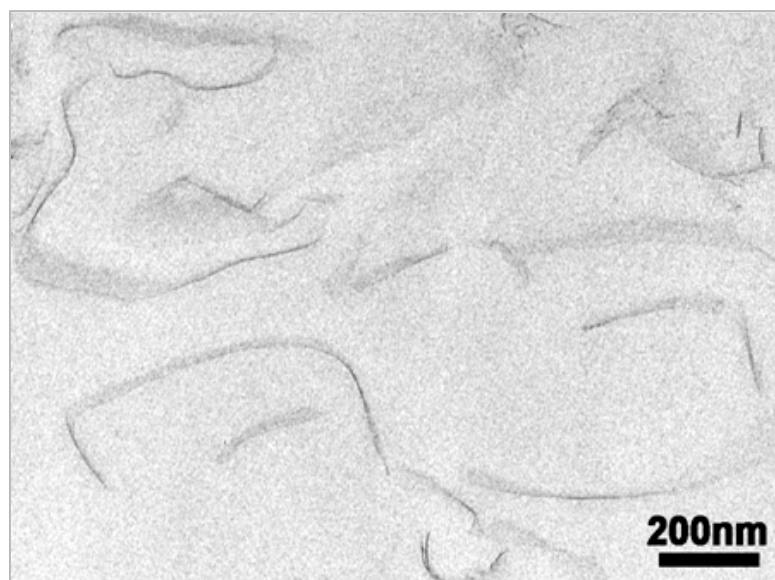
(c)

Fig. 6.2. TEM of epoxy/ZrP-100 nanocomposite: (a) low magnification, (b) high magnification, and (c) the corresponding schematic.

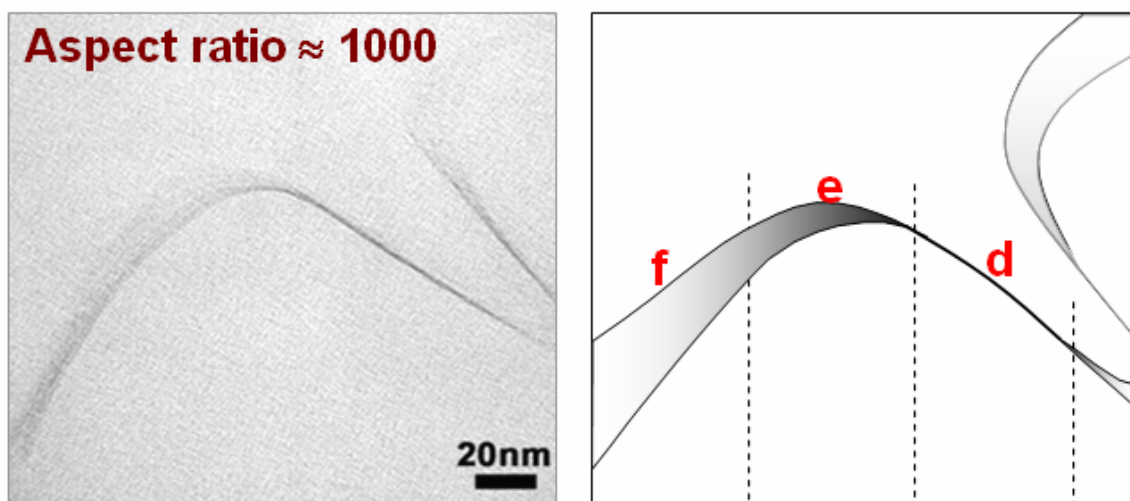
Furthermore, the frequency of α -ZrP oriented parallel to the thin-section direction, i.e., the surface of the micrograph, appears to be higher than that of the 1 and 2 vol% loading scenarios [82]. Fig. 6.2(b) presents a high magnification TEM image of epoxy/ α -ZrP from the same sample. As shown, the nanoplatelets show different morphology due to random orientation. The schematic in Fig. 6.2(c) aids to demonstrate the various orientations of nanoplatelets in detail: as noted **a**, **b**, and **c**. The α -ZrP nanoplatelets can appear as straight lines, tilted surfaces, or fully exposed flat surfaces.

In Fig. 6.3(a), high aspect ratio α -ZrP-1000 nanoplatelets also show complete exfoliation and random orientation in epoxy matrix. However, it is interesting to note that the high aspect ratio α -ZrP nanoplatelets exhibit a strong curvature instead of being straight. The high magnification TEM image in Fig. 6.3(b) shows a curved platelet. As depicted in **d**, **e**, and **f** (Fig. 6.3c), a single large nanoplatelet can appear as a straight line, a curved line in between, and a tilted surface at different locations of the TEM thin section. No evidence of completely flat ZrP-1000 is found in the thin section, probably because the TEM thin section is too thin (≈ 80 nm) to accommodate a complete curved α -ZrP nanoplatelet ($\approx 1,000$ nm) in the same thin section.

As pointed out earlier, the incorporation of 0.7 vol% of high aspect ratio α -ZrP in epoxy can drastically increase the viscosity of epoxy, making it extremely difficult to prepare void free epoxy plaques. As a result, only 0.7 vol% was incorporated in epoxy for this study.



(a)



(b)

(c)

Fig. 6.3. TEM of epoxy/ZrP-1000 nanocomposite: (a) low magnification, (b) high magnification, and (c) the corresponding schematic.

6. 3. 2. Mechanical Property

The tensile properties of epoxy/ZrP-100 and epoxy/ZrP-1000 are shown in Fig. 6.4. and summarized in Table 6.2. For comparison purposes, the plaques of neat epoxy (DGEBA/DDS) and an intercalating agent containing neat epoxy (epoxy/TBA) were also tested and compared. The tensile modulus of epoxy/ZrP-100 is found to increase only by 5% due to the low level of loading. Whereas, in the case of epoxy/ZrP-1000, an increase of about 12% in modulus is observed under the same condition. The larger increase in tensile modulus is explained from the higher aspect ratio of α -ZrP nanoplatelets. The decrease in elongation-at-break is greater for the high aspect ratio case and the trends correspond well with the results of Ray *et al.* [132].

Table 6.2. Tensile properties and fracture toughness of epoxy/ α -ZrP nanocomposites

	neat epoxy	epoxy/ZrP-100	epoxy/ZrP-1000	epoxy/TBA
Young's Modulus (GPa)	2.90 \pm 0.05	3.04 \pm 0.12	3.25 \pm 0.19	2.89 \pm 0.13
Tensile Strength (MPa)	75.3 \pm 6.4	54.7 \pm 4.9	46.0 \pm 4.4	43.2 \pm 4.3
Elongation at Break (%)	4.1 \pm 0.4	2.5 \pm 0.4	1.9 \pm 0.2	2.3 \pm 0.5
K _{IC} (MPa·m ^{1/2})	0.72 \pm 0.02	0.58 \pm 0.01	0.69 \pm 0.02	0.61 \pm 0.02

It should be noted that the tensile strength and elongation-at-break of both low and high aspect ratio cases are decreased due to the incorporation of the well-dispersed ZrP nanoplatelets. This finding is different from our earlier finding, which indicates that both strength and ductility of the epoxy nanocomposite can be maintained when the intercalating agent utilized is long-chain monoamine-based. This clearly suggests that the type of interaction agent utilized can have a significant impact on the strength and ductility of the polymer nanocomposites. This point will be further discussed later.

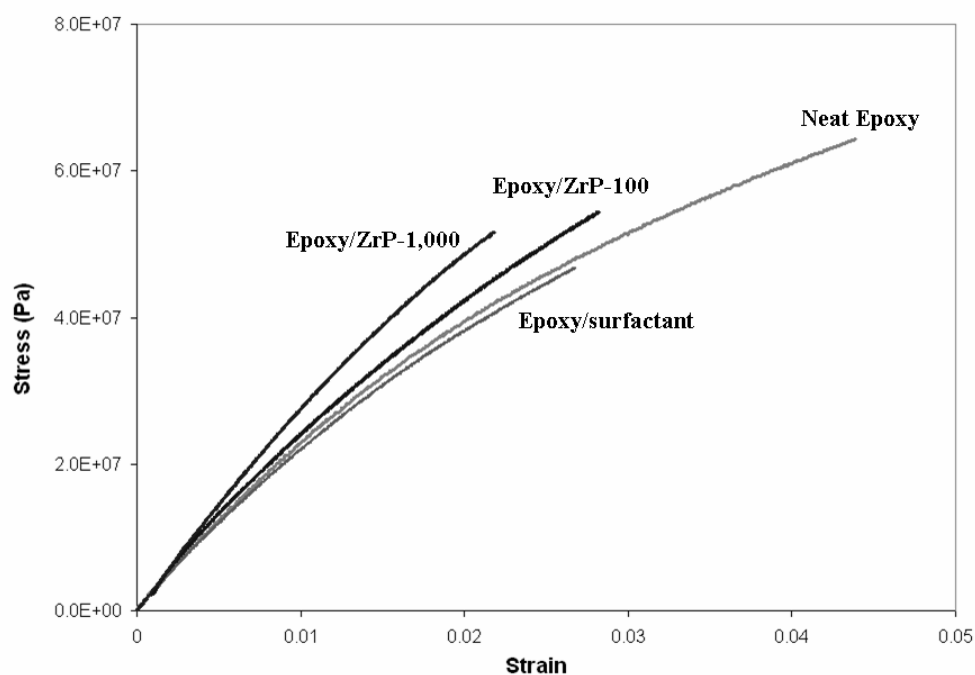


Fig. 6.4. Tensile behavior of neat epoxy and epoxy nanocomposites.

Fig. 6.5 shows DMA spectra of neat epoxy, epoxy/ZrP-100, and epoxy/ZrP-1000. The overall DMA behavior is consistent with our previous findings [28,82]. For comparison purposes, epoxy that contains intercalating agent (epoxy/TBA) was also tested and exhibits a T_g of 195°C (not shown). It is evident that the use of TBA as an intercalating agent is better for maintaining the T_g of epoxy than the long-chain monoamines [15,27,82]. It should be noted that the T_g of the epoxy/ZrP-100 and epoxy/ZrP-1000 are found to be 200 and 204°C, respectively. The above finding implies that the aspect ratio of the nanoplatelet does not play a significant role in affecting T_g at low nanoplatelet loadings. It appears that the incorporation of intercalating agent (surface modifier) may have a more significant effect on T_g for epoxy, simply because of the participation of the intercalating agent in the curing of epoxy.

By comparing the tensile and DMA results of the current epoxy nanocomposites that use TBA as intercalating agent and the previous nanocomposites that use monoamines as intercalating agent [40-43], it is evident that the T_g , strength, and ductility of the epoxy nanocomposite can be greatly influenced by the type of intercalating agents utilized. For instance, in our previous results [15,27,82], a significant T_g drop has been observed due to the unintended reaction between the monoamine intercalating agent and epoxy monomers. However, the nanocomposites in this study utilize TBA as an intercalating agent and show that the T_g of the epoxy nanocomposite remains close to as that of the neat epoxy.

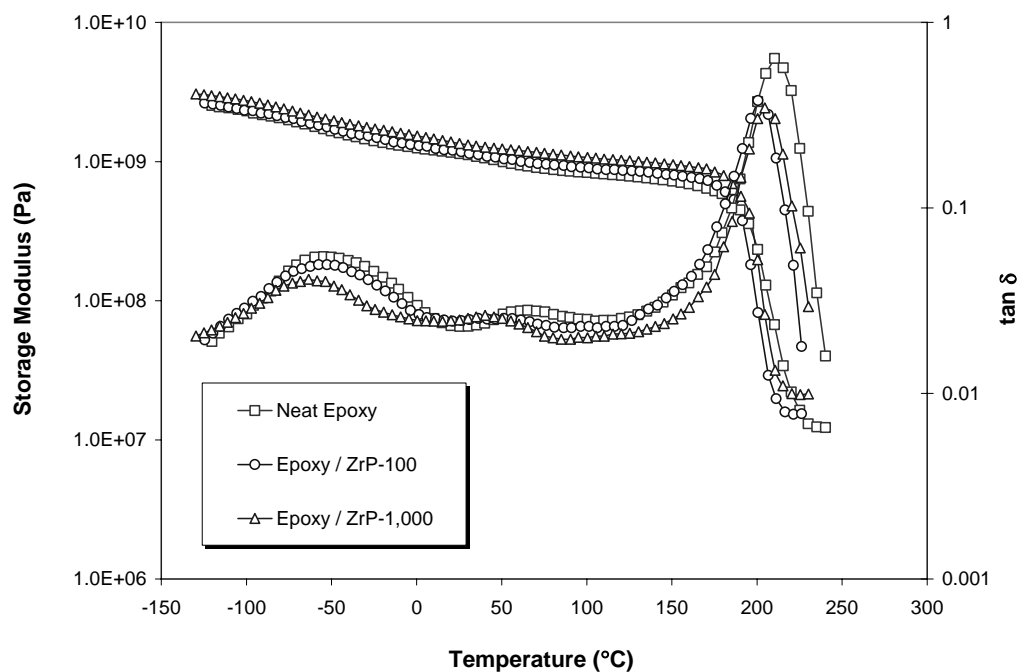
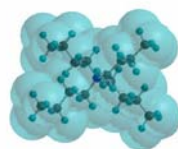


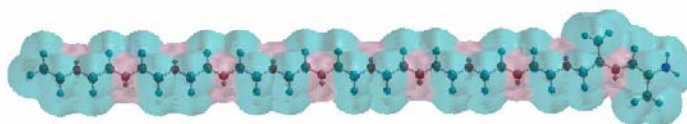
Fig. 6.5. DMA results of neat epoxy and epoxy nanocomposites.

Upon the use of TBA, the tensile strength and ductility of the epoxy nanocomposite are decreased. These drop in strength and ductility can be attributed not only to a more complete curing of epoxy with DDS but also to the more rigid interface between the polymer and the nanoplatelets, which restricts the segmental motion near the organic–inorganic interfaces [82]. The above hypothesis finds supports from the work of Kim *et al.* [98] and Ha *et al.* [133]. When TBA and monoamine are bonded to α -ZrP, TBA creates less flexible interface than monoamine-terminated polyether chains on and around α -ZrP layers. Fig. 6.6 shows the molecular structures of the TBA utilized in this

study and the monoamine-terminated polyether used in our previous reports [82]. As shown in Fig. 6.6(a), TBA has a much shorter aliphatic chain. They can be tightly packed and exhibit less flexibility, as opposed to the long single-chain monoamine structure (Fig. 6.6 (b)).



(a)



(b)

Fig. 6.6. Molecular structure and size comparison of the intercalating agents between (a) tetra-*n*-butyl ammonium hydroxide and (b) monoamine-terminated polyether.

6. 3. 3. Fracture Behavior Study

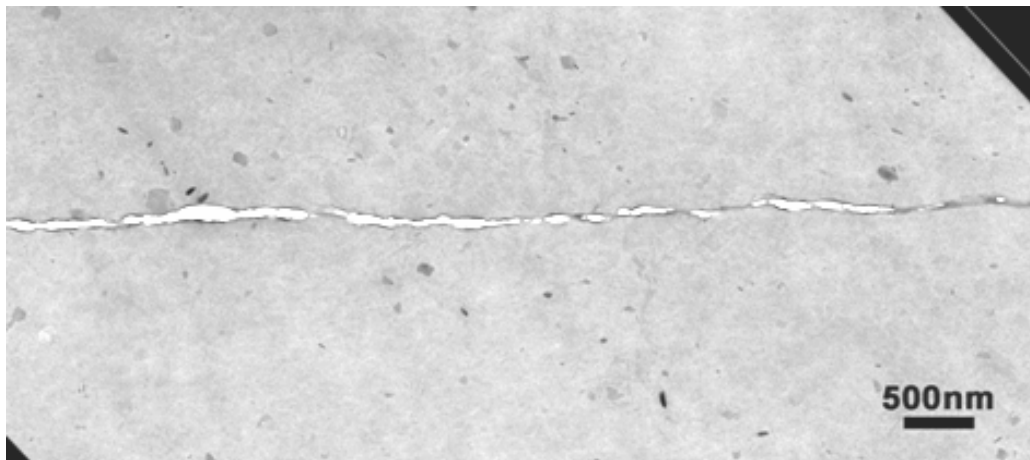
The Mode-I fracture toughness (K_{IC}) values of epoxy/ZrP-100 and epoxy/ZrP-1000 are measured and listed in Table 6.2. A neat epoxy and an epoxy/TBA are also tested as a control. As shown in Table 6.2, there is no substantial difference in K_{IC} values between neat epoxy and epoxy/ZrP-100. This result is consistent with our earlier study on both clay-filled and ZrP-reinforced epoxy nanocomposites systems [72]. In the case of epoxy/ZrP-1000, K_{IC} value is slightly higher than epoxy/ZrP-100. However, the difference is still limited. To investigate the fracture mechanisms in epoxy nanocomposites, the DN-4PB tests were carried out on epoxy/ZrP-100 and epoxy/ZrP-1000. TEM images from the arrested crack tip and crack wake are given in Figs 6.7 and 6.8, respectively.

As shown in Fig. 6.7, when the nanoplatelets are fully exfoliated, the subcritically propagated crack would grow more or less in a straight fashion. No signs of delamination or crack deflection can be found. This explains why the fracture toughness (K_{IC}) value is about the same as neat epoxy. This finding is also in good agreement with our previous results with various loading levels of α -ZrP in epoxy [82].

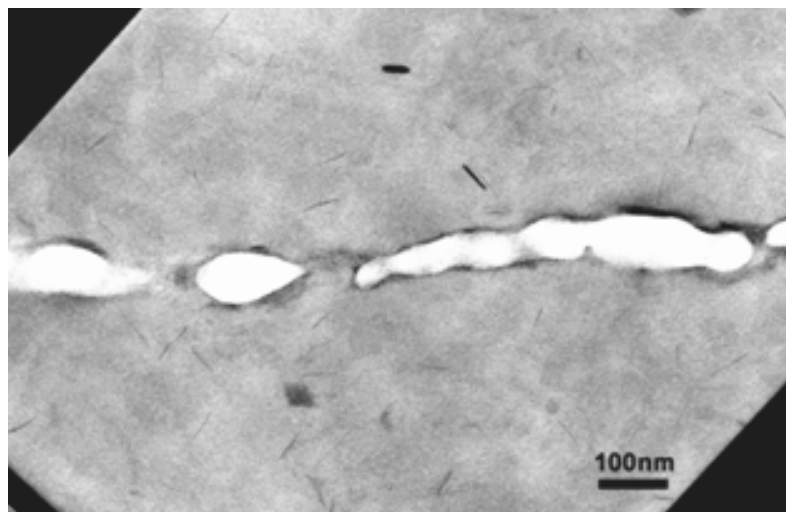
In the case of epoxy/ZrP-1000, significant crack deflection, crack bifurcation, and microcracking are observed (Fig. 6.8). Figs 6.8(a) and (b) are TEM taken from the crack wake, showing significant crack deflection at low and high magnifications, respectively. As shown in Fig. 6.8(c), the crack appears to grow along the interface of α -ZrP layers, suggesting a poorer interfacial adhesive strength than the cohesive strength of the epoxy matrix. As mentioned earlier [82], if the α -ZrP nanoplatelet aspect ratio is

around 100, the crack would propagate in a straight manner without sensing the presence of nanoplatelets. However, when the aspect ratio of the nanoplatelets becomes high, the crack begins to interact with the nanoplatelets to cause crack deflection, crack bifurcation, and even microcracking.

It should be noted that the crack deflection, crack bifurcation, and microcracking observed in epoxy/ZrP-1000 are not effective toughening mechanisms. These mechanisms are not as effective as shear banding or crazing [72]. Furthermore, in the case of the highly intercalated epoxy/ α -ZrP nanocomposite, modified by monoamine intercalating agent, the crack deflection observed does not give rise to any noticeable increase in K_{IC} [15]. This may be due to the presence of monoamine intercalating agent which greatly weakens the delamination strength of the intercalated ZrP. As a result, the toughening effect due to crack deflection mechanism is cancelled out by the weakening of the intercalating layers ahead of the crack tip.

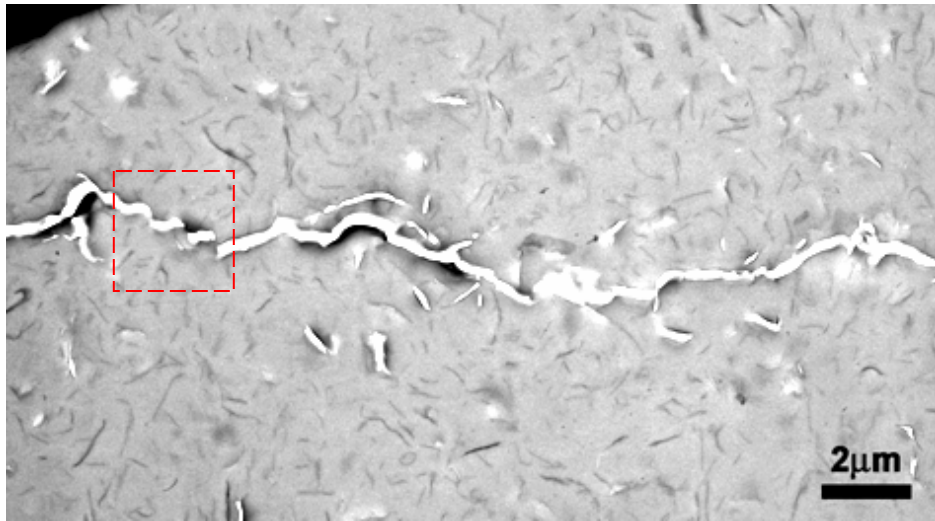


(a)

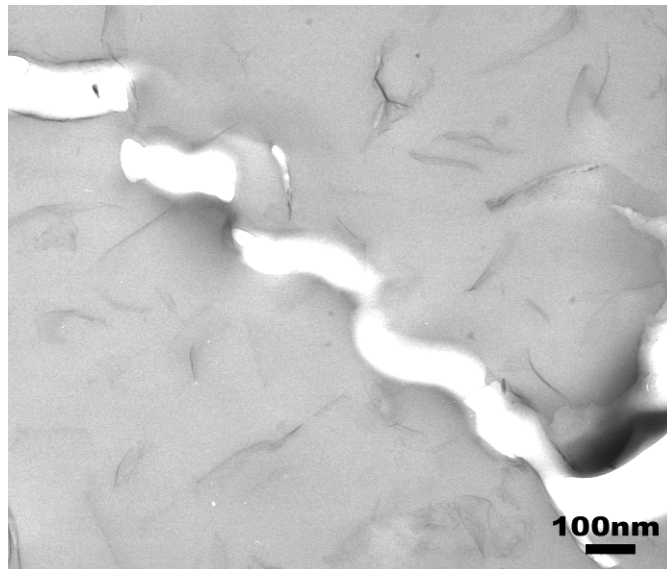


(b)

Fig. 6.7. TEM of DN-4PB damage zone of Epoxy/ZrP-100: (a) the crack wake and (b) the crack tip region. The crack propagates from left to right.

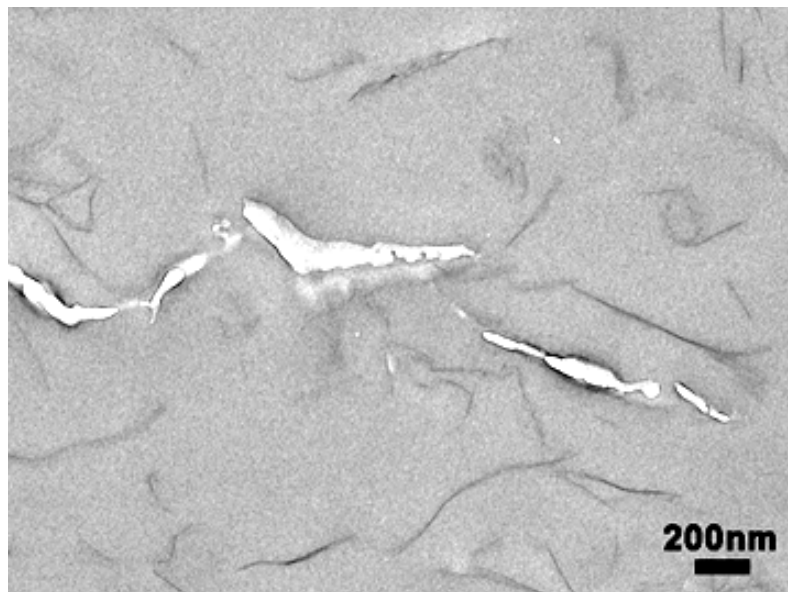


(a)



(b)

Fig. 6.8. TEM of DN-4PB damage zone of Epoxy/ZrP-1000 nanocomposite: (a) the crack wake region (low mag.) (b) the crack wake region (high mag.) and (c) the crack tip region. The crack propagates from left to right.



(c)

Fig. 6.8. Continued.

The present study clearly shows that, for polymer nanocomposite systems, the aspect ratio as well as the physical size of nanoplatelets can play an important role on their mechanical performance. Another important finding of the present study is that intercalating agent can greatly influence the mechanical properties of the polymer nanocomposites. Even though aspect ratio of the nanoplatelets does not show significant impact on the mechanical properties of epoxy due to their low loadings, it should be pointed out that aspect ratio is likely to significantly influence the gas barrier properties

and rheological behavior of the polymer matrix. The effect of the types of intercalating agents and their loadings on the gas barrier properties and rheological behavior of polymer nanocomposites will be reported in the near future.

6.4. Summary

To understand how the aspect ratio of nanoplatelets affects the mechanical property of polymer nanocomposites, epoxy/ α -ZrP nanocomposites with two different aspect ratios of 100 and 1,000 were prepared and characterized. Morphological differences between two distinctive sets of epoxy/ α -ZrP nanocomposites have been observed. Based on the present study, while the influence of aspect ratio on the mechanical properties are not significant due to the low loading level of nanoplatelets, it has a significant effect on the operative fracture mechanisms and dynamic mechanical behaviors. The present study also shows that intercalating agent can greatly influence the tensile strength and ductility of the polymer nanocomposites.

CHAPTER VII

CONCLUDING REMARKS AND RECOMMENDATIONS

The objectives of this research effort are focused on better understanding the structure-property relationship of α -ZrP based nanoplatelet-reinforced polymer nanocomposites. In order to investigate the fundamental structure-property relationship between the structural parameters of nanofillers and the physical and mechanical properties of polymer nanocomposites, a series of experimental studies have been carried out. These efforts cover a wide range of structural parameter variations of nanofillers, including loading level, degree of exfoliation, aspect ratio and type of intercalating agents.

In order to probe the structural parameters of nanofillers and morphology of nanocomposites, various techniques such as wide-angle X-ray diffraction (WAXD), optical microscopy (OM), scanning electron microscopy (SEM), transmission electron microscopy (TEM) and etc, have been utilized to confirm morphology. In addition, several mechanical tests such as tensile, fracture, and thermo-mechanical tests have been performed to finally evaluate the physical and mechanical properties of nanocomposites with the incorporation of nanofillers

7.1 Intercalation and Exfoliation of Nanoplatelets in Epoxy Nanocomposites

A new surface modification approach for improving intercalation and exfoliation efficiency of layered nanoplatelets has been introduced based on α -ZrP nanoplatelets. The intercalation of α -ZrP nanoplatelets was carried out using a number of different organic surface modifiers and their combinations. It is found that porous pathways, which can be created by incorporating a combination of a linear long chain amine and a bulky, short chain amine as intercalating agents, can lead to speedier and more effective intercalation. As a result, exfoliation is enhanced and the preparation of fully exfoliated polymer nanocomposites can be achieved. The intercalation/exfoliation mechanisms accounting for the observed effectiveness have been discussed. The proposed approach allows for effective intercalation and exfoliation of nanoplatelets, and for practical manufacturing of polymer nanocomposites.

7.2 Morphology and Mechanical Behavior of Exfoliated Epoxy/ α -Zirconium Phosphate Nanocomposites

The mechanical properties of synthetic α -ZrP based epoxy nanocomposites with variations in loading level and degree of exfoliation of α -ZrP have been investigated. The state of exfoliation and dispersion were confirmed by XRD and direct TEM imaging at different locations in the samples. Incorporation of fully exfoliated α -ZrP nanoplatelets causes significant improvements in the observed tensile properties. The double-notch four-point-bend (DN-4PB) technique was employed to investigate the fracture behavior of fully exfoliated nanoplatelet-reinforced epoxy nanocomposites. The

result suggests that, for a fully exfoliated epoxy nanocomposite system, the fracture toughness will remain comparable to that of the neat system. Based on the observations, the crack propagated in a straight manner, and there was no sign of crack deflection or debonding of nanoplatelets from the matrix. The nanoplatelets ahead of the crack were broken into two halves as the crack propagated through, indicating strong bonding between the nanoplatelet and the epoxy matrix.

7.3 Effects of Nanoplatelet Dispersion on Mechanical Behavior of Polymer

Nanocomposites

Through the manipulation of processing conditions, three levels of exfoliation of synthetic α -ZrP nanoplatelets in epoxy matrices have been achieved. TEM and WAXS were utilized to confirm the three different levels of exfoliation of nanoplatelets in epoxy/ α -ZrP nanocomposites. As expected, it was found that modulus and strength of the nanocomposite are affected by the dispersion extent of the nanoplatelets. It was also found that the operative fracture mechanisms depend strongly on the state of the nanoplatelets dispersion. The crack deflection mechanism, which leads to a tortuous path crack growth, was only observed for poorly dispersed nanocomposites. Delamination of intercalated nanoplatelets and crack deflection were observed in a moderately dispersed system. In the case of fully exfoliated system, the crack only propagated in a straight fashion, which indicates that the fully exfoliated individual nanoplatelet have minimal effects on the propagation of the crack. The implication of the present findings for structural applications of polymer nanocomposites has been discussed in the chapter.

7.4 Effects of Nanoplatelet Aspect Ratio on Mechanical Properties of Epoxy

Nanocomposites

To study the effect of the aspect ratio of nanoplatelets on the mechanical properties of polymer nanocomposites, epoxy/ α -zirconium phosphate nanocomposites with two distinctive aspect ratios of approximately 100 and 1,000 have been prepared and characterized. SEM and TEM were utilized to confirm the two different sizes and aspect ratios of nanoplatelets in epoxy. From the results, it is found that mechanical properties of the nanocomposite are affected by the aspect ratio of nanoplatelets in epoxy. That is, a higher aspect ratio renders a better improvement in modulus. It is also found that the interfacial characteristics between the nanoplatelets and polymer matrix are most critical in affecting the strength and ductility of the polymer. The operative fracture mechanisms depend strongly on the aspect ratio of the nanoplatelets incorporated. The crack deflection mechanism, which leads to a tortuous path crack growth, is only observed for the high aspect ratio system. The implication of the present findings for structural applications of polymer nanocomposites has been discussed.

7.5 Recommendations for Future Work

The fundamental structure-property relationship of nanoplatelet-reinforced polymer nanocomposites is a complex issue. To further investigate this complicated relationship between structural parameters of nanofillers and mechanical/physical properties of polymer nanocomposites, a great deal of effort is still needed. In order to

develop a more fundamental understanding of this complex issue, some recommendations for future work have been presented in the following.

7.5.1 Intercalating Agent and Interface Study

The dissertation addresses the mechanical properties of epoxy nanocomposites loaded with synthetic α -ZrP clay, specifically looking at how the degree of exfoliation or dispersion, and aspect ratio of the nanoplatelets impact the mechanical and physical properties. However, there are still some unanswered questions particularly in terms of the surface modifier and interface between the nanoplatelets and epoxy matrix.

Apparently, in the monoamine-based systems, some of the unreacted monoamine used to intercalate the α -ZrP nanoplatelets ends up reacting with the epoxy, effectively reducing the cross-link density of the matrix. Therefore, there is a dramatic drop in the T_g of the nanocomposite for all loading levels (Chapter V). However in the case of quaternary ammonium salt-based systems, the T_g of the nanocomposites are only slightly affected (Chapter VI).

Therefore, it can be noticed that the type of intercalating agent (surface modifier) incorporated may have a more significant effect on the T_g of epoxy. Furthermore, considering the tensile strength and ductility of the epoxy nanocomposites, the observed drops in strength and ductility can be attributed not only to higher curing levels of the epoxy matrix but also to the more rigid interface between the polymer and the nanoplatelets which restricts the segmental motion near the organic–inorganic interfaces (Chapter VI). It has been found that the interfacial properties between dispersed

nanoplatelets and matrix play an important role on the structure-property relationship of nanocomposites.

In this respect, further studies in terms of the types of intercalating agent and their effects on the matrix and the interface should be performed in a systematic fashion.

7.5.2 Toughenability Study of Nanoplatelet-Dispersed Epoxy Nanocomposites

In this study, it has been shown that, when the nanoplatelets are fully exfoliated and well-dispersed, and have at smaller sizes than the crack tip radius, the propagating crack would grow more or less in a straight fashion and no signs of crack deflection or bifurcation can be observed. Also, there was no increase in the observed fracture toughness of the model systems.

The above finding was observed based on brittle DGEBA/DDS epoxy. A question may arise if such a finding can be extended to ductile epoxy matrices. Thus, if a more ductile epoxy system was chosen, would they show the same outcome? If we were to adopt a relatively ductile epoxy system for the study, would we have a similar result? The toughening mechanisms and their effectiveness in fully exfoliated epoxy nanocomposites are not always intuitively clear due to the scale differences. Kinloch *et al.* [73] has also emphasized this issue in his reports. However, the above-mentioned question has not yet been completely addressed and clarified. Performing a set of experiments with a set of well-defined model systems with ductile epoxy matrices can help clarify the ambiguities.

In summary, the α -ZrP nanoplatelet-reinforced epoxy nanocomposites are a set of highly suitable model systems for studying the fundamental structure-property relationship of nanoplatelet-reinforced polymer nanocomposites. For a well-controlled experimental study, each control factor of α -ZrP-based model system can be altered independently with certainty. Therefore, further studies focusing on α -ZrP nanoplatelets with variations in intercalating agents, interface, matrix properties, and toughenability can be of great importance, and should be pursued.

REFERENCES

- [1] Balakrishnan S, Raghavan D. *Macromolecular Rapid Communications* 2004;25:481.
- [2] Miyagawa H, Rich MJ, Drzal LT. *Journal of Polymer Science Part B-Polymer Physics* 2004;42:4384.
- [3] Miyagawa H, Rich MJ, Drzal LT. *Journal of Polymer Science Part B-Polymer Physics* 2004;42:4391.
- [4] Miyagawa H, Jurek RJ, Mohanty AK, Misra M, Drzal LT. *Composites Part A-Applied Science and Manufacturing* 2006;37:54.
- [5] Balakrishnan S, Raghavan D. *Journal of Reinforced Plastics and Composites* 2005;24:785.
- [6] Massam J, Wang Z, Pinnavaia TJ, Lan T, Beall G. *Abstr Pap Am Chem S* 1998;215:U344.
- [7] Wang MS, Pinnavaia TJ. *Chemistry of Materials* 1994;6:468.
- [8] Ratna D, Manoj NR, Varley R, Raman RKS, Simon GP. *Polymer International* 2003;52:1403.
- [9] Pinnavaia TJ, Lan T, Wang Z, Shi HZ, Kaviratna PD. *Nanotechnology* 1996;622:250.
- [10] Jan IN, Lee TM, Chiou KC, Lin JJ. *Industrial & Engineering Chemistry Research* 2005;44:2086.

- [11] Wu DF, Zhou CX, Yu W, Xie F. *Journal of Applied Polymer Science* 2006;99:340.
- [12] Miyagawa H, Drzal LT. *Journal of Adhesion Science and Technology* 2004;18:1571.
- [13] Miyagawa H, Mohanty A, Drzal LT, Misra M. *Industrial & Engineering Chemistry Research* 2004;43:7001.
- [14] Shah D, Maiti P, Jiang DD, Batt CA, Giannelis EP. *Advanced Materials* 2005;17:525.
- [15] Sue HJ, Gam KT, Bestaoui N, Clearfield A, Miyamoto M, Miyatake N. *Acta Mater* 2004;52:2239.
- [16] Wang Z, Pinnavaia TJ. *Abstracts of Papers of the American Chemical Society* 1998;216:U308.
- [17] Shi HZ, Lan T, Pinnavaia TJ. *Chemistry of Materials* 1996;8:1584.
- [18] Giannelis EP. *Adv Mater* 1996;8:29.
- [19] Lan T, Pinnavaia TJ. *Chem Mater* 1994;6:2216.
- [20] Lan T, Kaviratna PD, Pinnavaia TJ. *Chemistry of Materials* 1994;6:573.
- [21] Pinnavaia TJ, Lan T, Kaviratna PD, Wang Z, Shi HH. *Abstracts of Papers of the American Chemical Society* 1995;210:61.
- [22] Kojima Y, Usuki A, Kawasumi M, Okada A, Fukushima Y, Kurauchi T, Kamigaito O. *J Mater Res* 1993;8:1185.
- [23] Kojima Y, Usuki A, Kawasumi M, Okada A, Kurauchi T, Kamigaito O. *J Polym Sci Pol Chem* 1993;31:983.

- [24] Usuki A, Kojima Y, Kawasumi M, Okada A, Fukushima Y, Kurauchi T, Kamigaito O. *Journal of Materials Research* 1993;8:1179.
- [25] Yano K, Usuki A, Okada A, Kurauchi T, Kamigaito O. *J Polym Sci Pol Chem* 1993;31:2493.
- [26] Zhu J, Start P, Mauritz KA, Wilkie CA. *Polym Degrad Stabil* 2002;77:253.
- [27] Sue HJ, Gam KT, Bestaoui N, Spurr N, Clearfield A. *Chemistry of Materials* 2004;16:242.
- [28] Sun L, Boo WJ, Browning RL, Sue H-J, Clearfield A. *Chem Mater* 2005;17:5606.
- [29] Clearfield A, Berman JR. *Journal of Inorganic & Nuclear Chemistry* 1981;43:2141.
- [30] Saber-Samandari S, Khatibi AA, Basic D. *Composites Part B-Engineering* 2007;38:102.
- [31] Yasmin A, Luo JJ, Abot JL, Daniel IM. *Composites Science and Technology* 2006;66:2415.
- [32] Chen L, Wang K, Toh ML, Kotaki M, He CB. *Abstracts of Papers of the American Chemical Society* 2005;230:U3563.
- [33] Wang H, Hoa SV, Wood-Adams PM. *Journal of Applied Polymer Science* 2006;100:4286.
- [34] Wang Q, Song CF, Lin WW. *Journal of Applied Polymer Science* 2003;90:511.
- [35] Lee CR, Ihn KJ, Gong MS. *Polymer-Korea* 2003;27:392.
- [36] Yasmin A, Abot JL, Daniel IM. *Scripta Materialia* 2003;49:81.
- [37] Park JH, Jana SC. *Macromolecules* 2003;36:2758.

- [38] Triantafillidis CS, LeBaron PC, Pinnavaia TJ. *Chemistry of Materials* 2002;14:4088.
- [39] Agag T, Takeichi T, Toda H, Kobayashi T. *International Journal of Materials & Product Technology* 2001;2:706.
- [40] Kornmann X, Lindberg H, Berglund LA. *Polymer* 2001;42:4493.
- [41] Ke YC, Lu JK, Yi XS, Zhao J, Qi ZN. *Journal of Applied Polymer Science* 2000;78:808.
- [42] Uhl FM, Webster DC, Davuluri SP, Wong SC. *European Polymer Journal* 2006;42:2596.
- [43] Ma HY, Fang ZP, Tong LF. *Polymer Degradation and Stability* 2006;91:1972.
- [44] Miyagawa H, Drzal LT, Miyagawa H, Carsello JA. *Polymer Engineering and Science* 2006;46:452.
- [45] Wang K, Chen L, Wu JS, Toh ML, He CB, Yee AF. *Macromolecules* 2005;38:788.
- [46] Lu HJ, Liang GZ, Ma XY, Zhang BY, Chen XB. *Polymer International* 2004;53:1545.
- [47] Daniel IM, Miyagawa H, Gdoutos EE, Luo JJ. *Experimental Mechanics* 2003;43:348.
- [48] Myskova MZ, Zelenka J, Spacek V, Socha F. *Mechanics of Composite Materials* 2003;39:119.
- [49] Park SJ, Seo DI, Lee JR. *Journal of Colloid and Interface Science* 2002;251:160.

- [50] Lee A, Lichtenhan JD, Reinerth WA. Abstracts of Papers of the American Chemical Society 2000;219:U485.
- [51] Lee A, Lichtenhan JD. Journal of Applied Polymer Science 1999;73:1993.
- [52] Skowronski JM, Shioyama H. Carbon 1995;33:1473.
- [53] Shioyama H. Carbon 1997;35:1664.
- [54] Harris DJ, Bonagamba TJ, Schmidt-Rohr K. Macromolecules 1999;32:6718.
- [55] Spurr NA, Bestaoui N, Gam KT, Sue HJ, Clearfield A. Abstracts of Papers of American Chemical Society 2003;225:U51.
- [56] Usuki A, Kojima Y, Kawasumi M, Okada A, Kurauchi T, Kamigaito O. Abstracts of Papers of the American Chemical Society 1990;200:218.
- [57] Messersmith PB, Giannelis EP. Chemistry of Materials 1994;6:1719.
- [58] Burnside SD, Giannelis EP. American Chemical Society 1996;212:19.
- [59] Messersmith PB, Giannelis EP. Chem Mater 1993;5:1064.
- [60] Wang H, Zeng CC, Elkovitch M, Lee LJ, Koelling KW. Polym Eng Sci 2001;41:2036.
- [61] Wang Z, Lan T, Pinnavaia TJ. Abstracts of Papers of American Chemical Society 1996;211:455.
- [62] Wang Z, Pinnavaia TJ. Chemistry of Materials 1998;10:1820.
- [63] Lan T, Wang Z, Shi HZ, Pinnavaia TJ. Abstracts of Papers of the American Chemical Society 1995;210:157.
- [64] Pinnavaia TJ, Lan T, Kaviratna PD, Wang Z, Shi HH. Abstracts of Papers of the American Chemical Society 1995;210:61.

- [65] Masenelli-Varlot K, Reynaud E, Vigier G, Varlet J. *J Polym Sci Pol Phys* 2002;40:272.
- [66] Chan CM, Wu JS, Li JX, Cheung YK. *Polymer* 2002;43:2981.
- [67] Thio YS, Argon AS, Cohen RE, Weinberg M. *Polymer* 2002;43:3661.
- [68] Liu TX, Tjiu WC, Tong YJ, He CB, Goh SS, Chung TS. *J Appl Polym Sci* 2004;94:1236.
- [69] Zerda AS, Lesser AJ. *J Polym Sci Pol Phys* 2001;39:1137.
- [70] Sue HJ, Yee AF. *J Mater Sci* 1989;24:1447.
- [71] Liu WP, Hoa SV, Pugh M. *Compos Sci Technol* 2005;65:307.
- [72] Gam KT, Miyamoto M, Nishimura R, Sue HJ. *Polym Eng Sci* 2003;43:1635.
- [73] Kinloch AJ, Taylor AC. *J Mater Sci Lett* 2003;22:1439.
- [74] Juwono A, Edward G. *Journal of Nanoscience and Nanotechnology* 2006;6:3943.
- [75] Karak N. *Journal of Polymer Materials* 2006;23:1.
- [76] Gyoo PM, Venkataramani S, Kim SC. *Journal of Applied Polymer Science* 2006;101:1711.
- [77] Oh TK, Hassan M, Beatty C, El-Shall H. *Journal of Applied Polymer Science* 2006;100:3465.
- [78] Wang K, Wang L, Wu JS, Chen L, He CB. *Langmuir* 2005;21:3613.
- [79] Gam KT, Sue HJ. *American Chemical Society* 2000;219:U498.
- [80] Weon JI, Sue HJ. *Polymer* 2005;46:6325.
- [81] Alexandre M, Dubois P. *Mat Sci Eng R* 2000;28:1.
- [82] Boo W-J, Sun L, Liu J, Clearfield A, Sue H-J. *Compos Sci Technol* 2007;67:262.

- [83] Liu J, Boo WJ, Clearfield A, Sue HJ. *Materials and Manufacturing Processes* 2006;22:829.
- [84] Vaia RA, Giannelis EP. *Macromolecules* 1997;30:7990.
- [85] Vaia RA, Giannelis EP. *Macromolecules* 1997;30:8000.
- [86] Blumstei.A. *Journal of Polymer Science Part A-General Papers* 1965;3:2665.
- [87] Krishnamoorti R, Vaia RA, Giannelis EP. *Chem Mater* 1996;8:1728.
- [88] Xu B, Zheng Q, Song YH, Shangguan Y. *Polymer* 2006;47:2904.
- [89] Kim BK, SEO JW, Jeong HM. *Euro. Polymer* 2003;39:85.
- [90] Lan T, Kaviratna PD, Pinnavaia TJ. *Chem Mater* 1995;7:2144.
- [91] Clearfield A, Medina AS, Duax WL, Garces JM. *J Inorg Nucl Chem* 1972;34:329.
- [92] Sun L, Boo WJ, Clearfield A, Sue HJ. *New Journal of Chemistry* 2006;DOI: 10.1039/b604054c
- [93] Vaia RA, Teukolsky RK, Giannelis EP. *Chem Mater* 1994;6:1017.
- [94] Ajayan PM, Schadler LS, Braun PV. *Nanocomposite Science and Technology* Weinheim: Wiley-VCH, 2003.
- [95] Ginzburg VV, Gendelman OV, Manevitch LI. *Physical Review Letters* 2001;86:5073.
- [96] Boo WJ, Sun L, Liu J, Moghbelli E, Clearfield A, Sue HJ. *J Polym Sci Pol Phys* 2007;submitted.
- [97] Boo W-J, Sun LY, Warren GL, Moghbelli E, Pham H, Clearfield A, Sue H-J. *Polymer* 2007;48:1075.

- [98] Kim HN, Keller SW, Mallouk TE, Schmitt J, Decher G. *Chemistry of Materials* 1997;9:1414.
- [99] Chen L, Wang K, Toh ML, He CB. *Macromolecular Materials and Engineering* 2005;290:1029.
- [100] Clearfield A, Duax WL, Medina AS, Smith GD, Thomas JR. *Journal of Physical Chemistry* 1969;73:3424.
- [101] Sue HJ, Yee AF. *Journal of Materials Science* 1993;28:2975.
- [102] Chin IJ, Thurn-Albrecht T, Kim HC, Russell TP, Wang J. *Polymer* 2001;42:5947.
- [103] Gam KT, Sue HJ. *PMSE* 2000;219:U498.
- [104] Lu HJ, Zhang BY, Chen XB. *Transactions of Nonferrous Metals Society of China* 2005;15:211.
- [105] Nigam V, Setua DK, Mathur GN, Kar KK. *Journal of Applied Polymer Science* 2004;93:2201.
- [106] Miyagawa H, Foo KH, Daniel IM, Drzal LT. *Journal of Applied Polymer Science* 2005;96:281.
- [107] Shen MM, Lu MG, Chen YL, Ha CY. *Polymer International* 2005;54:1163.
- [108] Kong D, Park CE. *Chemistry of Materials* 2003;15:419.
- [109] Sun L, Boo WJ, Tien CW, Clearfield A, Sue HJ. *Chemistry of Materials* 2007; accepted.
- [110] Ray SS, Okamoto M. *Progress in Polymer Science* 2003;28:1539.
- [111] Kim JK, Hu CG, Woo RSC, Sham ML. *Composites Science and Technology* 2005;65:805.

- [112] Altintzi I, Chrissopoulou K, Anastasiadis SH, Pitsikalis M, Hadjichristidis N, Theophilou N, Giannelis EP. Abstracts of Papers of the American Chemical Society 2005;229:1127.
- [113] Chrissopoulou K, Altintzi I, Anastasiadis SH, Giannelis EP, Pitsikalis M, Hadjichristidis N, Theophilou N. Polymer 2005;46:12440.
- [114] Kawasumi M, Hasegawa N, Kato M, Usuki A, Okada A. Macromolecules 1997;30:6333.
- [115] Hasegawa N, Kawasumi M, Kato M, Usuki A, Okada A. J Appl Polym Sci 1998;67:87.
- [116] Sue HJ, Pearson RA, Parker DS, Huang J, Yee AF. Abstracts of Papers of the American Chemical Society 1988;196:62.
- [117] Fornes TD, Yoon PJ, Hunter DL, Keskkula H, Paul DR. Polymer 2002;43:5915.
- [118] Mohan TP, Kumar MR, Velmurugan R. Polymer International 2005;54:1653.
- [119] Velmurugan R, Mohan TP. Journal of Materials Science 2004;39:7333.
- [120] Kornmann X, Lindberg H, Berglund LA. Polymer 2001;42:1303.
- [121] Triantafillidis CS, LeBaron PC, Pinnavaia TJ. Journal of Solid State Chemistry 2002;167:354.
- [122] Hasegawa N, Okamoto H, Kato M, Usuki A. J Appl Polym Sci 2000;78:1918.
- [123] Kato M, Usuki A, Okada A. J Appl Polym Sci 1997;66:1781.
- [124] Tyan HL, Liu YC, Wei KH. Chemistry of Materials 1999;11:1942.
- [125] Hasegawa N, Okamoto H, Kawasumi M, Usuki A. J Appl Polym Sci 1999;74:3359.

- [126] Essawy HA, Badran AS, Youssef AM, Abd El Haki AEA. *Macromol Chem Phys* 2004;205:2366.
- [127] Morgan AB, Harris JD. *Polymer* 2004;45:8695.
- [128] Kellar JJ, Herpfer MA, Moudgil BM, Society for Mining Metallurgy and Exploration (U.S.). *Functional fillers and nanoscale minerals*. Littleton, CO.: Society for Mining Metallurgy and Exploration, 2003.
- [129] Hasegawa N, Okamoto H, Kawasumi M, Kato M, Tsukigase A, Usuki A. *Macromol Mater Eng* 2000;280:76.
- [130] Maiti P, Yamada K, Okamoto M, Ueda K, Okamoto K. *Chemistry of Materials* 2002;14:4654.
- [131] Osman MA, Mittal V, Lusti HR. *Macromol Rapid Comm* 2004;25:1145.
- [132] Ray SS, Maiti P, Okamoto M, Yamada K, Ueda K. *Macromolecules* 2002;35:3104.
- [133] Ha B, Char K, Jeon HS. *J Phys Chem B* 2005;109:24434.

APPENDIX A

RHEOLOGICAL BEHAVIOR OF MODEL EPOXY NANOCOMPOSITES

A1. Introduction

Since the introduction of polymer nanocomposites which contain exfoliated nanoplatelets two decades ago, polymer nanocomposites research in academia and industry has been both intensive and extensive. When fully exfoliated, nanoplatelet-reinforced polymer nanocomposites exhibit enhanced material properties, including higher modulus, better thermal stability, superior flame retardancy and improved barrier properties.

Until recently, research work on polymer nanocomposites has been mainly focused on morphology, barrier properties, and mechanical properties. With more and more expected engineering applications of polymer nanocomposite in the near future, it is necessary that the rheological behavior of polymer nanocomposites be investigated. The rheological behaviors of several polymer nanocomposite systems have recently been reported. However, no systematic analysis or modeling was performed to establish structure-rheology relationship. Thus, more work is needed to fundamentally understand the rheological behavior of polymer nanocomposites for engineering applications.

It has been shown that, based on the rheological behavior studies, precious insights for improving processability of polymer nanocomposites can be gained. It is also possible that molecular scale interactions between molecules and nanoplatelets may be revealed. For example, Galgali *et al.* reported that the typical rheological responses in

nanocomposite system, such as increased viscosity and solid-like rheological response, were caused by the frictional interactions between the dispersed nanoplatelets, rather than due to the immobilization of confined polymer. Wagener *et al.* also found that shear thinning was a characteristic feature of truly nanodispersed composites. They demonstrated that the shear thinning exponent, n , was a semi-quantitative indicator of the degree of exfoliation and dispersion. Also, they claimed that shear thinning was triggered and prolonged by the shear-induced alignment of dispersed nanoplatelets.

In addition to the aforementioned studies with molten-state thermoplastic-based nanocomposites, rheological behaviors of prepolymers, such as uncured epoxy resin, have also been studied. For example, Wang *et al.* chose diglycidyl ether of bisphenol-A (DGEBA) epoxy resin and organically modified montmorillonite (MMT) clay to study the effects of well-dispersed nanoplatelets on the rheological behavior of epoxy prepolymers. They proposed that a good dispersion of nanoplatelets led to high viscosity and strong shear thinning behavior in the uncured system due to two reasons: (1) increased interactions between the clay and epoxy molecules and (2) increased clay-clay frictional forces. They also learned that this increase in viscosity was not from the introduction of free amine groups, nor from the presence of water molecules in epoxy.

After numerous research efforts, it has been accepted that the presence of nanoplatelets in polymers or prepolymers usually causes viscosity increase and shear thinning phenomenon. However, the exact reasons why the nanoplatelets bring about such phenomena are still unclear. Furthermore, it is still uncertain how the degree of

dispersion and aspect ratio of nanoplatelets influence the rheological behavior of polymer nanocomposites.

To address above important issues, systematic investigations of two sets of model epoxy systems, i.e., epoxy/synthetic α -Zirconium phosphate (epoxy/ZrP) with variations in nanoplatelet degree of dispersion and changes in aspect ratio have been carried out. In this study, polymer nanocomposites containing three distinctive levels of dispersion and two different aspect ratios of ZrP nanoplatelets have been prepared. The chemical compositions and processing have been kept the same for samples in each set of model systems. Thus, these model samples are suitable for unambiguous investigations of the effects of nanoplatelet dispersion and aspect ratio on the rheological behaviors of epoxy prepolymer. Additionally, by employing an established physical model, the rheological behavior of the model epoxy nanocomposite systems has been modeled against surface area, aspect ratio, and hydrodynamic volume. Implication of the current research for the processing and fabrication of polymer nanocomposites based parts for engineering applications are also addressed.

A2. Experimental

A2.1. Materials

The ZrP crystals with two distinctively different aspect ratios of 100 (ie, ZrP-100) and 1000 (ie, ZrP-1000) were prepared. Detailed chemistry and procedures for the synthesis of α -ZrP and control of its aspect ratios can be found elsewhere. Fig. A1 displays the SEM micrographs of the ZrP-100 and ZrP-1000 crystals, respectively.

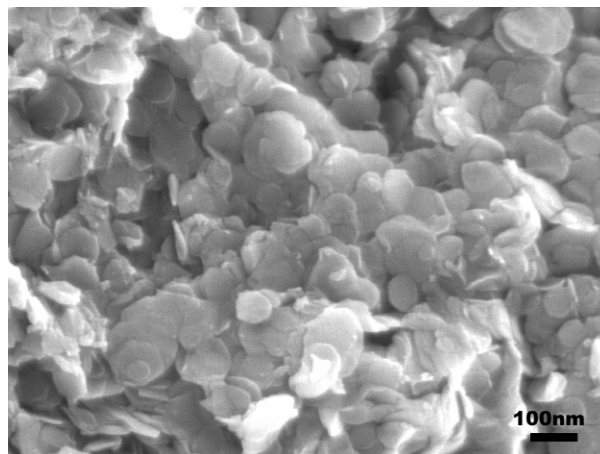
Commercially available monoamine, polyoxyalkyleneamine (Jeffamine[®] M600, Huntsman Chemical) and tetra-*n*-butyl ammonium hydroxide (TBA) were used as intercalating agents for ZrP. DGEBA epoxy resin (D.E.R.[™] 332 epoxy resin, The Dow Chemical Company) was chosen as the matrix resin for the rheology study. All the chemicals, except the epoxy resin which was dried in a vacuum oven for 24 hrs prior to sample preparation, were used as received.

A2. 2. Preparation of ZrP Dispersion in Epoxy Resin

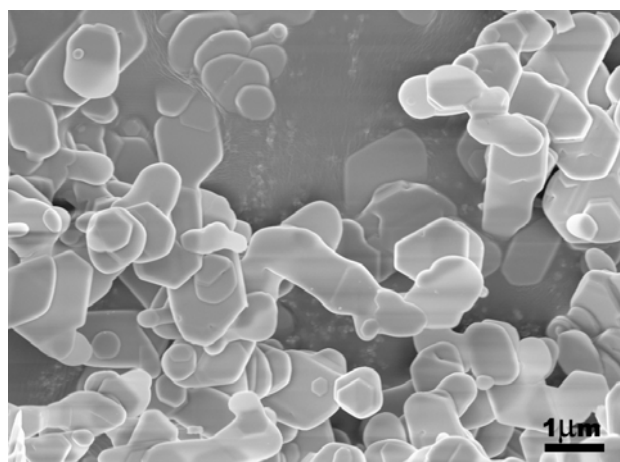
To systematically investigate how the degree of exfoliation and aspect ratio affect rheological behavior, two sets of model epoxy/ZrP systems were prepared. The detailed information of the samples is summarized in Table A1.

Table A1. Prepared sample and loading level, level of exfoliation, and aspect ratio of α -ZrP

Sample	Vol %	Degree of Exfoliation	Aspect Ratio of α -ZrP	Intercalating agent
Epoxy/M600	0	–	–	Jeffamine [®] M600
Poor exfoliation	2.0	Poor	100	Jeffamine [®] M600
Moderate Exfoliation	2.0	Moderate	100	Jeffamine [®] M600
Good exfoliation	2.0	Good	100	Jeffamine [®] M600
Epoxy/TBA	0	–	–	TBA
High aspect ratio	0.7	Good	100	TBA
Low aspect ratio	0.7	Good	1,000	TBA



(a)



(b)

Fig. A1. SEM images of α -ZrP nanoplatelets with aspect ratio of about (a) 100 and (b) 1,000.

To control the degree of exfoliation of ZrP in epoxy, the intercalation processing conditions using Jeffamine[®] M600 were systematically altered to achieve various levels of ZrP dispersion in the epoxy resin. The detailed procedures for achieving the intercalation and exfoliation of ZrP in epoxy can be found elsewhere. To prepare epoxy/ZrP-100 and epoxy/ZrP-1000 samples, tetra-n-butyl ammonium was utilized as the intercalating agent to achieve exfoliation in epoxy. The detailed procedures for sample preparation can be found elsewhere.

After the intercalation and exfoliation processes in epoxy, solvent was removed by using Rotavapor[®] in a water bath. The uncured epoxy/ZrP samples were then prepared for rheological study.

A2. 3. Morphology Characterizations

Wide angle X-ray diffraction (WAXD) analysis was performed on a Bruker D8 diffractometer with Bragg-Brentano θ - 2θ geometry at a set operating voltage and current of 40 kV and 40 mA, respectively. Diffraction patterns were obtained for 2θ in the range from 2° to 30° with a step size of 0.04° and a count time of 2 seconds per step.

Scanning electron microscopy (SEM) images of α -ZrP nanoplatelets were acquired using a Zeiss Leo 1530 VP Field Emission-SEM (FE-SEM). The samples were sputter-coated with a thin layer (ca. 3 nm) of Pt/Pd (80/20) prior to SEM observation. For transmission electron microscopy (TEM) observation, a JEOL 1200 EX electron microscope operated at an accelerating voltage of 100 kV was utilized. Details of the microtomy and microscopy techniques employed here are given elsewhere^{29,30}.

A2. 4. Rheological Property Measurement

Rheological behavior characterization was performed using a Brookfield (Essex, UK) DV-III⁺ rheometer equipped with Thermosel[®] heating chamber and a programmable temperature controller. An HT-2 sample chamber (10.5 mL) and an SCH-27 link hanging spindle with extension link were used. The testing temperatures were set at 28, 50 and 80°C, respectively. Before testing, the system was stabilized for 30 min to equilibrate at the set temperature between the sample and spindle. The shear rate was set from 0.1 to 80/s. The data acquired were recorded and processed by program Brookfield Rheocalc (v. 2.4).

A3. Results and Discussion

The significance of this study is that three distinctive levels of exfoliation and two different aspect ratios of ZrP nanoplatelets in epoxy have been successfully achieved and characterized. No structural or compositional changes were made in each set of model system. As a result, the present study can unambiguously reveal how the level of dispersion and aspect ratio of nanoplatelets can affect rheological behavior of epoxy nanocomposites before curing.

The characterization of the structure and morphology of the model epoxy/ZrP systems with variations in degree of dispersion and aspect ratio have presented elsewhere. They will not be repeated here. For convenience, the typical morphologies of the model epoxy/ZrP systems are shown in Figs. A2 and A3. As shown in Fig. A2, three different levels of dispersion of ZrP nanoplatelets in epoxy can be clearly differentiated:

(a) poorly exfoliated, (b) moderately exfoliated, and (c) fully exfoliated. All the samples contain 2.0 vol% of ZrP nanoplatelets. Fig. A3 displays the TEM images showing exfoliated ZrP-100 and ZrP-1000 nanoplatelets (0.7 vol%) in epoxy. Fig. A3(a) clearly shows random orientation of ZrP nanoplatelets. In Fig. A3(b) and A3(c), ZrP-1000 nanoplatelets exhibit significant curvature in epoxy. It should be noted that when the ZrP-1000 has a concentration above 0.7 vol%, the viscosity becomes too high for handling and removal of trapped air. As a result, only 0.7 vol% of ZrP is utilized for the investigation of aspect ratio effect on rheological behaviors.

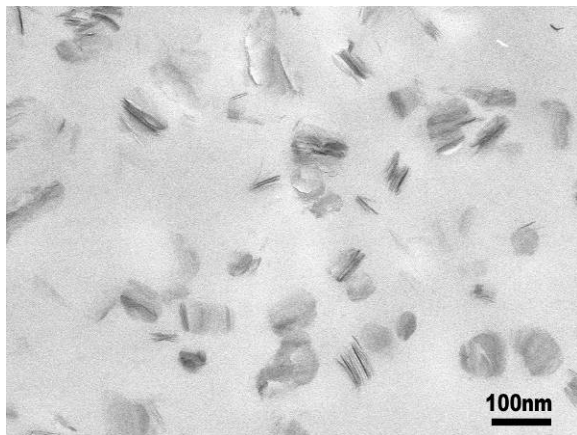
Once the viscosity data as a function of shear rate at three different temperatures are collected, the Power Law model which takes the form of:

$$\tau = KD^n \quad (1)$$

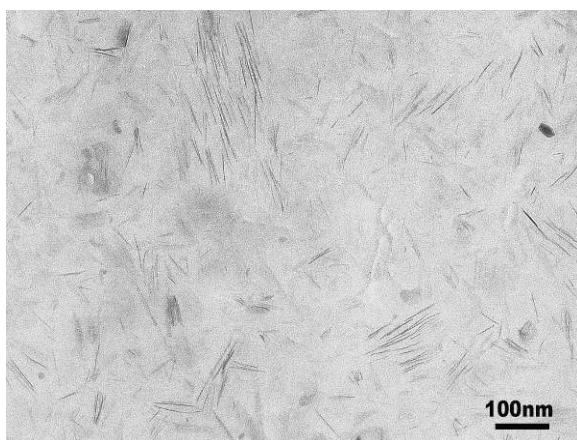
is utilized to fit the experimental findings; where, τ is shear stress, D is shear rate ($\dot{\gamma}$), K is consistency index, and n is flow behavior index.

In order to determine the K and n , logarithmic plots of τ vs. $\dot{\gamma}$ are constructed and fitted to a straight line. The n value ranges from unity to zero. As $n=1$, the equation reduces to the constitutive equation of a Newtonian fluid. When n is < 1 , shear thinning behavior is observed. The lower the n value, the more pronounced is the shear thinning behavior. The value of the consistency index (K) is taken from the intercept from the τ axis and therefore represents the viscosity at unit shear rate. As has been well known, K is sensitive to temperature, whereas n is much less sensitive. The calculated results from

the rheological behavior study of various levels of exfoliation and aspect ratios of ZrP nanoplatelets in epoxy are presented in Tables A2 and A3, respectively.

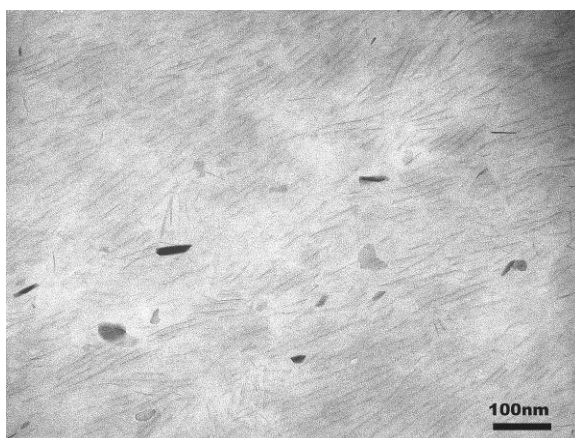


(a)



(b)

Fig. A2. TEM of epoxy/ α -ZrP showing (a) poor exfoliation, (b) moderate exfoliation and (c) good exfoliation. All samples contain the same amount of α -ZrP (2.0 vol%) and intercalating agent in epoxy.

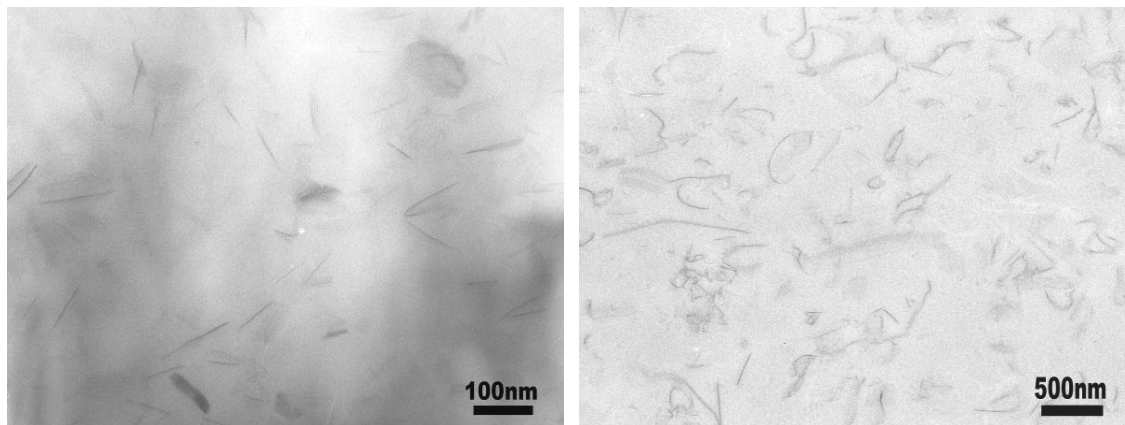


(c)

Fig. A2. Continued.

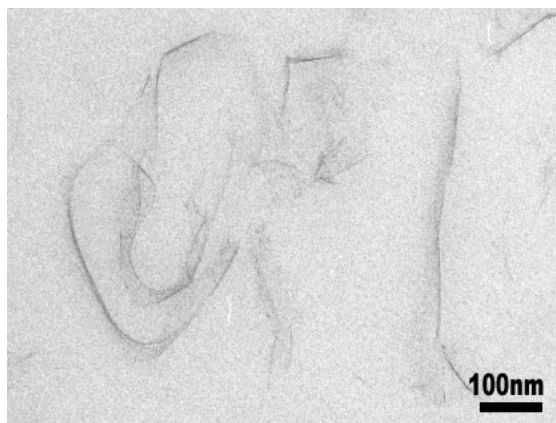
Table A2. Power law factors affected by level of exfoliation of α -ZrP

Temperature (°C)	Samples / exfoliation level	Consistency index (K)	Flow index (n)	Confident of Fit (%)
28	Neat epoxy	3352	0.96	97.1
	Epoxy/Jeffamine	2560	0.96	98.6
	Poor	6630	0.92	99.6
	Good	7209	0.91	99.1
50	Neat epoxy	428	0.96	97.7
	Poor	840	0.91	99.4
	Good	1142	0.85	99.2
80	Neat epoxy	52	0.96	98.6
	Poor	313	0.80	97.9
	Good	834	0.53	98.7



(a)

(b)



(c)

Fig. A3. TEM images of nanocomposites reinforced with (a) α -ZrP of aspect ratio of 100 at high magnification, aspect ratio of 1,000 (b) at low magnification, and (c) high magnification.

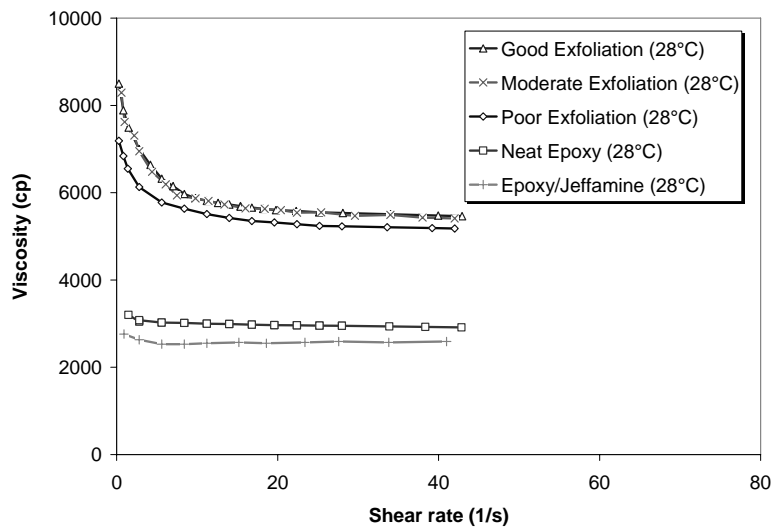
Table A3. Power law factors in terms of aspect ratio of α -ZrP

Temperature (°C)	Samples / aspect ratio	Consistency index (K)	Flow index (n)	Confident of Fit (%)
28	Neat epoxy	3352	0.96	97.1
	Epoxy/TBA	4125	0.95	98.1
	100	8469	0.93	97.9
	1,000	53928	0.37	97.5
50	Neat epoxy	428	0.96	97.7
	100	1561	0.81	97.9
	1,000	27467	0.29	97.8
80	Neat epoxy	52	0.96	98.6
	100	504	0.73	97.9
	1,000	11027	0.17	99.7

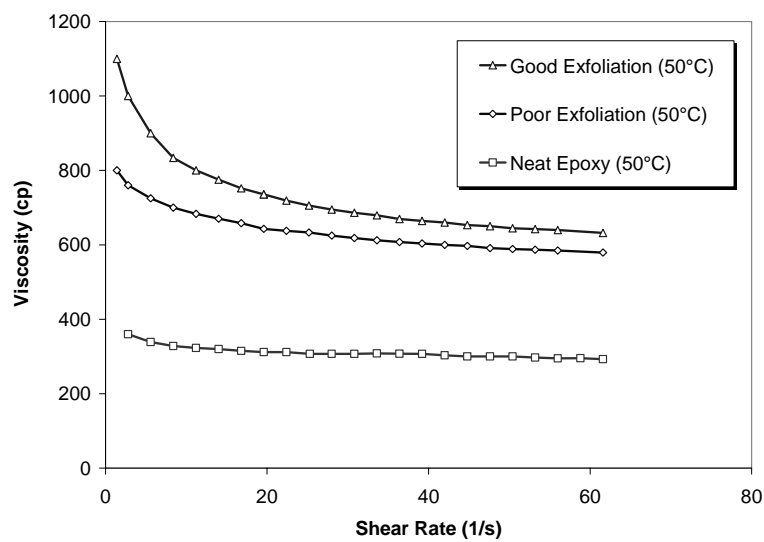
Fig. A4 shows the representative plots revealing the shear viscosity dependence of how the level of nanoplatelet exfoliation in epoxy affects viscosity at three different temperatures. As shown in Fig. A4(a), there is no appreciable differences in rheological behavior between the exfoliated and moderately exfoliated systems. Thus, viscosity curves of moderately exfoliated system are omitted from Figs. A4(b) and A4(c) to prevent overcrowding of the Figs.

From Fig. A4, as expected, all three epoxy nanocomposites show a strong dependence on temperature. The neat epoxy prepolymer can be considered a Newtonian fluid at all temperatures tested. The incorporation of 2.0 vol% of exfoliated ZrP

nanoplatelets can lead to significant shear thinning behavior of epoxy resin and reduce the flow behavior index from 0.96 to 0.53 (Table A2), especially at high temperature (80°C). When the concentration of the nanoplatelet is high, Sternstein *et al.* explained that the primary underlying mechanism for reinforcement and nonlinear behavior appears to be due to the filler-matrix interactions, but not because of filler agglomeration or percolation. However, since there is no chain entanglement in the uncured epoxy resin in this study, the shear thinning behavior can be attributed mainly to the shear-induced rotation and realignment of exfoliated individual nanoplatelet to the shear stress direction. This realignment reduces nanoplatelets physical networking, which serves a similar role as the entanglement of polymer chains. This finding is consistent with the results by Nguyen-Thuc *et al.*, who reported that sphere-shaped nanoparticles dispersed in epoxy resin only cause an increase in viscosity but no shear thinning effect. This is due to the absence of molecular entanglement or physical network. Interestingly, the addition of the same amount of poorly dispersed ZrP nanoplatelets does not play any significant role in affecting the rheological behavior of epoxy prepolymer (Figs. A4). Thus, the significant change in shear thinning behavior in epoxy is surely because of the high level of exfoliation of ZrP nanoplatelets. The temperature effects will be discussed later.



(a)



(b)

Fig. A4. Viscosity of neat epoxy and α -ZrP nanoplatelet dispersed epoxy resins with variation in the degree of exfoliation of nanoplatelets, measured at (a) 28, (b) 50, and (c) 80°C.

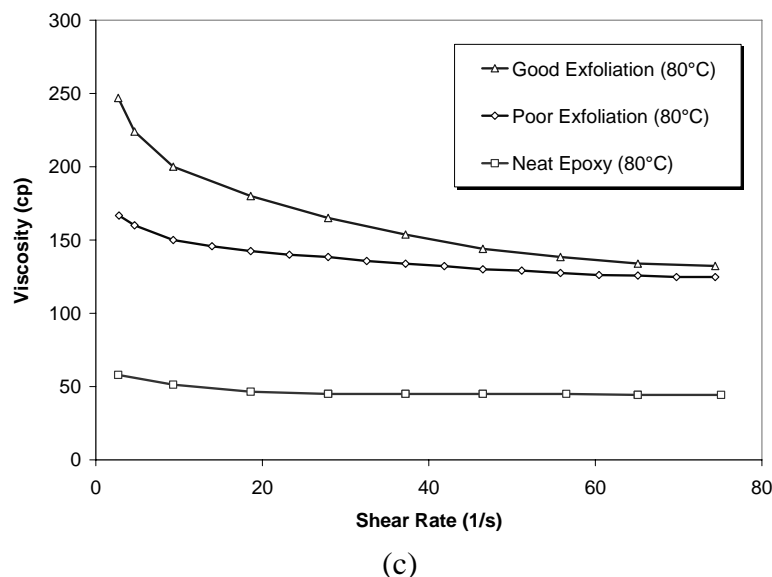
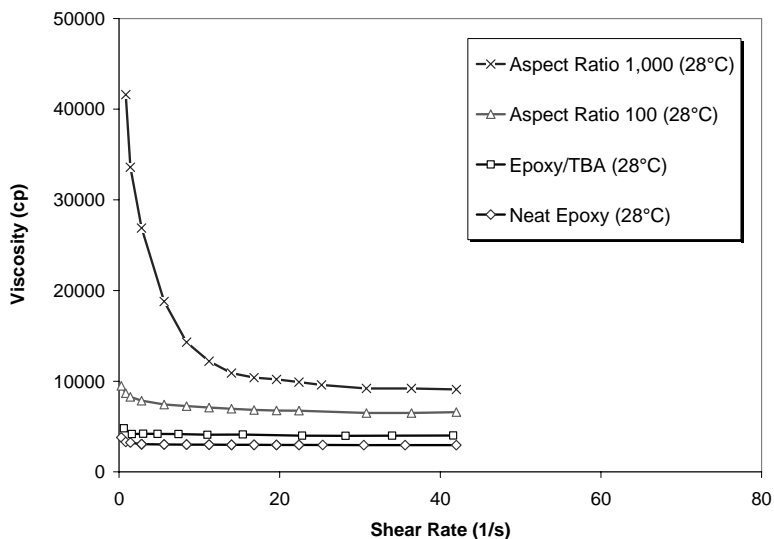


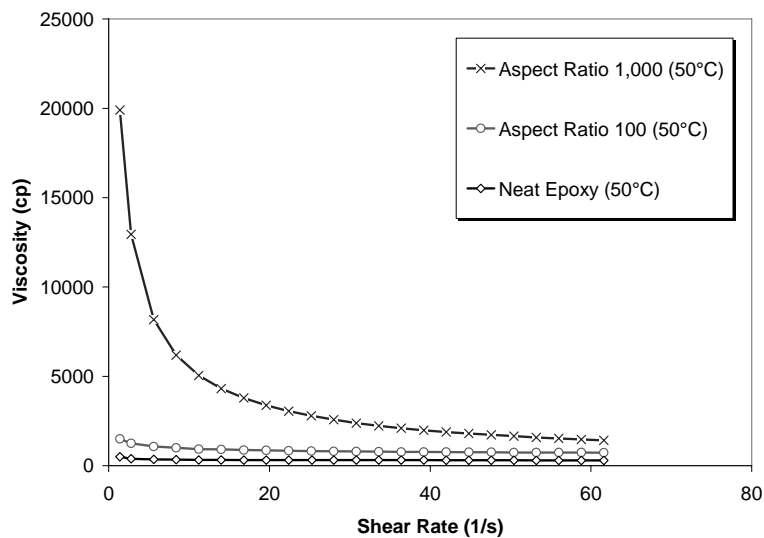
Fig. A4. Continued.

Fig. A5 presents the typical viscosity curves on how the aspect ratio of exfoliated ZrP nanoplatelets affects the rheological behavior of epoxy prepolymer at three different temperatures. Unlike the 2.0 vol% loading case, the incorporation of exfoliated ZrP-100 nanoplatelets does not induce noticeable shear thinning but only increases the shear viscosity at each testing temperature. This is probably due to the low loading level (0.7 vol%) of the dispersed nanoplatelets, which form insignificant physical networks to affect viscosity. Whereas, the addition of the same amount of ZrP-1000 nanoplatelets not only causes an increase in shear viscosity but also result in significant shear thinning behavior of epoxy resin. The flow indexes (n) representing the shear thinning effects are listed in Table A3. The strong shear thinning behavior of epoxy resin with exfoliated ZrP-1000 is

believed due to the high shear stress required to rotate and align dispersed ZrP layers along the direction of shear force.



(a)



(b)

Fig. A5. Viscosity of neat epoxy and α -ZrP nanoplatelet dispersed epoxy resins with variation in the aspect ratio of nanoplatelets, measured at (a) 28, (b) 50, and (c) 80°C.

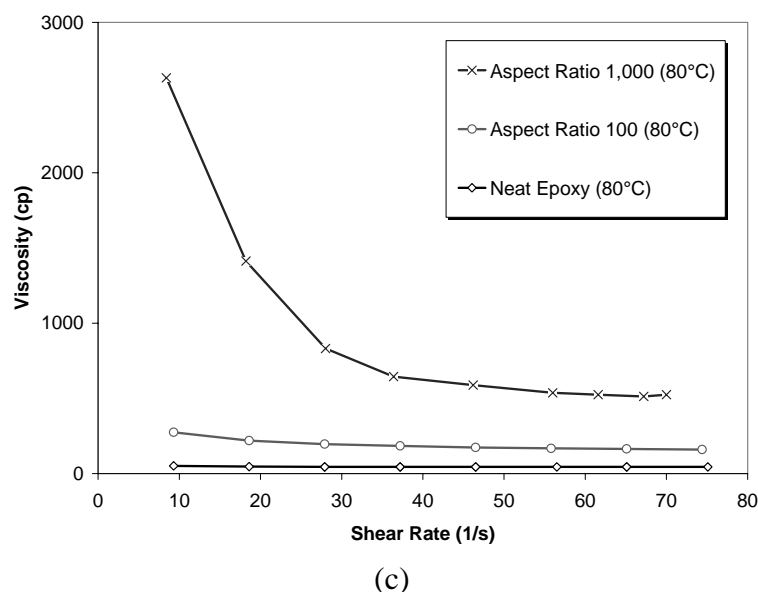
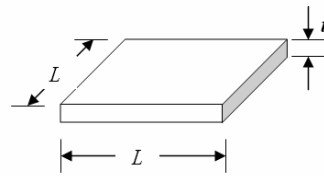


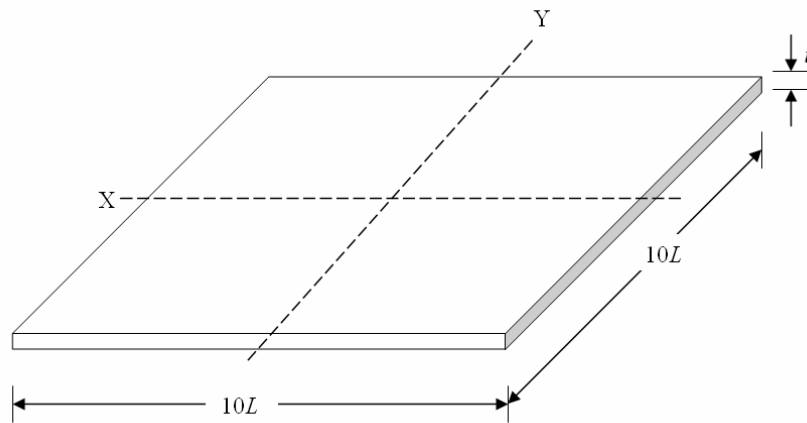
Fig. A5. Continued.

It is surprising that note that a mere 0.7 vol% of ZrP-1000 can create such a high viscososity build up at low shear rate and exhibit significant shear thinning behavior at high shear rate. To determine whether or not the observed strong shear thinning behavior in epoxy/ZrP-1000 is because of the possible higher surface area of the ZrP-1000 over that of the ZrP-100, an idealized schematics of ZrP-100 and ZrP-1000 nanoplatelets are drawn in Fig. A6. In Figs. A6(a) and A6(b), the ZrP layers dispersed in epoxy resin are simplified into square platelets with a length of L and $10L$ for ZrP-100 and ZrP-1000, respectively. Since both ZrP-100 and ZrP-1000 nanoplatelets in epoxy have been fully exfoliated, the thickness (t) of each nanoplatelet is the same. According to Fig. A6, it is evident that, at the same volume fraction of 0.7vol%, the ZrP-100 actually has a slightly higher surface area than ZrP-1000 simply because more nanoplatelet edges are present for

the epoxy/ZrP-100 system. Thus, it is reasonable to claim that the observed strong shear thinning behavior of the ZrP-1000 is not because it has a higher overall surface area. The continuity of surface area can be considered as the same concept of the aspect ratio of the dispersed nanoplatelets.



(a)



(b)

Fig. A6. Schematic diagram for the surface area comparison of α -ZrP nanoplatelets with aspect ratio of (a) 100 and (b) 1,000. A single layer structure of α -ZrP has been simplified as a square.

When considering the rotational volumes and moments of inertia of ZrP-100 and ZrP-1000, we can notice that, on an average, ZrP-1000 requires 10 times larger rotational volume and 100 times higher moment of inertia than that of 100 pieces of ZrP-100 nanoplatelets. The moment of inertia of a surface area with respect to X axis (I_x) can be expressed as:

$$I_x = \int y^2 dA \quad (2)$$

where, y is certain distance from x axis to an element, and dA is differential element of area.

Consequently, much higher resistance, or viscosity, is introduced for ZrP-1000 to rotate and align themselves along the shear orientation at low shear rate. When the shear rate is high, once the high aspect ratio nanoplatelets have aligned along the shear direction, significant drop in viscosity is expected. This leads to the observed significant shear thinning behavior of epoxy resin.

It is intuitively clear that temperature will have a strong effect on rheological behavior of polymers. As shown in Figs. A4 and A5 and based on the power law parameters listed in Tables A2 and A3, the shear thinning dependency on temperature is evident. Generally the viscosity of non-Newtonian fluids decreases as temperature increases, and vice versa. Thus, at a higher temperature, intrinsic viscosity of epoxy resins decrease. A higher shear rate is needed to induce the rotation and alignment of dispersed nanoplatelets in epoxy resin at the higher temperature.

The viscosity data obtained is compared with the Krieger–Dougherty (KD) model, which has been shown to be effective for describing the rheological behavior of particle-filled polymers. This model indicates that the viscosity of the polymer will increase if particles are added, and the magnitude of viscosity increase depends on the concentration and shape (aspect ratio) of the particles:

$$\frac{\eta}{\eta_0} = \left(1 - \frac{\phi}{\phi_c}\right)^{-[\eta]\phi_c} \quad (3)$$

where, η is the viscosity of the suspension, η_0 is the viscosity of medium (ie, epoxy resin in this case), ϕ is the volume fraction of fillers, ϕ_c is the effective maximum packing volume fraction when the free-rotational motion is hindered due to geometric constraint. The intrinsic viscosity $[\eta]$ and ϕ_c can be calculated from the theory of Wang *et al.* Also, Jeon *et al.* has reported that the K-D model describes the nanoplatelet-dispersed prepolymers well.

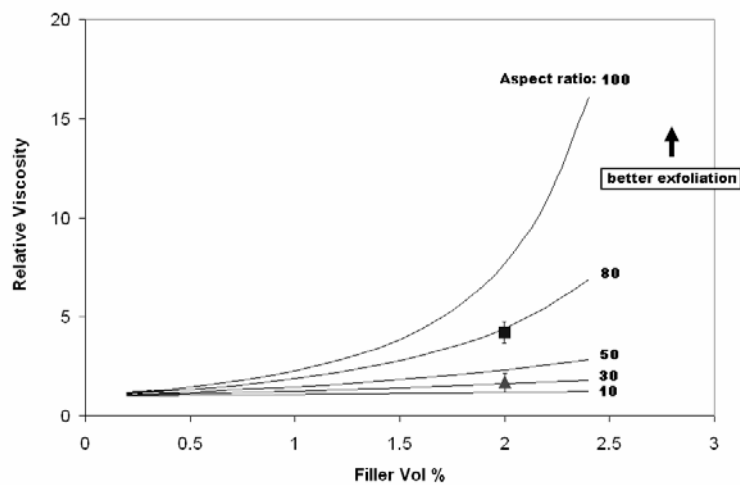
Fig. A7 shows the comparison between the K-D models for the viscosity profiles of the model epoxy/ZrP systems at 28°C. In Fig. A7(a), the degree of exfoliation of nanoplatelet is being expressed in terms of effective aspect ratio, meaning that the higher aspect ratio, the better level of exfoliation of nanoplatelets. It can be noticed that the K-D model predicts that the effective aspect ratios of 2.0 vol% of good and poor exfoliation systems are about 80 and 30, respectively. Since the aspect ratio of an individual nanoplatelet has been found to be about 100 and is fully exfoliated via TEM, a lower

number of effective aspect ratio of dispersed filler indicates either the use of surface modifier, monoamine, has inadvertently caused an increase in viscosity or the model has overestimated the particle-polymer interaction forces. Additional work may be needed to address this issue.

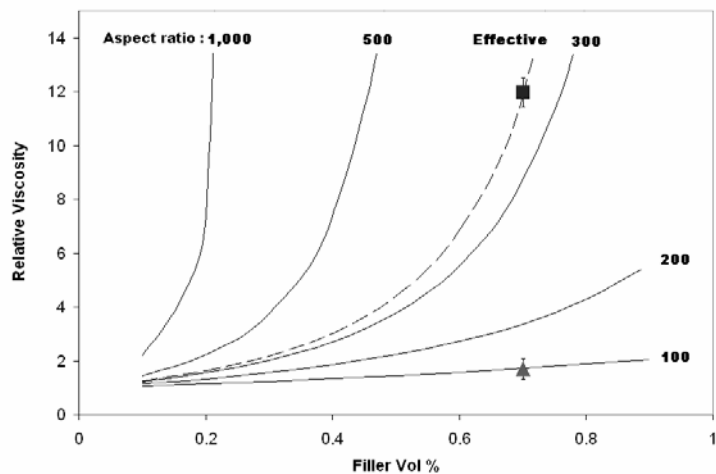
The K-D model in Fig. A7(b) describes the relative viscosity prediction affected by the aspect ratio of nanoplatelets ranging from 100 to 1,000. It shows that the higher aspect ratio nanoplatelets can increase the viscosity of suspension more dramatically. In the case of ZrP-100, the viscosity profile follows relatively well with the model. However, It should be noted that the K-D model is only valid for filler loading level below 0.2 vol%. As for ZrP-1000, the effective aspect ratio is found to be about 350. The large discrepancy between the effective and the actual particle aspect ratios can be explained with the strong curvature of high aspect ratio α -ZrP nanoplatelets shown in the TEM images in Fig. A3 (c) and (d).

As stated in the experimental sections (Table A2), to observe the intercalating agent effects, two types of intercalating agents, i.e., Jeffamine M600 and TBA, have been utilized in this study. From Tables A2 and A3, the consistency index (K) of TBA intercalated and exfoliated ZrP dispersed epoxy is higher than that treated with Jeffamine, even at a lower (0.7 vol%) loading level. To make a fair comparison, neat epoxy resins that contain only surface modifiers (Jeffamine or TBA) were also prepared. As shown in Figs. A4 (a) and A5 (a), by adding Jeffamine into epoxy decreases the viscosity of epoxy resin, whereas incorporation of TBA into epoxy shows the opposite. Also, it can be noticed from Tables A2 and A3, the flow indexes have not been changed much. With this

trend, it is possible to explain that the higher shear viscosity values found in TBA treated epoxy/ZrP even at lower nanoplatelet loading level.



(a)



(b)

Fig. A7. Constitutive model (K-D model) prediction and relative viscosity data at 28°C in terms of (a) degree of exfoliation (α -ZrP aspect ratio 100; ■ and ▲ represent good and poor exfoliation, respectively.) and (b) aspect ratio (■ and ▲ represent α -ZrP aspect ratio 1,000 and 100, respectively). The numbers in bold font express aspect ratios of dispersed fillers in suspension.

A4. Conclusion

A systematic study on the rheological behavior of α -ZrP nanoplatelets dispersed into epoxy resins varying in the degree of exfoliation and aspect ratio has been performed. Neat epoxy resin exhibits Newtonian-like rheological behavior while the addition of exfoliated nanoplatelets into epoxy resin has shown to result in a non-Newtonian behavior, which is characterized as shear thinning. Furthermore, the higher degree of exfoliation and the high aspect ratio of incorporated nanoplatelets lead to increased viscosity and significant shear thinning behavior of epoxy resins. By employing the concept of moment of inertia and surface area calculation, it has been explained that the increase of viscosity and shear thinning phenomena is mainly attributed to the high aspect ratio of dispersed nanoplatelets. Additionally by using K-D model, the effective aspect ratios of dispersed nanoplatelets in epoxy resin have been predicted and compared with the rheological data and TEM images.

A5. References

- Becker, O., Sopade, P., Bourdonnay, R., Halley, P. J., & Simon, G. P. (2003). Layered silicate nanocomposites based on various high-functionality epoxy resins. Part II: The influence of an organoclay on the rheological behavior of epoxy prepolymers. *Polymer Engineering and Science*, 43, 1683.
- Boo, W.-J., Sun, L., Liu, J., Clearfield, A., & Sue, H.-J. (2007). Morphology and Mechanical Behavior of Exfoliated Epoxy/ α -Zirconium Phosphate Nanocomposites. *Composites Science and Technology*, 67, 262.

- Boo, W.-J., Sun, L. Y., Warren, G. L., Moghbelli, E., Pham, H., Clearfield, A., & Sue, H.-J. (2007). Effect of Nanoplatelet Aspect Ratio on Mechanical Properties of Epoxy Nanocomposites *Polymer*, 48, 1075.
- Boo, W. J., Sun, L., Liu, J., Moghbelli, E., Clearfield, A., & Sue, H. J. (2007). Effect of Nanoplatelet Dispersion on Mechanical Behavior of Polymer Nanocomposites. *Journal of Polymer Science Part B-Polymer Physics*, submitted.
- Choi, H. J., Kim, S. G., Hyun, Y. H., & Jhon, M. S. (2001). Preparation and rheological characteristics of solvent-cast poly(ethylene oxide)/montmorillonite nanocomposites. *Macromolecular Rapid Communications*, 22, 320.
- Clearfield, A., & Berman, J. R. (1981). On the Mechanism of Ion-Exchange in Zirconium-Phosphates .34. Determination of the Surface-Areas of Alpha-Zr(Hpo4)2-H2o by Surface Exchange. *Journal of Inorganic & Nuclear Chemistry*, 43, 2141.
- Clearfield, A., Duax, W. L., Medina, A. S., Smith, G. D., & Thomas, J. R. (1969). On Mechanism of Ion Exchange in Crystalline Zirconium Phosphates .I. Sodium Ion Exchange of Alpha-Zirconium Phosphate. *Journal of Physical Chemistry*, 73, 3424.
- Clearfield, A., Medina, A. S., Duax, W. L., & Garces, J. M. (1972). Mechanism of Ion-Exchange in Crystalline Zirconium Phosphates .4. Potassium Ion-Exchange of Alpha-Zirconium Phosphate. *Journal of Inorganic & Nuclear Chemistry*, 34, 329.
- Galgali, G., Ramesh, C., & Lele, A. (2001). A rheological study on the kinetics of hybrid formation in polypropylene nanocomposites. *Macromolecules*, 34, 852.

- Iversen, J. D. (1979). Autorotating Flat-Plate Wings - Effect of the Moment of Inertia, Geometry and Reynolds-Number. *Journal of Fluid Mechanics*, 92, 327.
- Jeon, H. S., Rameshwaram, J. K., Kim, G., & Weinkauf, D. H. (2003). Characterization of polyisoprene-clay nanocomposites prepared by solution blending. *Polymer*, 44, 5749.
- Kojima, Y., Usuki, A., Kawasumi, M., Okada, A., Fukushima, Y., Kurauchi, T., & Kamigaito, O. (1993). Mechanical-Properties of Nylon 6-Clay Hybrid. *Journal of Materials Research*, 8, 1185.
- Kojima, Y., Usuki, A., Kawasumi, M., Okada, A., Kurauchi, T., & Kamigaito, O. (1993). Synthesis of Nylon-6-Clay Hybrid by Montmorillonite Intercalated with Epsilon-Caprolactam. *Journal of Polymer Science Part a-Polymer Chemistry*, 31, 983.
- Koo, C. M., Kim, M. J., Choi, M. H., Kim, S. O., & Chung, I. J. (2003). Mechanical and rheological properties of the maleated polypropylene-layered silicate nanocomposites with different morphology. *Journal of Applied Polymer Science*, 88, 1526.
- Lee, H., Hsieh, A., & Mckinley, G. (2002). Rheological properties of clay/PMMA nanocomposites. *Abstracts of Papers of the American Chemical Society*, 224, 526.
- Lim, S. T., Choi, H. J., & Jhon, M. S. (2003). Dispersion quality and rheological property of polymer/clay nanocomposites: Ultrasonification effect. *Journal of Industrial and Engineering Chemistry*, 9, 51.

- Lim, S. T., Lee, C. H., Choi, H. J., & Jhon, M. S. (2002). Rheological analysis of melt intercalated polymer/organoclay nanocomposites. *Abstracts of Papers of the American Chemical Society*, 224, U385.
- Lim, Y. T., & Park, O. O. (2001). Microstructure and rheological behavior of block copolymer/clay nanocomposites. *Korean Journal of Chemical Engineering*, 18, 21.
- Nguyen-Thuc, B. H., & Maazouz, A. (2002). Morphology and rheology relationships of epoxy/core-shell particle blends. *Polymer Engineering and Science*, 42, 120.
- Pintao, C. A. F., de Souza, M. P., Grandini, C. R., & Hessel, R. (2004). Experimental study of the conventional equation to determine a plate's moment of inertia. *European Journal of Physics*, 25, 409.
- Sternstein, S. S., Ramorino, G., Jiang, B., & Zhu, A. J. (2005). Reinforcement and nonlinear viscoelasticity of polymer melts containing mixtures of nanofillers. *Rubber Chemistry and Technology*, 78, 258.
- Sternstein, S. S., & Zhu, A. J. (2002). Reinforcement mechanism of nanofilled polymer melts as elucidated by nonlinear viscoelastic behavior. *Macromolecules*, 35, 7262.
- Sun, L., Boo, W. J., Browning, R. L., Sue, H.-J., & Clearfield, A. (2005). Effect of Crystallinity on the Intercalation of Monoamine in a-Zirconium Phosphate Layer Structure. *Chemistry of Materials*, 17, 5606.

- Sun, L., Boo, W. J., Clearfield, A., & Sue, H. J. (2007). Preparation of α -zirconium phosphate nanoplatelets with wide variations in aspect ratios. *New Journal of Chemistry*, DOI: 10.1039/b604054c.
- Tindwa, R. M., Ellis, D. K., Peng, G. Z., & Clearfield, A. (1985). Intercalation of Normal-Alkylamines by Alpha-Zirconium Phosphate. *Journal of the Chemical Society-Faraday Transactions I*, 81, 545.
- Usuki, A., Kojima, Y., Kawasumi, M., Okada, A., Fukushima, Y., Kurauchi, T., & Kamigaito, O. (1993). Synthesis of Nylon 6-Clay Hybrid. *Journal of Materials Research*, 8, 1179.
- Usuki, A., Kojima, Y., Kawasumi, M., Okada, A., Kurauchi, T., & Kamigaito, O. (1990). Characterization and Properties of Nylon-6 - Clay Hybrid. *Abstracts of Papers of the American Chemical Society*, 200, 218.
- Wagener, R., & Reisinger, T. J. G. (2003). A rheological method to compare the degree of exfoliation of nanocomposites. *Polymer*, 44, 7513.
- Wang, H., Hoa, S. V., & Wood-Adams, P. M. (2006). New method for the synthesis of clay/epoxy nanocomposites. *Journal of Applied Polymer Science*, 100, 4286.
- Wang, Z., & Pinnavaia, T. J. (1998). Hybrid organic-inorganic nanocomposites: Exfoliation of magadiite nanolayers in an elastomeric epoxy polymer. *Chemistry of Materials*, 10, 1820.
- Werner, F., & Mersmann, A. (1998). About the rheology of polymer solutions Part 2: A model for the prediction of the concentration dependence of the rheological parameters of power-law fluids. *Chemical Engineering & Technology*, 21, 644.

- Werner, F., & Mersmann, A. (1998b). Rheology of polymer solutions - Part 2: A model for prediction of the the concentration dependence of the rheological parameters of power-law fluids. *Chemie Ingenieur Technik*, 70, 1027.
- Wierenga, A. M., & Philipse, A. P. (1998). Low-shear viscosity of isotropic dispersions of (Brownian) rods and fibres; a review of theory and experiments. *Colloids and Surfaces a-Physicochemical and Engineering Aspects*, 137, 355.
- Wu, D. F., Zhou, C. X., Fan, X., Mao, D. L., & Bian, Z. (2005). Linear rheological behaviour and thermal stability of poly(butylene terephthalate)/epoxy/clay ternary nanocomposites. *Polymer Degradation and Stability*, 87, 511.
- Wu, D. F., Zhou, C. X., Yu, W., & Xie, F. (2006). Effect of blending sequence on the morphologies of poly(butylene terephthalate)/epoxy/clay nanocomposites by a rheological approach. *Journal of Applied Polymer Science*, 99, 340.
- Yano, K., Usuki, A., Okada, A., Kurauchi, T., & Kamigaito, O. (1991). Synthesis and Properties of Polyimide-Clay Hybrid. *Abstracts of Papers of the American Chemical Society*, 201, 16.
- Yano, K., Usuki, A., Okada, A., Kurauchi, T., & Kamigaito, O. (1993). Synthesis and Properties of Polyimide Clay Hybrid. *Journal of Polymer Science Part a-Polymer Chemistry*, 31, 2493.

VITA

Woong Jae Boo was born in Seoul, Republic of Korea. He received his B.S. degree in mechanical engineering from Hankook Aviation University in 1995. After serving as a Lieutenant J.G. in the R.O.K. Navy for four years, he received his M.S degree in mechanical engineering from Texas A&M University (College Station, Texas, USA) in December 2003 under the guidance of Dr. Roger J. Morgan. He furthered his studies in the Ph.D. program of materials science and engineering under the supervision of Dr. Hung-Jue Sue. His research interests include development, characterization and the structure-property relationship of polymer nanocomposites. His permanent address is: 207-1203 Jukong, Daebang-dong, Dongjak-ku, Seoul, Korea.